Modeling and analysis of the dynamics of dry-friction-damped structural systems

Olivier Poudou

MODELING AND ANALYSIS OF THE DYNAMICS OF DRY-FRICTION-DAMPED STRUCTURAL SYSTEMS

by

Olivier J. Poudou

A dissertation submitted in partial fulfillment
of the requirements for the degree of
Doctor of Philosophy
(Mechanical Engineering)
in The University of Michigan
2007

Doctoral Committee:

Professor Christophe Pierre, Chair
Associate Research Scientist Matthew P. Castanier
Assistant Professor Bogdan I. Epureanu
Professor Armin W. Troesch

ACKNOWLEDGEMENTS

I wish to express my deepest gratitude to Prof. Christophe Pierre for his guidance, support and mentorship throughout this doctoral work. I would like to thank the Société Nationale D'Étude et de Construction de Moteurs D'Aviation (SNECMA) - and in particular Marc Berthillier, Eric Seinturier, Jean-Pierre Lombard and Christian Dupont - for their trust, support and input. I am also grateful to Dr. Matthew P. Castanier, my colleagues, and the visiting students at the Structural Dynamics Laboratory for their insights and suggestions.

Finally, I would like to extend my sincere thanks to my friends in Ann Arbor who supported me throughout these wonderful years at the University of Michigan.

TABLE OF CONTENTS

LIST OF FIGURES

Figure

LIST OF TABLES

Table

LIST OF APPENDICES

Appendix

CHAPTER I

INTRODUCTION

1.1 Foreword

Friction is often considered by engineers as detrimental to the design of mechanisms with moving parts, but it has long been established that it can also provide a very efficient means of damping out vibrations in elastic structures. In applications such as turbomachinery bladed disks, where structural damping is negligible, dry-friction damping has been widely used to reduce the resonant response of the blades so as to limit the occurrence of wear and premature failure. In such systems, friction is obtained either by appending special passive devices (friction dampers) to selected locations of the elastic structure to be damped, or by direct frictional interaction between two or more of its constitutive parts. Once properly modeled, the parameters describing these frictional interfaces can be optimized so as to maximize the benefits of friction damping, namely reducing the vibratory response.

The figures 1.1 and 1.2 depict a complete bladed disk assembly and the typical components of a cyclic sector for such a structure. Both models are provided by the Société Nationale d'Étude et de Construction de Moteurs d'Aviation (SNECMA). Friction dampers are usually inserted in specifically designed cavities located under the platforms of the blades. Since these dampers straddle two adjacent sectors of the assembly, the relative

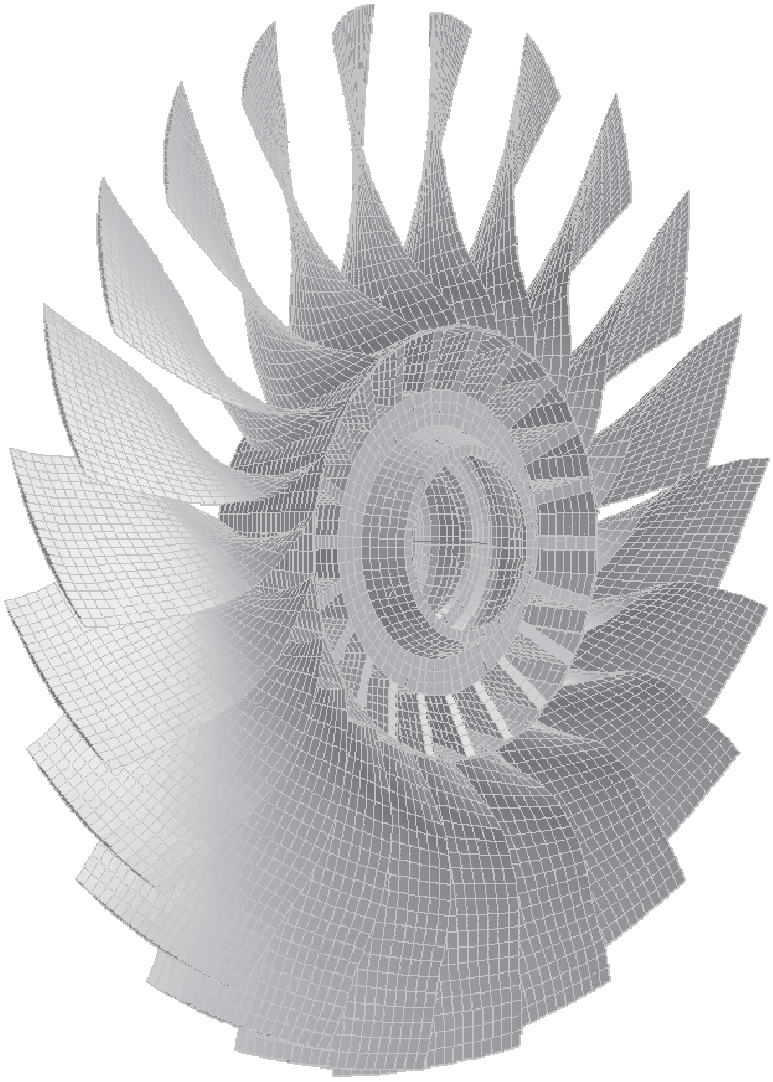

Figure 1.1: Model of bladed disk assembly. (Model provided by SNECMA.)

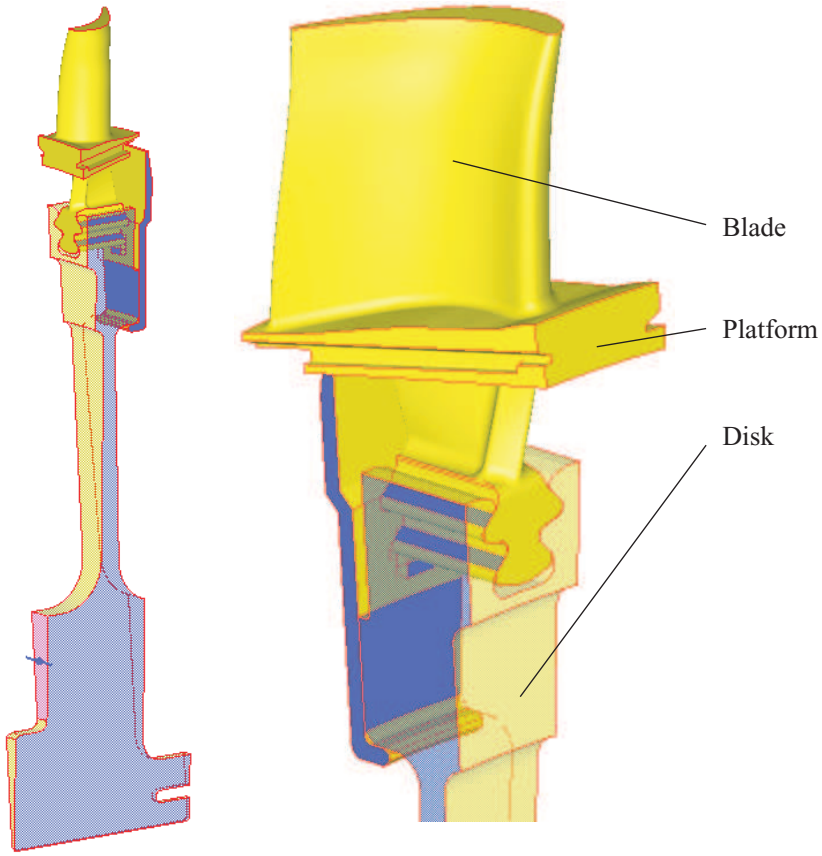

Figure 1.2: Model of a single sector of a bladed disk assembly. The sector is comprised of the blade and a section of the disk. The entire bladed disk can be deduced by successive rotations of this sector due to its properties of cyclic symmetry. Friction dampers are usually located in specially designed cavities or grooves underneath the platforms. (Model provided by SNECMA.)

motion of these two sectors due to the vibration of the entire structure generates friction at the damper/platform interfaces. Although they are not structurally connected to the blades, the centrifugal force created by the rotation of the engine presses them against the platforms and thus provides positive normal contact forces at the frictional damper/platform interfaces. In addition to these interfaces, friction can also occur directly between the contacting parts of two adjacent platforms, and between two adjacent blades if these blades feature shrouds or if their design includes interlocking teeth at their tip. Finally, most bladed disk assemblies can experience frictional interactions between the blades and the disk and the blades and the casing of the engine; such interactions are however beyond the scope of this work and are not investigated.

The benefits of an intentional friction damping mechanism is illustrated in Fig. 1.3, which presents the forced response of a simple dry-friction damped beam for various values of the normal contact load characterizing the frictional interface. This behavior shows that a careful analysis of the parameters that define a frictional interface can lead to a substantial reduction of the response of the friction-damped structure. In the case of friction dampers the design parameters that can be optimized usually include their stiffness, the centrifugal force applied to them, and the friction coefficient of their interfaces with the blade. These parameters are derived from the dampers geometry and material, and the location of the frictional interfaces. For direct contact - such as between two adjacent platforms - the design parameters are limited to the friction coefficient of the contacting components of the assembly.

However, the optimization of such parameters is hampered by the highly nonlinear behavior of friction-damped systems, which makes their modeling and analysis complicated. Difficulties stem from the modeling of the frictional interactions as well as from the highly nonlinear nature of the resulting set of equations of motion. Since an accurate description

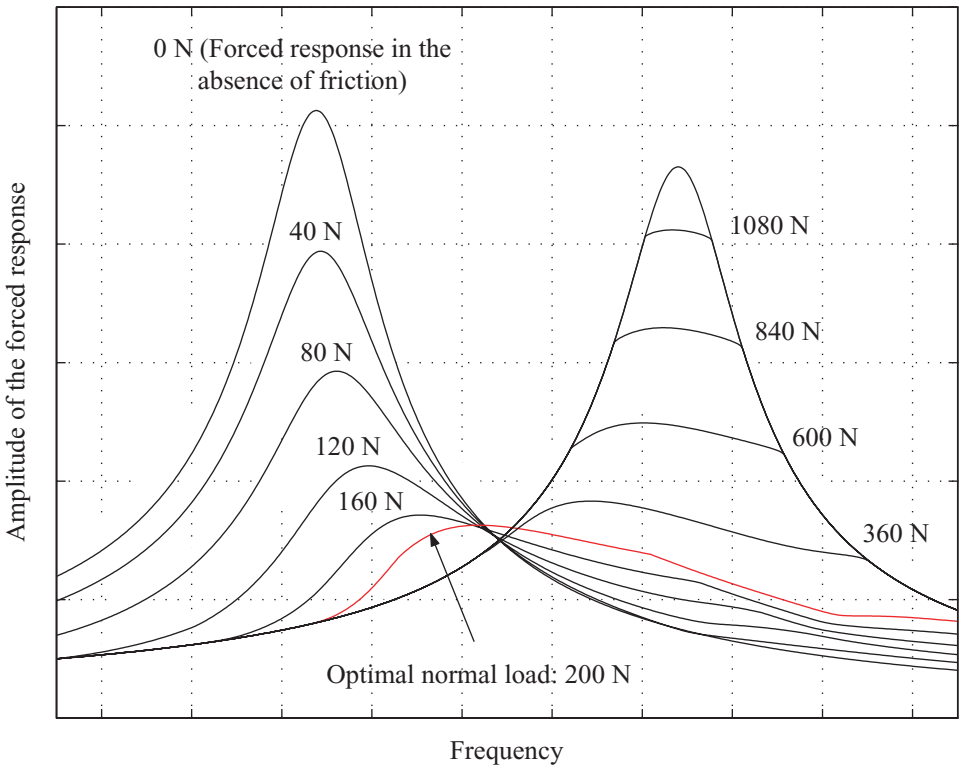

Figure 1.3: Typical forced response of a dry-friction damped beam subject to a periodic excitation, for various values of the normal contact load characterizing the frictional interface.

of the forced response of realistic systems is usually not amenable to the traditional means of analysis (e.g. closed-form solutions or direct time-integration methods) because of the complexity of these systems and/or the computational costs involved, most of the research efforts to date have yielded approximate methods sacrificing one or more of the following aspects of the modeling: (1) realism of the modeling of the friction-damped structures, (2) realism of the models of friction dampers, (3) accuracy of the kinematics of the contact interfaces, (4) ability of the modeling method to capture accurately the complexity of the forced response of the damped system.

The objective of this dissertation is to introduce new methods of analysis that overcome some of these obstacles. This research is aimed at the development and implementation of methods of analysis and models of dampers adapted to the study of the steady-state, forced

response of realistic friction-damped structures. It is based on the Alternating Frequency-Time (AFT) method originally proposed by Cameron and Griffin [1], which parallels the Fast Galerkin (FG) method introduced by Ling and Wu [2]. Guillen and Pierre [3–6] have further developed this theoretical approach – also known as the Hybrid Frequency-Time (HFT) method.

In this doctoral work, Guillen's approach is modified and extended so as to be applied to large-scale, industrial structural systems. Complex models of elastic, structure-like under-platform dampers are introduced, and the modeling of direct friction (e.g. without a friction damper) between two contacting parts of the same structure is also investigated.

1.2 Literature review

Friction has been an extremely active field of research since the early studies by den Hartog [7] of a simple friction-damped system. Recent survey papers by Ibrahim [8, 9] and Feeny *et al.* [10] show the variety and complexity of friction-related mechanisms, which blend contact mechanics, tribology and nonlinear dynamics. Friction damping modeling and its applications have been reviewed by Ferri [11]. Given the scope of this research, it is of particular interest to note that the existing works on dry-friction damping can be broadly divided into two categories: (1) research efforts undertaken to model and analyze the nonlinear behavior of friction-damped systems and (2) studies that have principally focused on the modeling of the friction dampers.

1.2.1 Nonlinear methods for the analysis of friction-damped systems

Early studies have focused on exact solution methods. den Hartog [7] was first to propose the exact steady-state solution for a simple single degree of freedom (DOF) oscillator subject to harmonic excitation. His work was further extended by Levitan [12] to the same model subject to a harmonic base excitation, and by Hundal [13] to a different

frictional configuration. Yeh [14] investigated the dynamics of a two-DOF system with friction, and Pratt and Williams [15] introduced a mixed analytical/numerical procedure for the study of two spring-mass systems contacting each other. The rapid increase of the complexity of the solutions for the dynamics of systems involving friction has however limited closed-form solutions to extremely simplified models.

Early on it has also been recognized that the conceptually opposite approach based on direct time integration methods was leading to almost intractable computational issues when realistic models where studied. Ferri [11] noted that time integration can be very inefficient if one is primarily interested in the steady-state response to periodic excitation, since the very low amount of structural damping present in turbomachinery structures requires one to perform the integration of the system equations over hundreds of periods, until the transient response dies out. Furthermore, several authors have underscored the significant difficulties involved in the implementation of the transition criteria between the various states of the contact interfaces – stick, slip or separation –, usually leading to the costly choice of unusually small time steps to detect these phase changes accurately. As a consequence, exact time integration methods have been mainly used for (1) the study of small frictional oscillators, (2) verifications of the results produced by faster, approximate solutions for the dynamics of larger systems and (3) parametric studies (often coupled with experimental investigations) of the dynamics of specific systems. Among the works falling in the last category, Korkmaz *et al.* [16] have analyzed the behavior of a cantilever beam damped by a dry friction damper using Newmark's method, Whiteman and Ferri [17] have investigated the interactions between bending-torsion flutter and friction for gas turbines, and Toufine *et al.* have focused on the dynamics of a simple friction-damped mechanical system [18] and a more complex structure with flexion-torsion coupling [19].

Since closed-form solutions are available only for extremely simplified models, and

direct time integration techniques lead to prohibitive computational costs, approximate methods have been continuously introduced over the past 20 years. Among them, the Harmonic Balance Method (HBM) developed by Nayfeh and Mook's [20] has been successfully applied to various friction-damped structures. It is based on the assumption that the forced response of the system is mainly harmonic. Using this approximation, the behavior of cantilevered beams subject to the action of friction dampers has been studied by Dowell [21], Dowell and Schwartz [22, 23], Ferri and Dowell [24], Ferri and Bindemann [25], Menq and Griffin [26], Whiteman and Ferri [27, 28], and Go *et al.* [29], among others. Bazan *et al.* [30] extended the approach to linear structures with multiple frictional interfaces. In the context of turbomachinery, Griffin [31], Srinivasan and Cutts [32], Muszyńska and Jones [33], Sinha and Griffin [34] and Sanliturk *et al.* [35] have applied the Harmonic Balance Method (or equivalent approximation techniques) to the study of the forced response of jet engine blades. Sinha and Griffin [36–39] also extensively investigated the effect of friction damping on various flutter configurations and analyzed the dynamics of mistuned bladed disk assemblies with friction dampers [40]. Cha and Sinha [41–43] investigated the influence of white noise and narrow band excitations on the computation of the normal load applied to friction dampers featured in mistuned bladed disks.

The Harmonic Balance Method has been later used for the modeling of systems involving friction dampers of increased complexity, as shown in the following section. Yet, it has also been noted that its inability to represent accurately the periodic waveform of the nonlinear forced response as well as the contact friction force could be a significant source of error, especially when hysteretic models of dampers were considered.

In order to overcome the modeling limitations of the Harmonic Balance Method, multiharmonic techniques have been developed. They can be traced back to the introduction

by Lau *et al.* [44–46] of the Incremental Harmonic Balance method (IHB) to solve for the nonlinear periodic and quasi-periodic vibrations of continuous systems. Ferri [47] showed the equivalence of the IHB and the Galerkin/Newton-Raphson (GNR) form of the Harmonic Balance Method. Pierre and Dowell [48], and Pierre *et al.* [49] used an extended IHB approach to analyze the steady state of systems featuring perfectly plastic friction dampers, and Ferri and Dowell [50] used a multiharmonic GNR method to model damped systems where Coulomb's friction law was approximated by a ramp. Wei and Pierre [51] applied a similar approach to the modeling of mistuned assemblies with several rigid dampers. Shiau *et al.* [52, 53] combined a multi-harmonic approach with a trigonometric collocation method to investigate the behavior of frictionally-damped composite blades.

A significant breakthrough was made by Ling and Wu [2] (Fast Galerkin Method), Cameron and Griffin [1] (Alternating Frequency-Time domain Method), as well as Kim and Noah [54] and Cardona [55], when it was realized that the nonlinearities due to the friction force could be accurately described in the time domain over a single period of motion of the structure, and then transformed back in the frequency domain using a Fast Fourier Transform, to form a set of nonlinear equations which can be solved by a Newton-Raphson or a Broyden procedure. Berthillier *et al.* [56, 57] applied this procedure to the forced response of turbomachinery blades with an approximation of Coulomb's friction law. Guillen and Pierre [3–6] further expanded the capabilities of the method to study the forced and free response of systems with multiple friction dampers, and clearly demonstrated that (1) approximations of Coulomb's friction law were no longer required and (2) complex models of dampers were compatible with this method, referred to herein as the Hybrid Frequency-Time (HFT) domain method.

Other methods of less general scope have been introduced for the modeling of spe-

cific nonlinear systems. A multi-harmonic method associated with an exact, analytical expression of the friction force has been developed by Wang and Chen [58] for the study of a single-DOF system with a hysteretic model of damper, but this approach becomes rather cumbersome for larger systems, and is not applicable to more complex frictional configurations (e.g., variable normal load). Ren and Beards [59] introduced a receptance-based multi-harmonic method that is almost as costly as a direct time integration. Ge and Leung [60, 61] developed a method based on Toeplitz Jacobian Matrices, which so far has not been applied to frictional systems. The stick-slip motion of frictionally-damped turbine airfoils has been studied by Wang [62] using a Finite Element in Time approach applied to a single-DOF system. A simple hysteretic model of damper was used, yet it was noted that the computation of the friction force contributed to a significant portion of the overall computation time, and therefore this approach did not seem as appropriate as the HFT method to study systems involving more complex frictional mechanisms. The same author [63] proposed an analytical solution for the periodic response of elastic friction-damped systems, yet again the procedure was applied to a single DOF system with simple dampers. Ferri and Heck [64] recently used the Singular Perturbation Theory to investigate the effect of the mass of the friction damper on a spring-mass-dashpot system, but significant deviations from the exact solution were observed. A similar investigation was carried out by Berger and Krousgrill [65] with bilinear hysteresis elements to model the frictional interfaces.

Finally, specially tailored analytical techniques have been developed for the analysis of mistuned bladed disk systems, which involve as many frictional interfaces as there are friction-damped blades. Chen and Sinha [66] investigated the behavior of a mistuned bladed disk with friction dampers attached, while Lin and Mignolet [67] increased the complexity of such systems by considering an additional mistuning of the characteristics

of the dampers.

1.2.2 Models of dampers

As mentioned above, the development of further-refined means of analysis of the dynamics of nonlinear systems has been paralleled by the increase in the complexity of the modeling of the frictional interfaces. It must be noticed, however, that the description of the friction mechanisms has evolved somewhat faster than the ability of the methods of analysis to solve the resulting nonlinear systems. Practically, the harmonic balance method (i.e., with a single temporal harmonic) has been overwhelmingly used for the study of complex frictional interfaces, notwithstanding the noted limited accuracy of the method for realistic configurations.

The frictional interfaces encountered in the literature on friction damping can be classified according to the following criteria:

1. **Type of friction interface**. Possible friction sources are (1) the contact between the root of the blade and the disk, (2) blade-to-ground dampers, (3) blade-to-blade under-platform dampers and their variant called wedge – or cottage-roof – dampers, and (4) shroud-to-shroud or similar direct contact between two parts of the bladed disk assembly.

2. **Type of friction law used**. Although Hertzian contact may have been used occasionally, there is a widespread consensus on the ability of Coulomb's classical law of dry friction to capture the mechanisms of interest for friction damping. Yet, many approximations have been made for its implementation. Among them, one can note (1) the choice of a constant normal load over that of a variable normal load, and (2) the approximation of the hysteretic relation between the tangential displacement and the friction force by simplified laws, such as ramp or sign functions, usually

involving arbitrary numerical coefficients.

3. **Type of frictional mechanism**. Micro- or macroslip approaches have to be considered, according to the complexity of the contact interfaces.

4. **Type of kinematics at the friction interfaces**. It can be one-dimensional (1-D), but in general the contacting interfaces have a complex, two-dimensional (2-D) or three-dimensional (3-D) relative motion – an extended 2-D case with variable normal load and possibly separation.

Works based on single-harmonic approximations have investigated several of these characteristics. Menq *et al.* have examined a 1-D microslip approach applied to the vibratory response of a single-DOF system [68], the influence of a variable normal load on the forced vibration of a similar system [69], and the particular case of 2-D (circular or elliptic) relative motion. The effect of a variable load, including separation, was later analyzed by Yang and Menq [70] for the 1-D frictional interaction of shrouded blades. Wang and Shieh [71] have investigated the influence of a variable friction coefficient for the 1-D friction-damped motion of a single-DOF system. Also considering a single DOF system, Anderson and Ferri [72] have studied the influence of various generalized friction laws. Griffin and Menq [73] also developed a circular model of friction damping, and applied it to a 2-DOF system. They later suggested that this elliptical model could be applied to a new damping mechanism involving friction dampers located within internal cavities of hollow airfoils [74]. Sanliturk and Ewins [75] proposed a more complex 2-D model of friction damper, which does not rely on the analytical approximations of the previous models for the computation of the friction force. Menq and Yang [76] reexamined Menq's first 2-D model and also proposed a refined version based on a step-by-step, time-domain evaluation of the friction force when the relative motion of the contacting interfaces is

elliptic.

Still under the assumption that the forced response of the system is mono-harmonic, the modeling of 3-D frictional constraints has been developed by Yang and Menq [77–79] for the analysis of shroud contact. Csaba [80–82], Jareland and Csaba [83] and Jareland [84] investigated various 1-D and 2-D models of under-platform and wedge dampers combining macroslip and microslip approaches. Sanliturk and Ewins [85] also proposed a non-flexible wedge damper, whose contact interfaces with the platforms are described by a microslip model whose characteristics are deduced from experimental data.

Other non-flexible models of wedge dampers have been studied with time integration methods by Pfeiffer and Hajek [86] and more recently by Kaiser *et al.* [87]. Panning *et al.* [88] also used a direct time integration and a non-flexible model of wedge damper to investigate various possible geometric configurations, but he augmented his model by assuming that Hertzian contact represents the frictional interfaces with the platform.

Finally, the most advanced works on friction damping have been based on the multi-harmonic HFT method or variations thereof. Guillen *et al.* [6] introduced a simplified flexible structure-like damper model featuring four contact points, where each of the contact points experiences Coulomb friction with a constant normal load along a fixed direction, and studied the free response and stability of simple friction-damped systems. Chen and Menq [89–91] extended Yang's model of 3-D shroud contact to several harmonics. Nacivet *et al.* [92, 93] introduced a variant of the HFT method based on Dynamic Lagrangians so as to model the dynamics of periodic frictional contact in finite elements models. Seinturier *et al.* [94] as well as Petrov and Ewins [95–97] presented several successful applications of multi-harmonic methods to the analysis of the forced response of realistic bladed disk assemblies for various contact configurations, including ones that include mistuned damper characteristics [98]. Finally, recent work by Nacivet [99], Charleux *et al.* [100, 101] and

Petrov and Ewins [102, 103] have focused on applying these methods to the analysis of the friction phenomena occuring at the dovetail attachments of the blades on the disks.

These studies strongly suggest that the multi-harmonic HFT technique is now the method of choice for the modeling of complex periodic frictional interactions in realistic structures.

1.3 Research topics addressed in this dissertation

In this research, extensions of the multi-harmonic HFT method are proposed for the efficient study of the forced response of realistic, complex structures featuring displacement-dependent nonlinearities, such as the friction and impact phenomena that may occur in the presence of friction dampers or when two parts of the same structure periodically contact each other. Particular attention is paid to the theoretical formulation of the method for large scale, realistic industrial bladed disk structures that may feature cyclic symmetry or that may be mistuned. Two analysis techniques are developed for the modeling of such displacement-dependent nonlinearities. The first technique corresponds to the modeling of the friction dampers as nonlinear operators representing the contact forces acting on the bladed disk assembly, from the simple case of mono-directional friction with constant normal load to the more complex case of three dimensional contact with variable normal load. The analysis of the forced response of several nonlinear systems illustrates the capabilities of this approach as well as the complexity of the typical behavior exhibited by friction damped structures. The second technique introduced helps analyze structures experiencing intermittent contact or friction between two parts or sub-components of these structures. This method is applied to the study of the forced response of several simple systems and is used with great efficiency to predict the nonlinear behavior of a beam with a crack. This second technique also allows the dampers to be modeled realistically as stand-

alone components appended to the bladed disk assembly. In this approach the bladed disk assembly as well as the friction dampers are modeled as independent structures that interact at their contacting interfaces. This allows the exact elastic properties of the friction dampers to be retained without making assumptions regarding their geometry. These two methods are applied to the study of the nonlinear forced response a realistic bladed disk assembly featuring a wedge damper model and a structure-like damper model.

1.4 Dissertation outline

The remaining chapters of this dissertation are based on five technical papers that have been prepared for submission to the scientific community. As a consequence, some background information as well as some theoretical developments are repeated in various chapters. These chapters are organized as follows:

In chapter II the theoretical formulation of the multi-harmonic HFT method is presented. Modifications of the original HFT method are introduced to allow the accurate and efficient analysis of the nonlinear forced response of large-scale, realistic structures with or without cyclic symmetry. The specific features of the response exhibited by structures with cyclic symmetry and subject to a traveling excitation are investigated. In particular, the special relationship between the temporal harmonics of the forcing and the spatial harmonics of the response of the structure is highlighted. The concept of modeling friction dampers as nonlinear operators is presented, as well as a detailed analysis of the procedures used to calculate the time-domain, periodic waveforms of the contact efforts for damper models. These procedures are delineated for models of dampers which feature either mono-directional friction with constant normal load or more complicated three-dimensional contact with variable normal load.

In chapter III a series of numerical examples that illustrate the capabilities of the multi-

harmonic HFT method is presented. The forced response of simple systems is obtained for different types of damper models, in the case of structures which are tuned (that is, structures with cyclic symmetry), or mistuned (that is, structures that require the modeling of a large number of frictional interfaces).

In chapter IV, a variation of the multi-harmonic HFT method is proposed to analyze the periodic forced response of structural systems undergoing intermittent contact and frictional interactions between some of their components. In this new approach, the dynamics of the structure is still described by a set of Fourier coefficients representing the motion of the nonlinear DOFs where impact or friction occur, but the corresponding forces are no longer taken into account in the resulting set of nonlinear equations to be solved. Instead, this method is based on the nonlinear kinematic conditions associated with the contact forces, that is, it solves directly for the nonlinear DOFs displacements which satisfy the friction and non-penetration conditions associated with these nonlinear forces. Simple spring-mass systems with displacement-dependent, non-smooth nonlinearities are studied, as well as an application of the method to a more realistic finite element model representing two example shrouded blades impacting each other. The robustness and accuracy of the method is demonstrated.

In chapter V, the multi-harmonic HFT method is extended so as to allow for the analysis of structures with cracks. The method is applied to a finite element model of cracked beam, and the influence of the method's parameters on the accuracy of the prediction of the crack-induced frequency shift is investigated. The results highlight the importance of the modeling of the crack interface, and they demonstrate the method's ability to handle with great accuracy and at a very low computational cost the dynamics of such complex structures.

In chapter VI, the forced response of a realistic bladed disk assembly is investigated

for various frictional and contact configurations that highlight the capabilities of the extensions of the multi-harmonic HFT method introduced in the previous chapters. Using the nonlinear-operator approach, a new model of flexible wedge damper is introduced and a parametric study of its influence on the overall response of the bladed disk assembly is carried out. Then, the behavior of the structure with a new model of structure-like damper featuring several contact points under the blades' platform is analyzed. In this case the damper is modeled as a flexible structure independent from the bladed disk, and it is only subject to the centrifugal load due to the rotation of the engine and the boundary conditions at the contact interfaces under the blades platforms. The analysis exhibits the complexity of the nonlinear forces at the contact points, which feature friction with variable normal load.

Finally, chapter VII summarizes the main contributions of this research and investigates possible ways to further extend them in future investigations, both in terms of theoretical advancements as well as in terms of possible applications.

CHAPTER II

HYBRID FREQUENCY-TIME DOMAIN METHODS FOR THE ANALYSIS OF COMPLEX STRUCTURAL SYSTEMS WITH DRY FRICTION DAMPING

2.1 Introduction

Many studies on the dynamics of periodically excited structural systems with friction damping use the Harmonic Balance Method (HBM) introduced By Nayfeh and Mook [20]. This method is based on the representation of the dynamics of the structure using a linear combination of temporal harmonics, and it is particularly well suited to the analysis of the steady state response of nonlinear systems. If a sufficient number of harmonics are retained, both the motion of selected degrees of freedom of the structure and the friction force at the contact points can be approximated with excellent accuracy. Early studies on the subject of dry-friction damping were limited to single harmonic approximations. Among them, work by Dowell and Schwartz [22], Ferri *et al.* [24, 25] and Whiteman and Ferri [27] on cantilevered beams; and Griffin [31], Srinivasan and Cutts [32], and Sinha and Griffin [37] on simple turbomachinery applications have successfully focused on models of dampers of increasing complexity. Menq *et al.* studied the effect of microslip [68] and variable normal load [69]. An elliptic motion of the contact point was later considered by Griffin and Menq [73], Sanliturk and Ewins [75], and Menq and Yang [76]. The

case of three-dimensional (3-D) contact kinematics has also been investigated by Yang *et al.* [104]. However, it was also noted that the single harmonic approximation used in these studies was often unable to accurately capture the periodic waveforms of the nonlinear response and the friction force.

This issue was first addressed by the introduction of an incremental variant of the HBM introduced by Lau [45] and Ferri [47], but the first multi-harmonic studies still required complicated analytical work to calculate the nonlinear force, as shown by Pierre *et al.* [49]. A significant breakthrough was made possible when the Alternating Frequency-Time domain method was introduced in 1989 by Cameron and Griffin [1]. It was realized that the nonlinearities due to the friction force can be accurately evaluated in the time domain and transformed back in the frequency domain, so as to form a set of nonlinear equations which can be solved by a Newton-Raphson-like procedure. Guillen and Pierre [5] recently proposed a variant of the AFT method, called Hybrid Frequency-Time (HFT) domain method, and confirmed that large scale, friction-damped systems can be efficiently studied with this approach. Finally, the most recent works show that the HFT method is adapted to the study of systems featuring complex frictional nonlinearities with an accurate, multi-harmonic approach. Guillen *et al.* [6] introduced a flexible, structure-like damper model. Chen and Menq [91] developed a three-dimensional model of shroud contact, and Nacivet *et al.* [92, 93] introduced an alternative to the HFT method based on dynamic lagrangians. Recently, Petrov introduced a multi-harmonic method for the study of realistic turbomachinery applications for various frictional configurations [95–98, 102, 103]

This chapter presents two extensions of the Hybrid Frequency-Time domain method: The first one is based on Lagrange's work on the modeling of the forced response of spatially cyclic structures with friction dampers [105]. Previous works on this subject assumed that the sectors of the assembly are structurally independent, that is, they are

represented by independent structures connected to a rigid support. Coupling between these structures was assumed to occur only through the nonlinear forces, which depend from the motion of two adjacent sectors, such as the forces created by shroud-to-shroud contact or by under-platform dampers. In other words, these studies considered that for a bladed-disk assembly subject to nonlinear forces applied to the blades only, the coupling between two adjacent sectors due to the flexibility of the disk is zero. The theory presented here is based *a contrario* on the exact derivation of the properties of fully flexible, cyclic systems. It allows one to reduce the study of the structure to the analysis of the behavior of one of its sectors. It also shows that there exists a special relation between the spatial modes of vibration of the structure and the temporal harmonics of the excitation.

The second extension of the HFT method concerns the generation of the equations of motion derived from the Harmonic Balance Method. More precisely, a new method of condensation of the equations of motion on the set of nonlinear degrees of freedom (DOFs) is introduced. This new method, based on a modal analysis of the part of the structure that is not subject to the nonlinear forces, allows one to study without incurring time penalties systems featuring a high ratio of linear DOFs to nonlinear DOFs.

In addition, this chapter introduces the theoretical analysis underlying the modeling of friction dampers. These dampers are defined in the HBM as nonlinear operators, and a detailed analysis of the time-domain calculation methods required to obtain the periodic waveform of the corresponding nonlinear forces is presented.

2.2 HBM for non-cyclic structures

The general equations of motion of a n-DOF elastic structure are

$$\mathbf{M}\ddot{\mathbf{x}}(t) + \mathbf{C}\dot{\mathbf{x}}(t) + \mathbf{K}\mathbf{x}(t) = \mathbf{f}_l(t) + \mathbf{f}_{nl}[\mathbf{x}](t), \tag{2.1}$$

where $\mathbf{M}$, $\mathbf{K}$ and $\mathbf{C}$ are, respectively, its mass, stiffness and viscous damping matrices; $\mathbf{f}_l$ is a periodic, external force, and $\mathbf{f}_{nl}$ is an external, nonlinear force modeled as an operator acting on the displacement of the structure. $\mathbf{x}$ is the vector representing the DOFs of the system.

2.2.1 Equations of motion in complex form

When the steady-state response of the structure is assumed to be periodic, the displacement $\mathbf{x}$ and the linear force $\mathbf{f}_l$ can be written as Fourier series of harmonic functions. Assuming that keeping n_h harmonics provides an accurate approximation of the dynamics of the structure, they can be written as

$$\mathbf{x}(t) \approx \mathrm{Re}\big[\sum_{k=0}^{n_h} \underline{\mathbf{x}}_k e^{jk\omega t}\big] \tag{2.2}$$

$$\mathbf{f}_l(t) \approx \mathrm{Re}\big[\sum_{k=0}^{n_h} \underline{\mathbf{f}}_{l,k} e^{jk\omega t}\big], \tag{2.3}$$

where $\frac{\omega}{2\pi}$ is the frequency of excitation of $\mathbf{f}_l$. Similarly, the expression of the nonlinear force $\mathbf{f}_{nl}$ as a function of the displacement $\mathbf{x}$ is given by:

$$\mathbf{f}_{nl}[\mathbf{x}](t) \approx \mathrm{Re}\big[\sum_{k=0}^{n_h} \underline{\mathbf{f}}_{nl,k}(\underline{\mathbf{x}}_0, \ldots, \underline{\mathbf{x}}_{n_h}) e^{jk\omega t}\big]. \tag{2.4}$$

Then, applying the Harmonic Balance Method to equation (2.1) yields a set of n_h complex, nonlinear, coupled equations

$$\underline{\mathbf{\Lambda}}_k \underline{\mathbf{x}}_k - \underline{\mathbf{f}}_{l,k} - \underline{\mathbf{f}}_{nl,k}(\underline{\mathbf{x}}_0, \ldots, \underline{\mathbf{x}}_{n_h}) \approx \mathbf{0}, \tag{2.5}$$

where

$$\underline{\mathbf{\Lambda}}_k = -(k\omega)^2\mathbf{M} + \underline{j}k\omega\mathbf{C} + \mathbf{K}. \tag{2.6}$$

2.2.2 Condensation of the system

Since industrial, realistic structures are in general represented by very large finite element models, it is usually not possible to solve efficiently the set of nonlinear equa-

tions (2.5) when the unknowns $\underline{\mathbf{x}}_k$ consist of the harmonic components of *all* the physical degrees of freedom present in the finite element (FE) model. In lieu thereof, models of significantly smaller size are used to represent the structure. Assuming that the structure's DOFs can be classified as *nonlinear* DOFs (i.e., DOFs where a nonlinear external force is applied), and *linear* DOFs (i.e., all the other DOFs of the structure), these reduced-order models are usually obtained from component mode synthesis techniques, which substitute most of the linear DOFs of the structure by a few modal coordinates and leave the nonlinear DOFs unchanged. Therefore, when the nonlinearities are localized (i.e., the number of nonlinear DOFs is a small fraction of the total number of DOFs), significant gains in term of size reduction are achieved.

In turbomachinery applications, such localized nonlinearities are exhibited by bladed disk assemblies with dry friction dampers attached to adjacent blades. Applying the Craig-Bampton condensation method [106] to these systems yields reduced-order models in which DOFs are partitioned as described in Fig. 2.1. These reduced-order models consist in:

- A subset of the physical DOFs of the original FE model. It is made of the nonlinear friction DOFs as well as any other physical DOFs (referred to as *retained, linear DOFs*) of particular importance for the analysis and the understanding of the dynamics of the structure.

- A subset of *modal coordinates* corresponding to the free vibration normal modes of the structure fixed at the retained, linear and nonlinear DOFs.

This condensation of the FE model is computationally costly and is usually done once and for all. As a consequence, when for instance parametric studies are carried out to optimize the characteristics of the dampers, it is necessary to make sure that the subset of

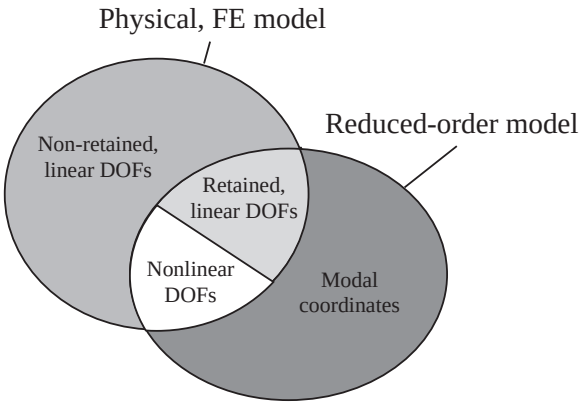

Figure 2.1: Partition of physical, FE model DOFs and reduced-order model DOFs.

retained physical DOFs of the reduced-order model is large enough, so that various frictional configurations can be tested without performing the condensation of the FE model for each configuration. For bladed-disk assemblies with underplatform friction dampers, one might retain for instance several candidate friction DOFs under each platform to assess the benefits of various locations of the damper. Similarly, it is usually beneficial to keep a relatively large number of normal modes of vibration so as to approximate best the dynamics of the structure.

Therefore, although the size of the reduced-order model can be several orders of magnitude smaller than the size of the original FE model, the ratio of the actual nonlinear DOFs – for a given frictional configuration – to the other DOFs of the reduced-order model (i.e., the other candidate friction DOFs not considered in this configuration, the retained linear DOFs, and the modal coordinates) can still be rather small, and makes solving the set of equations (2.5) difficult.

The Harmonic Balance Method provides an elegant means of reducing the system to the actual nonlinear DOFs. Let the superscript ^{r} denote the *retained* DOFs (i.e., the DOFs actually subject to a nonlinear force for a given friction configuration), and let ^{d} denote the *deleted* DOFs, i.e., all the other DOFs of the reduced-order model. Since the DOFs in the

^{d} set are not subject to a nonlinear force, the set of equations (2.5) can be written as

$$\begin{bmatrix} \underline{\mathbf{\Lambda}}_k^{dd} & \underline{\mathbf{\Lambda}}_k^{dr} \\ \underline{\mathbf{\Lambda}}_k^{rd} & \underline{\mathbf{\Lambda}}_k^{rr} \end{bmatrix} \begin{bmatrix} \underline{\mathbf{x}}_k^d \\ \underline{\mathbf{x}}_k^r \end{bmatrix} - \begin{bmatrix} \underline{\mathbf{f}}_{l,k}^d \\ \underline{\mathbf{f}}_{l,k}^r \end{bmatrix} - \begin{bmatrix} \mathbf{0} \\ \underline{\mathbf{f}}_{nl,k} \end{bmatrix} = \mathbf{0}. \tag{2.7}$$

This set of equations can be expressed as a function of $\underline{\mathbf{x}}_k^r$ only

$$\underline{\mathbf{\Lambda}}_k^{red} \underline{\mathbf{x}}_k^r - \underline{\mathbf{f}}_{l,k}^{red} - \underline{\mathbf{f}}_{nl,k}(\underline{\mathbf{x}}_0^r, \ldots, \underline{\mathbf{x}}_{n_h}^r) = \mathbf{0}, \tag{2.8}$$

where the reduced quantities $\underline{\mathbf{\Lambda}}_k^{red}$ and $\underline{\mathbf{f}}_{l,k}^{red}$ are defined as:

$$\underline{\mathbf{\Lambda}}_k^{red} = \underline{\mathbf{\Lambda}}_k^{rr} - \underline{\mathbf{\Lambda}}_k^{rd} \underline{\mathbf{\Lambda}}_k^{dd^{-1}} \underline{\mathbf{\Lambda}}_k^{dr} \tag{2.9}$$

$$\underline{\mathbf{f}}_{l,k}^{red} = \underline{\mathbf{f}}_{l,k}^r - \underline{\mathbf{\Lambda}}_k^{rd} \underline{\mathbf{\Lambda}}_k^{dd^{-1}} \underline{\mathbf{f}}_{l,k}^d. \tag{2.10}$$

If required, a simple backsubstitution allows one to express the value of the harmonic components of the deleted DOFs, $\underline{\mathbf{x}}_k^d$, as a function of the harmonic components of the retained nonlinear DOFs, $\underline{\mathbf{x}}_k^r$:

$$\underline{\mathbf{x}}_k^d = \underline{\mathbf{\Lambda}}_k^{dd^{-1}} [\underline{\mathbf{f}}_{l,k}^d - \underline{\mathbf{\Lambda}}_k^{dr} \underline{\mathbf{x}}_k^r]. \tag{2.11}$$

As a consequence of this transformation, the set of nonlinear equations (2.8) does not involve a combination of linear and nonlinear variables anymore. It is made of the n_h harmonic components of the n_r retained nonlinear DOFs only, resulting in a compact system of $n_r(2n_h - 1)$ real, nonlinear variables[1].

Traditional implementations of the HBM generate the n_h reduced matrices $\underline{\mathbf{\Lambda}}_k^{red}$ by a direct application of Eq. (2.9). When the response of the structure is desired over a range of frequencies, the steps described in Eqs. (2.9) and (2.10) must be repeated for each frequency. In particular, the matrices $\underline{\mathbf{\Lambda}}_k^{dd}$ have to be inverted for each value of ω,

[1]For each DOF, the coefficients of the Fourier series are complex (they are represented by a real and an imaginary part corresponding to the cosine and sine components of the series), except the coefficient corresponding to the harmonic 0, which is always real.

and these inversions can become very costly as the fidelity of the reduced-order model increases, i.e., as the ratio of nonlinear DOFs to deleted DOFs decreases. In some cases, the CPU time consumed by these linear operations significantly exceeds the CPU time required to solve the condensed, nonlinear problem.

The reduced matrices $\underline{\mathbf{\Lambda}}_k^{red}$ can be generated in a simple way which alleviates this problem. Assuming that the damping matrix $\mathbf{C}$ is proportional to the mass and stiffness matrices of the structure, that is,

$$\mathbf{C} = \alpha\mathbf{K} + \beta\mathbf{M}, \tag{2.12}$$

and defining the complex scalars $\underline{\varepsilon}_k$ and $\underline{\delta}_k$ as

$$\underline{\varepsilon}_k = 1 + \underline{j}k\omega\alpha \tag{2.13}$$

$$\underline{\delta}_k = -(k\omega)^2 + \underline{j}k\omega\beta, \tag{2.14}$$

$\underline{\mathbf{\Lambda}}_k^{dd}$ can be written as

$$\underline{\mathbf{\Lambda}}_k^{dd} = \underline{\varepsilon}_k\mathbf{K}^{dd} + \underline{\delta}_k\mathbf{M}^{dd}, \tag{2.15}$$

with similar expressions available for $\underline{\mathbf{\Lambda}}_k^{rr}$, $\underline{\mathbf{\Lambda}}_k^{rd}$ and $\underline{\mathbf{\Lambda}}_k^{dr}$. Then, solving the eigenproblem

$$[\mathbf{K}^{dd} + \lambda\mathbf{M}^{dd}]\mathbf{x}^d = \mathbf{0} \tag{2.16}$$

yields

$$\mathbf{M}^{dd^{-1}}\mathbf{K}^{dd} = \mathbf{P}\mathbf{D}\mathbf{P}^{-1}, \tag{2.17}$$

where $\mathbf{D}$ is a diagonal matrix. Now, defining the diagonal matrices $\underline{\mathbf{\Theta}}_k$ as

$$\underline{\mathbf{\Theta}}_k = \underline{\varepsilon}_k\mathbf{D} + \underline{\delta}_k\mathbf{I}, \tag{2.18}$$

where $\mathbf{I}$ is the identity matrix, and combining Eqs. (2.15), (2.17) and (2.18), one obtains the following expression for the inverse of $\underline{\mathbf{\Lambda}}_k^{dd}$:

$$\underline{\mathbf{\Lambda}}_k^{dd^{-1}} = \mathbf{P}\underline{\mathbf{\Theta}}_k^{-1}\mathbf{P}^{-1}\mathbf{M}^{dd^{-1}}. \tag{2.19}$$

Introducing the constant matrices $\mathbf{U}$, $\mathbf{U}'$, $\mathbf{V}$, and $\mathbf{V}'$ defined as

$$\mathbf{U} = \mathbf{K}^{rd}\mathbf{P} \tag{2.20}$$

$$\mathbf{U}' = \mathbf{M}^{rd}\mathbf{P} \tag{2.21}$$

$$\mathbf{V} = \mathbf{P}^{-1}\mathbf{M}^{dd^{-1}}\mathbf{K}^{dr} \tag{2.22}$$

$$\mathbf{V} = \mathbf{P}^{-1}\mathbf{M}^{dd^{-1}}\mathbf{M}^{dr}, \tag{2.23}$$

and substituting these expressions in equation (2.9), the reduced matrices $\underline{\mathbf{\Lambda}}_k^{red}$ can finally be expressed as:

$$\begin{aligned}\underline{\mathbf{\Lambda}}_k^{red} = \underline{\mathbf{\Lambda}}_k^{rr} - \mathbf{U}[\underline{\varepsilon}_k^2\underline{\mathbf{\Theta}}_k^{-1}\mathbf{V} + \underline{\varepsilon}_k\underline{\delta}_k\underline{\mathbf{\Theta}}_k^{-1}\mathbf{V}'] \\ -\mathbf{U}'[\underline{\delta}_k\underline{\varepsilon}_k\underline{\mathbf{\Theta}}_k^{-1}\mathbf{V} + \underline{\delta}_k^2\underline{\mathbf{\Theta}}_k^{-1}\mathbf{V}'].\end{aligned} \tag{2.24}$$

The advantage of this formulation is that $\mathbf{U}$, $\mathbf{U}'$, $\mathbf{V}$, and $\mathbf{V}'$ can be computed once and for all (they are independent of ω), and that the inversion of the matrices $\underline{\mathbf{\Lambda}}_k^{dd}$ is replaced by the trivial inversion of the diagonal, complex matrices $\underline{\mathbf{\Theta}}_k$. When large models are considered (e.g., mistuned bladed disk assemblies with as many friction dampers as blades), significant CPU-time gains ensue.

2.3 HBM for cyclic structures

Unlike the general structures described in the previous section, a typical friction-damped, bladed disk is a structure which exhibits a cyclic symmetry. In other words, the geometry of the complete assembly (i.e., the disk, the blades and the underplatform dampers) can be deduced by successive rotations of one of its sectors. Such a structure can be fully described by (1) the geometry and the mechanical properties of a single sector, and (2) the number of sectors n_s of the assembly.

As the bladed disk rotates, it is subject to a constant, non-uniform pressure field, and the variations of pressure experienced by the sectors due to the rotation of the structure

result in a vibratory response of the assembly.

2.3.1 Temporal periodicity of the response

For the sake of clarity, we introduce the two following reference frames:

- (R) is a reference frame fixed with respect to the structure. In this frame, the position of a point Q of the structure is expressed in polar coordinates as $Q(r, \alpha, z)$, where z corresponds to the axis of rotation of the disk.

- (R') is a reference frame fixed with respect to the pressure field. The position of a point Q' fixed with respect to (R') is expressed in polar coordinates as $Q'(r, \theta, z)$.

It is somehow more convenient to carry out the analysis of the response of the structure by considering that the disk is fixed in space and that the pressure field rotates, resulting in a traveling excitation which excites the bladed disk assembly, as shown in Fig. 2.2.

Since the pressure field is time invariant in (R'), the pressure observed at any point $Q'(r, \theta, z)$ fixed in (R') can be described by an infinite Fourier series:

$$P\big(Q'\big) = \mathrm{Re}\big[\sum_{k=0}^{\infty} \underline{p}_k(r, z) e^{jk\theta}\big]. \tag{2.25}$$

In most turbomachinery applications however, the pressure field features a spatial periodicity defined by an integer e_o, referred to as "engine order". That is, the pressure field can be fully described by any angular sector of size $2\pi/e_o$ repeated e_o times, and $P\big(Q'\big)$ is given by:

$$P\big(Q'\big) = \mathrm{Re}\big[\sum_{k=0}^{\infty} \underline{p}_k(r, z) e^{jke_o\theta}\big]. \tag{2.26}$$

Figure 2.2 shows an example of traveling excitation when e_o – also referred to as the number of nodal diameters of the excitation – is equal to 4.

Now, defining Ω as the angular velocity of (R') with respect to (R), and assuming that the two reference frames coincide at $t = 0$, the angular coordinates of two points Q (fixed

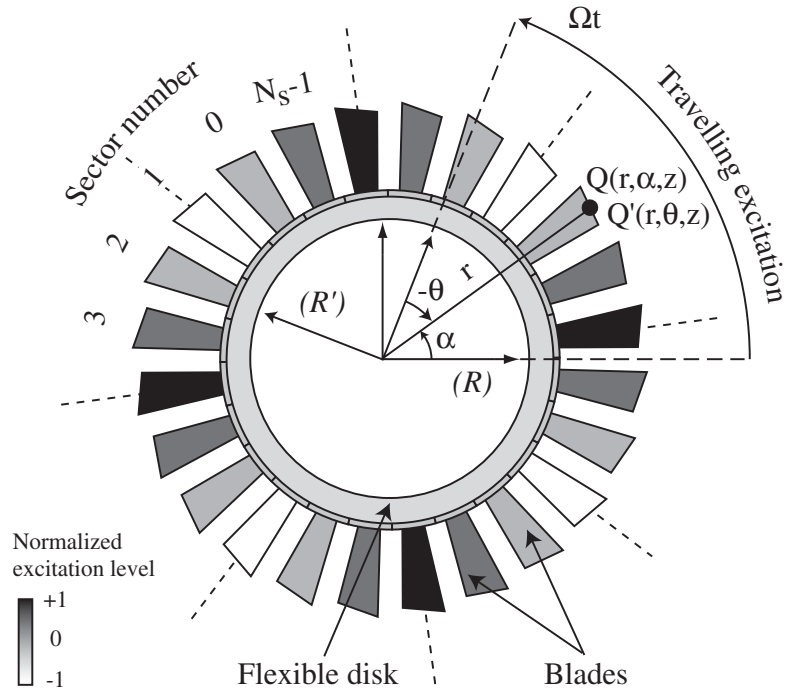

Figure 2.2: Model of a rotating structure with cyclic symmetry subject to a traveling excitation.

in (R)) and Q' (fixed in (R')) coinciding at t must satisfy:

$$\theta = \Omega t - \alpha. \tag{2.27}$$

As a consequence, the pressure observed at t at a fixed point $Q(r, \alpha)$ of the structure is expressed as:

$$P\big(Q, t\big) = \mathrm{Re}\big[\sum_{k=0}^{\infty} \underline{p}_k(r, z) e^{jke_o(\Omega t - \alpha)}\big]. \tag{2.28}$$

Then, defining ω as

$$\omega = \Omega e_o, \tag{2.29}$$

and integrating Eq. (2.28) over the elements of the structure, one obtains the expression of the linear, traveling excitation in the reference frame (R):

$$\tilde{\mathbf{f}}_l(t) = \mathrm{Re}\Big[\sum_{k=0}^{\infty} \underline{\tilde{\mathbf{f}}}_{l,k} e^{jk\omega t}\Big]. \tag{2.30}$$

Thus, the spatial harmonics which define the constant, rotating pressure field correspond to the temporal harmonics of the linear excitation acting on the bladed disk, and the pulsation of the fundamental temporal harmonic of $\tilde{\mathbf{f}}_l$ is ω.

Now, assuming that gyroscopic effects are neglected, the equations of motions of the complete structure can be expressed as

$$\tilde{\mathbf{M}}\ddot{\tilde{\mathbf{x}}}(t) + \tilde{\mathbf{C}}\dot{\tilde{\mathbf{x}}}(t) + \tilde{\mathbf{K}}\tilde{\mathbf{x}}(t) = \tilde{\mathbf{f}}_l(t) + \tilde{\mathbf{f}}_{nl}[\tilde{\mathbf{x}}](t), \tag{2.31}$$

where $\tilde{}$ indicates that the variable refers to *all* the $\tilde{n}$ DOFs of the structure, $\tilde{n}$ being defined as the product of n_s by the number n of DOFs per sector. As in the previous section, $\tilde{\mathbf{f}}_{nl}$ represents the nonlinear forces due to the friction dampers.

Labeling the n_s sectors of the assembly as indicated in Fig. 2.2, the displacement of the structure as well as the linear and nonlinear forces can be written as

$$\tilde{\mathbf{x}}(t) = \big[\mathbf{x}^{0^T}(t), \ldots, \mathbf{x}^{n_s-1^T}(t)\big]^T \tag{2.32}$$

$$\tilde{\mathbf{f}}_l(t) = \big[\mathbf{f}_l^{0^T}(t), \ldots, \mathbf{f}_l^{n_s-1^T}(t)\big]^T \tag{2.33}$$

$$\tilde{\mathbf{f}}_{nl}[\tilde{\mathbf{x}}](t) = \big[\mathbf{f}_{nl}^{0^T}[\tilde{\mathbf{x}}](t), \ldots, \mathbf{f}_{nl}^{n_s-1^T}[\tilde{\mathbf{x}}](t)\big]^T, \tag{2.34}$$

and in the following, the sector numbered "0" will be referred to as the *reference* sector.

Since $\tilde{\mathbf{f}}_l$ corresponds to a wave rotating at the angular velocity Ω, the external excitations applied at time t to two adjacent sectors differ only by a simple temporal phase ϕ_t, defined as:

$$\phi_t = \frac{2\pi}{\Omega n_s}. \tag{2.35}$$

Thus, the excitation applied to the q-th sector of the assembly can be fully deduced from the excitation applied to the reference sector:

$$\mathbf{f}_l^q(t) = \mathbf{f}_l^0(t - q\phi_t). \tag{2.36}$$

Now, assuming that the response of the structure exhibits the same temporal phase, the displacement of the whole structure can also be expressed as a function of the displacement of the reference sector, that is,

$$\mathbf{x}^q(t) = \mathbf{x}^0(t - q\phi_t). \tag{2.37}$$

As a consequence, the definition of the nonlinear forces $\mathbf{f}_{nl}^q$ as operators acting on $\tilde{\mathbf{x}}$ can be modified so as to involve $\mathbf{x}^0$ only,

$$\mathbf{f}_{nl}^q[\tilde{\mathbf{x}}](t) = \mathbf{f}_{nl}^q[\mathbf{x}^0](t), \tag{2.38}$$

and the phase relation (2.37) yields:

$$\mathbf{f}_{nl}^q[\tilde{\mathbf{x}}](t) = \mathbf{f}_{nl}^0[\mathbf{x}^0](t - q\phi_t). \tag{2.39}$$

2.3.2 Equations of motion in complex form

Since the pulsation of the excitation $\tilde{\mathbf{f}}_l$ is ω, and assuming that n_h-harmonic Fourier series are accurate enough to approximate the dynamics of the structure, the phase relations (2.36), (2.37) and (2.39) allow one to write in complex form $\tilde{\mathbf{x}}$, $\tilde{\mathbf{f}}_l$, and $\tilde{\mathbf{f}}_{nl}$ as:

$$\begin{aligned}\underline{\tilde{\mathbf{x}}}(t) = \sum_{k=0}^{n_h} \big[&\underline{\mathbf{x}}_k^{0^T} e^{jk\omega t}, \dots \\ &\dots, \underline{\mathbf{x}}_k^{0^T} e^{jk\omega(t-(n_s-1)\phi_t)}\big]^T,\end{aligned} \tag{2.40}$$

$$\begin{aligned}\underline{\tilde{\mathbf{f}}}_l(t) = \sum_{k=0}^{n_h} \big[&\underline{\mathbf{f}}_{l,k}^{0^T} e^{jk\omega t}, \dots \\ &\dots, \underline{\mathbf{f}}_{l,k}^{0^T} e^{jk\omega(t-(n_s-1)\phi_t)}\big]^T,\end{aligned} \tag{2.41}$$

and

$$\begin{aligned}\underline{\tilde{\mathbf{f}}}_{nl}[\tilde{\mathbf{x}}](t) = \sum_{k=0}^{n_h} \big[\underline{\mathbf{f}}_{nl,k}^{0^T}(\underline{\mathbf{x}}_0^0, \ldots, \underline{\mathbf{x}}_{n_h}^0) e^{jk\omega t}, \ldots \\ \ldots, \underline{\mathbf{f}}_{nl,k}^{0^T}(\underline{\mathbf{x}}_0^0, \ldots, \underline{\mathbf{x}}_{n_h}^0) e^{jk\omega(t-(n_s-1)\phi_t)}\big]^T.\end{aligned} \tag{2.42}$$

These equations can be written in a more compact form,

$$\underline{\tilde{\mathbf{x}}}(t) = \sum_{k=0}^{n_h} \big[\underline{\mathbf{u}}_k^{e_o} \otimes \underline{\mathbf{x}}_k^0\big] e^{jk\omega t} \tag{2.43}$$

$$\underline{\tilde{\mathbf{f}}}_l(t) = \sum_{k=0}^{n_h} \big[\underline{\mathbf{u}}_k^{e_o} \otimes \underline{\mathbf{f}}_{l,k}^0\big] e^{jk\omega t} \tag{2.44}$$

$$\underline{\tilde{\mathbf{f}}}_{nl}[\underline{\tilde{\mathbf{x}}}](t) = \sum_{k=0}^{n_h} \big[\underline{\mathbf{u}}_k^{e_o} \otimes \underline{\mathbf{f}}_{nl,k}^0(\underline{\mathbf{x}}_0^0, \ldots, \underline{\mathbf{x}}_{n_h}^0)\big] e^{jk\omega t}, \tag{2.45}$$

where the Kronecker product $\otimes$ and the vector $\underline{\mathbf{u}}_k^{e_o}$ are defined in Appendix A.

Then, using Eqs. (2.43-2.45), introducing the matrices $\underline{\tilde{\mathbf{\Lambda}}}_k$ as

$$\underline{\tilde{\mathbf{\Lambda}}}_k = -(k\omega)^2 \tilde{\mathbf{M}} + \underline{j} k\omega \tilde{\mathbf{C}} + \tilde{\mathbf{K}}, \tag{2.46}$$

and applying the harmonic balance method to Eq. (2.31), one obtains:

$$\begin{aligned}\underline{\tilde{\mathbf{\Lambda}}}_k(\underline{\mathbf{u}}_k^{e_o} \otimes \underline{\mathbf{x}}_k^0) - \underline{\mathbf{u}}_k^{e_o} \otimes \underline{\mathbf{f}}_{l,k}^0 \\ - \underline{\mathbf{u}}_k^{e_o} \otimes \underline{\mathbf{f}}_{nl,k}^0(\underline{\mathbf{x}}_0^0, \ldots, \underline{\mathbf{x}}_{n_h}^0) = \mathbf{0}.\end{aligned} \tag{2.47}$$

The last step in this analysis is based on the definition and properties of the extended Fourier matrix presented in Appendix B. In particular, since the bladed disk is spatially cyclic, (i.e., $\tilde{\mathbf{M}}$, $\tilde{\mathbf{K}}$ and $\tilde{\mathbf{C}}$ are block-circulant matrices), the trivial transformation

$$\begin{aligned}\underline{\tilde{\mathbf{E}}}^* \underline{\tilde{\mathbf{\Lambda}}}_k \underline{\tilde{\mathbf{E}}} \underline{\tilde{\mathbf{E}}}^* (\underline{\mathbf{u}}_k^{e_o} \otimes \underline{\mathbf{x}}_k^0) - \underline{\tilde{\mathbf{E}}}^* (\underline{\mathbf{u}}_k^{e_o} \otimes \underline{\mathbf{f}}_{l,k}^0) \\ - \underline{\tilde{\mathbf{E}}}^* (\underline{\mathbf{u}}_k^{e_o} \otimes \underline{\mathbf{f}}_{nl,k}^0(\underline{\mathbf{x}}_0^0, \ldots, \underline{\mathbf{x}}_{n_h}^0)) = \mathbf{0}\end{aligned} \tag{2.48}$$

yields the block-diagonal form of Eq. (2.47):

$$\begin{aligned}&\mathbf{BDiag}[\underline{\mathbf{\Lambda}}_k^0, \ldots, \underline{\mathbf{\Lambda}}_k^{n_s-1}](\underline{\mathbf{E}}^* \otimes \mathbf{I}_n)(\underline{\mathbf{u}}_k^{e_o} \otimes \underline{\mathbf{x}}_k^0) \\ &- (\underline{\mathbf{E}}^* \otimes \mathbf{I}_n)(\underline{\mathbf{u}}_k^{e_o} \otimes \underline{\mathbf{f}}_{l,k}^0) \\ &- (\underline{\mathbf{E}}^* \otimes \mathbf{I}_n)(\underline{\mathbf{u}}_k^{e_o} \otimes \underline{\mathbf{f}}_{nl,k}^0(\underline{\mathbf{x}}_0^0, \ldots, \underline{\mathbf{x}}_{n_h}^0)) = \mathbf{0},\end{aligned} \tag{2.49}$$

Engine order \ Temporal harmonic	0	1	2	3	4	5	6	7	8	9	10	11	12	13	...
0	0	0	0	0	0	0	0	0	0	0	0	0	0	0	...
1	0	1	2	3	4	5	6	7	8	9	10	11	12	0	...
2	0	2	4	6	8	10	12	1	3	5	7	9	11	0	...
3	0	3	6	9	12	2	5	8	11	1	4	7	10	0	...
4	0	4	8	12	3	7	11	2	6	10	1	5	9	0	...
5	0	5	10	2	7	12	4	9	1	6	11	3	8	0	...
6	0	6	12	5	11	4	10	3	9	2	8	1	7	0	...

Spatial harmonic

Table 2.1: Relation between the *spatial harmonics* of the response of a 13-sector cyclic structure and the *temporal harmonics* of the excitation applied to one of its sectors, for various engine orders.

where

$$\underline{\mathbf{\Lambda}}_k^q = -(k\omega)^2 \underline{\mathbf{M}}^q + \underline{j} k\omega \underline{\mathbf{C}}^q + \underline{\mathbf{K}}^q. \tag{2.50}$$

Then, the distributivity property of the Kronecker product allows one to rewrite Eq. (2.49) as:

$$\begin{aligned} &\mathbf{BDiag}[\underline{\mathbf{\Lambda}}_k^0, \ldots, \underline{\mathbf{\Lambda}}_k^{n_s-1}](\underline{\mathbf{E}}^* \underline{\mathbf{u}}_k^{e_o}) \otimes \underline{\mathbf{x}}_k^0 \\ &- (\underline{\mathbf{E}}^* \underline{\mathbf{u}}_k^{e_o}) \otimes \underline{\mathbf{f}}_{l,k}^0 \\ &- (\underline{\mathbf{E}}^* \underline{\mathbf{u}}_k^{e_o}) \otimes \underline{\mathbf{f}}_{nl,k}^0(\underline{\mathbf{x}}_0^0, \ldots, \underline{\mathbf{x}}_{n_h}^0)) = \mathbf{0}. \end{aligned} \tag{2.51}$$

Finally, the property of the product $\underline{\mathbf{E}}^* \underline{\mathbf{u}}_k^{e_o}$ explained in the appendix yields the most compact form of the n_h equations of motion:

$$\underline{\mathbf{\Lambda}}_k^{q(k,e_o)} \underline{\mathbf{x}}_k^0 - \underline{\mathbf{f}}_{l,k}^0 - \underline{\mathbf{f}}_{nl,k}^0(\underline{\mathbf{x}}_0^0, \ldots, \underline{\mathbf{x}}_{n_h}^0) = \mathbf{0}, \tag{2.52}$$

where

$$q(k, e_o) - k e_o \equiv 0 \; [n_s]. \tag{2.53}$$

If required, this set of nonlinear equations can be reduced to the nonlinear DOFs of the reference sector, in a fashion strictly similar to the method previously presented.

2.3.3 Comments

Although the set of nonlinear equations (2.52) obtained for a cyclic system shares many similarities with the set of equations (2.5) obtained in the general, non-cyclic case, some important differences should be noted:

- The unknowns involved in the set of equations (2.52) consist of the Fourier coefficients of the DOFs of the reference sector only. They represent the actual motion of the nodes of the reference sector. The gain in terms of reduction of the size of the nonlinear system is therefore extremely important, since the DOFs of the other sectors can be ignored.

- A simple temporal phase ϕ_t exists between the response of two adjacent sectors. This phase relation applies to the displacement of the structure, the linear and the nonlinear forces as well, and it depends on (1) the pulsation ω of the linear excitation applied on the reference sector, (2) the spatial repetitivity e_o of the traveling excitation; and (3), the number of sectors n_s of the assembly. ϕ_t is given by:

$$\phi_t = \frac{2\pi}{\omega e_o n_s}. \tag{2.54}$$

- Although the nonlinear force applied to the reference sector depends on the DOFs of this sector as well as the DOFs of other sectors of the assembly - as it is the case for underplatform friction dampers which straddle consecutive sectors – it can be expressed as a function of the motion of the reference DOFs only.

- The matrices $\underline{\mathbf{M}}^q$, $\underline{\mathbf{K}}^q$ and $\underline{\mathbf{C}}^q$ appearing in the definition of the matrices $\underline{\mathbf{\Lambda}}_k^q$ are complex, and they represent the structural matrices associated to the modes of vibrations of the reference sector when the response of the complete structure exhibits a spatial

cyclicity of order q. Since the complete structure features n_s sectors, the maximum value of q is $n_s - 1$.

The set of equations (2.52) is best understood by realizing that the nonlinear response of the complete structure is actually approximated by a finite series of linear responses. The set of nonlinear equations (2.52) is indeed made of n_h coupled linear systems, where each linear system corresponds to the equations of motion of the reference sector when the complete cyclic structure is subject to a mono-harmonic traveling wave. The nonlinearity of the complete set of equations stems from the coupling of the solutions of these linear systems by the nonlinear force.

For instance, for the linear system associated to $k = 1$, the structure is subject to a rotating, mono-harmonic traveling wave of spatial cyclicity e_0, or, in other words, the structure is subject to a rotating wave made of the spatial harmonic e_o only. The response of the structure is therefore a traveling wave of same characteristics, i.e., it features the spatial harmonic e_o only. This response is obtained for the reference sector – from which the response over all the assembly can be deduced – by selecting the structural matrices $\underline{\mathbf{M}}^1$, $\underline{\mathbf{K}}^1$, and $\underline{\mathbf{C}}^1$ which correspond to the modes of vibrations with one nodal diameter.

As long as the inequality $ke_o < n_s$ is verified, the spatial harmonic of the response matches exactly the spatial harmonic of the traveling excitation. However, when $ke_o \geq n_s$, the response of the structure cannot exhibit a spatial cyclicity of ke_o, since it is made of n_s sectors. Instead, the response of the structure exhibits a spatial harmonic $q(k, e_o)$, where $q(k, e_o)$ is defined in Eq. (2.53). Eq. (2.53) is of course also valid when ke_o is lower than n_s.

Since the spatial harmonic waves of the excitation are each associated to a temporal harmonic of the forcing applied to the reference sector, Eq. (2.53) can therefore be understood as the relation between the temporal harmonics of the linear and nonlinear forces

applied to the reference sector, and the spatial harmonics present in the response of the complete structure. This relation is illustrated in Table 2.1 for a 13-sector cyclic structure.

One should also note that although the linear excitation $\mathbf{f}_l^0(t)$ is approximated by a relatively low number of harmonics – less than 3 in general –, the nonlinear force $\mathbf{f}_{nl}^0[\mathbf{x}^0](t)$ has usually a much richer harmonic content. As a consequence, the number of spatial harmonics which are present in the response of the structure is in most cases not limited by the number of temporal harmonics, and it is determined by e_o and n_s only. For instance, considering a 160-sector assembly subject to a force featuring 64 nodal diameters, the only spatial harmonics potentially present are: 0, 32, 64, 128, and 96.

2.4 Solution method

As mentioned above, the equations of motion of both cyclic and non-cyclic structures are governed by a set of n_h similar matrix equations. They can also be written in real form and combined into a single nonlinear matrix equation, so that the harmonic coefficients that describe the dynamics of the system are solution of a nonlinear function $\mathbf{F}$, defined as

$$\mathbf{F}(\mathbf{u}) = \mathbf{\Lambda}\mathbf{u} - \mathbf{f} - \mathbf{f}_{nl}(\mathbf{u}), \tag{2.55}$$

where $\mathbf{u}$ consists of the harmonic cosine and sine coefficients of the motion of all or part of the nonlinear DOFs of the structure (depending on whether it is cyclic or not).

2.4.1 Hybrid Frequency-Time domain method

The nonlinear equation $\mathbf{F}(\mathbf{u}) = \mathbf{0}$ is solved using a nonlinear solver based on an implementation of the hybrid Powell algorithm [107] proposed by Garbow *et al*[108] . Given an initial approximation $\mathbf{u}^{(0)}$ of the solution, this algorithm generates successive estimations $\mathbf{u}^{(1)}$, $\mathbf{u}^{(2)}$, ..., $\mathbf{u}^{(m)}$, until satisfactory convergence of this series towards the

solution is detected. This algorithm requires one to evaluate the nonlinear function $\mathbf{F}$ and its jacobian $\mathbf{J}$ for any input motion $\mathbf{u}$.

In the Hybrid Frequency-Time domain method, this evaluation is performed by applying, to the displacement and the nonlinear force, alternate transformations from the frequency domain to the time domain. Its principal steps are outlined as follows:

1. Inverse Fast Fourier Transforms are applied to the harmonic coefficients stored in $\mathbf{u}$, so as to obtain the periodic time histories of the motion of the nonlinear DOFs of the structure.

2. The time histories of the nonlinear forces resulting from this imposed displacement are calculated.

3. Fast Fourier Transforms are applied to the time histories of the nonlinear forces, and they yield the harmonic coefficients stored in $\mathbf{f}_{nl}(\mathbf{u})$.

4. $\mathbf{F}(\mathbf{u})$ is evaluated according to Eq. (2.55).

The advantage of the HFT method is that the evaluation of the nonlinear forces is performed in the time domain. Therefore, the nonlinearities associated with these forces can be calculated with a very high accuracy. Also, evaluating these forces in the time domain allows one to capture complex hysteretic nonlinearities, such as the stick/slip behavior of friction dampers.

As a consequence, the accuracy of the HFT method is only limited by (1) the number of harmonics used in the HBM to generate the equations of motion, and (2), the ability of the nonlinear solver to converge towards the solution.

2.4.2 Structures with multiple frictional interfaces

For structures featuring several frictional interfaces, that is, non-cyclic structures with several friction dampers attached, or cyclic structures which feature more than one friction damper per sector, the jacobian of Eq. (2.55) can be computed in a very efficient way. Mistuned bladed disks are examples of such structures: since they do not satisfy the cyclic symmetry hypothesis, their dynamics cannot be deduced from the study of one sector only, and therefore their analysis must consider the complete assembly and all the friction dampers.

For such systems, the components of $\mathbf{u}$ can be ordered as:

$$\mathbf{u} = \left\{ \mathbf{u}^{1^T}, \ldots, \mathbf{u}^{n_d^T} \right\}^T, \tag{2.56}$$

where $\mathbf{u}^p$ consists of the cosine and sine harmonic coefficients of the nonlinear DOFs corresponding to the p-th friction damper, that is:

$$\mathbf{u}^p = \left\{ \mathbf{u}_0^{p^T}, \mathbf{u}_{1,c}^{p^T}, \mathbf{u}_{1,s}^{p^T}, \ldots, \mathbf{u}_{n_h,c}^{p^T}, \mathbf{u}_{n_h,s}^{p^T} \right\}^T. \tag{2.57}$$

Since the nonlinear friction forces exerted by the dampers depend on the motion of the corresponding frictional interfaces only, $\mathbf{f}_{nl}$ is expressed as:

$$\mathbf{f}_{nl}(\mathbf{u}) = \left\{ \mathbf{f}_{nl}^{1^T}(\mathbf{u}^1), \ldots, \mathbf{f}_{nl}^{n_d{}^T}(\mathbf{u}^{n_d}) \right\}^T. \tag{2.58}$$

Thus, the jacobian of the nonlinear function $\mathbf{F}$ is given by:

$$\mathbf{J} = \mathbf{\Lambda} - \mathbf{BDiag}\left[\mathbf{J}^1, \ldots, \mathbf{J}^{n_d} \right], \tag{2.59}$$

where

$$\mathbf{J}^p = \frac{\partial \mathbf{f}_{nl}^p(\mathbf{u}^p)}{\partial \mathbf{u}^p}. \tag{2.60}$$

$\mathbf{\Lambda}$ is the linear part of the jacobian. As observed in the derivation of the equations of motion obtained by the harmonic balance method, it depends only on the structural matrices and the frequency of excitation ω.

Therefore, when Eq. (2.55) is solved for a given frequency, $\mathbf{\Lambda}$ can be computed once and for all at the beginning of the solution process. If the nonlinear solver needs a new estimate of the jacobian as it converges towards the solution, $\mathbf{\Lambda}$ does not need to be recalculated, and only a new, simple evaluation of the blocks $\mathbf{J}^p$ is necessary. These blocks are easily calculated by finite differences with successive evaluations of the nonlinear functions $\mathbf{f}_{nl}^p$.

Thus, when n_d is very large, namely, when the structure features a large number of independent frictional interfaces, $\mathbf{J}$ is obtained in a very efficient fashion that does not penalize, in terms of CPU time, the solving of the nonlinear function $\mathbf{F}$.

The algorithm used for the HFT method is summarized in Fig. 2.3.

2.5 Time-domain analysis of nonlinear forces

The Hybrid Frequency-Time domain method is well suited for the analysis of structures featuring displacement-based nonlinear forces, such as the hysteretic forces produced at the structure interfaces which are subject to friction. The method's only requirement is that it must be possible to calculate these nonlinear forces for any type of periodic displacement of the structure DOFs, since the HFT method is based on the iterative generation of approximations of the correct periodic motion of the structure. In other words, one must be able to model these nonlinearities as nonlinear operators that act on the time-domain periodic waveforms of the DOFs of the structure, and that produce a time-domain periodic waveform of the corresponding nonlinear forces.

A consequence of this approach is that in the case of friction dampers for instance, the dampers can be modeled by a set of simple numerical parameters which define their stiffness, the friction coefficient and the contact pressure they have at their interface with the structure. In this approach it is not necessary to include a finite element representation

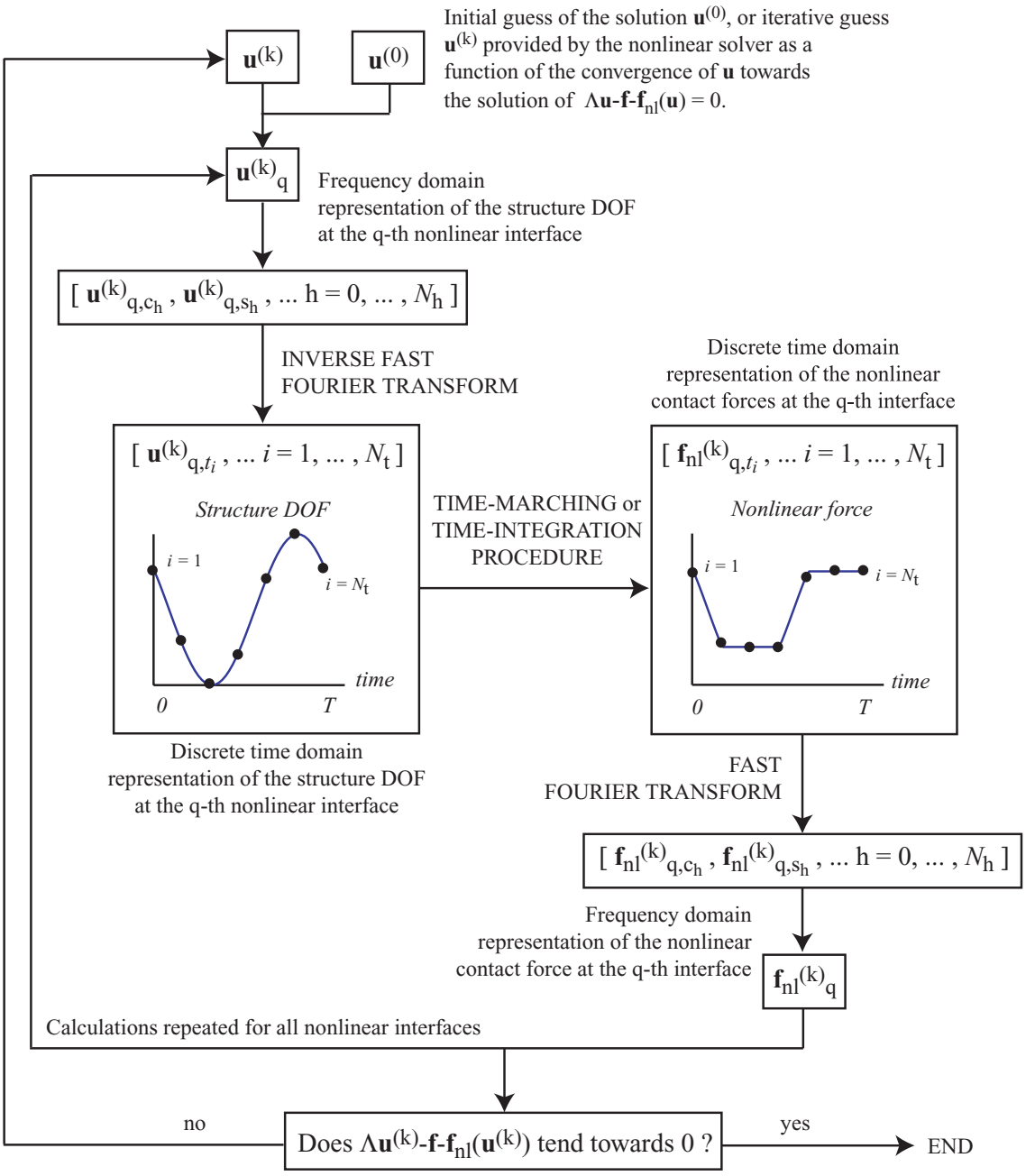

Figure 2.3: Algorithm of the Hybrid Frequency-Time domain method. The parameters of the method are the total number of harmonics N_h used to approximate the forced response of the structure, and the number of sample points in the time domain N_t. A real representation of the nonlinear quantities is used here: for instance, $\mathbf{u}^k_{q,c_h}$ corresponds to the cosine components of the h-th harmonic of the DOFs of the q-th contact interface, for the k-th guess generated by the nonlinear solver.

of the damper alongside with that of the structure in the nonlinear analysis. However, one should note that usually the numerical parameters defining the friction dampers characteristics are derived from independent, stand-alone analysis based on such FE models.

Another consequence of this approach is that the DOFs associated to the dampers do not need to be part of the set of nonlinear equations of the friction-damped structure. The complete structure-damper interface is usually described by two geometric points: the first one corresponds to the exact position of the contact point between the damper and the structure, while the second one is usually part of the finite element definition of the structure. With the exception of particular friction configurations, these two points do not always coincide in space when the structure-damper assembly responds to an external forcing, as the relative motion of the damper and the structure creates the frictional phenomena. However, since the order of magnitude of the relative displacement of the damper with respect to the structure is small (with respect to the typical mesh size of a finite element model), one can make the reasonable assumption that the nonlinear contact forces applied by the damper to the structure can be localized to that very point defined in the FE model. Therefore, the displacement in space of the actual contact point is not a quantity that explicitly appears in the set of nonlinear, frequency-domain equations of the system. It is instead a quantity that is calculated in the time domain to help create the time domain representation of the contact forces.

Depending on the type of nonlinear interaction modeled, the time domain calculation of these forces can be performed in two ways: for simple models of nonlinear forces, (e.g., simple models of friction dampers) a fast time-marching procedure can be used, whereas more complicated nonlinear interactions (such as those produced by friction damper models with complex contact kinematics) require a time-integration procedure to calculate the corresponding nonlinear forces.

2.5.1 Time-marching procedure

The simplest models of hysteretic friction dampers correspond to those that assume that the relative motion at the friction interface is rectilinear (1-D), and that the normal contact force between the damper and the rest of the structure is constant. Figure 2.4 depicts such a damper.

A time marching procedure is a very effective way of calculating the contact efforts for this type of damper. Following the classic Coulomb friction law, the damper can have only two distinct states:

1. *Stick state*. In this state there is no relative motion between the damper and the structure, and the contact force and DOFs verify

$$T = -kx_d, \tag{2.61}$$

$$\|T\| \leq \mu N, \tag{2.62}$$

and

$$\dot{x}_d = \dot{x}_s, \tag{2.63}$$

where x_d represents the position of the contact point, and x_s is the nonlinear DOF of the structure.

2. *Slip state*. In this state the tangential force applied by the damper to the structure is

$$T = -\mu N \quad \text{if} \quad \dot{x}_s > 0 \quad \text{or} \quad T = \mu N \quad \text{if} \quad \dot{x}_s < 0, \tag{2.64}$$

and the position of the contact point satisfy

$$x_d = \mu N/k \quad \text{if} \quad \dot{x}_s > 0 \quad \text{or} \quad x_d = -\mu N/k \quad \text{if} \quad \dot{x}_s < 0. \tag{2.65}$$

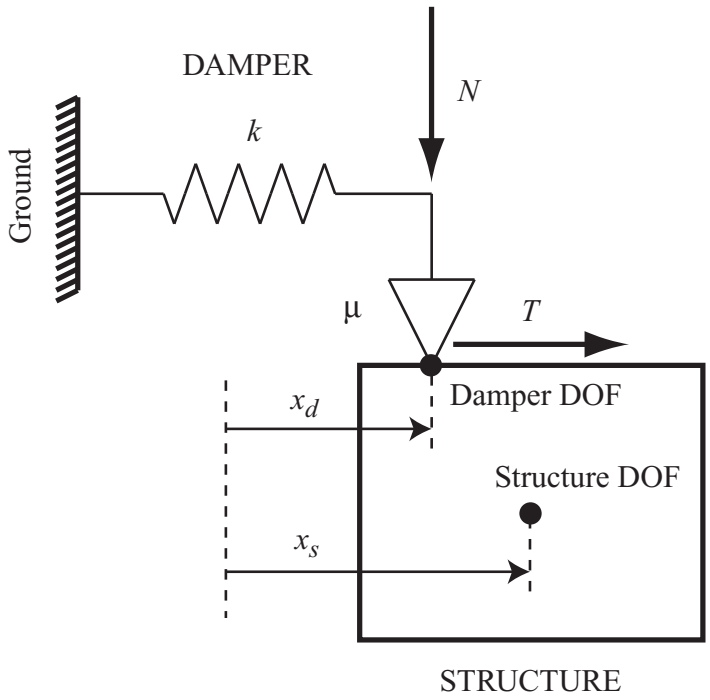

Figure 2.4: Simple model of a hysteretic friction damper. The friction is defined here as being mono-directional, with a constant normal load N. The damper is characterized by its stiffness k and by the friction coefficient μ. The tangential contact effort applied by the damper to the structure is T.

In addition to these two states, the behavior of the damper is also characterized by the mathematical conditions that describe the transitions between these states. Again, these transition criteria are simply derived from the laws of Coulomb friction:

1. *Stick-slip transition*. This type of transition occurs when the following conditions are met:

$$x_d = \mu N/k \quad \text{and} \quad \dot{x}_s > 0, \tag{2.66}$$

or

$$x_d = -\mu N/k \quad \text{and} \quad \dot{x}_s < 0, \tag{2.67}$$

according to the direction of the relative motion between the damper and the structure.

2. *slip-stick transition*. This type of transition occurs when the damper is in the slip state and the structure DOF reverts its direction of motion:

$$x_d = \mu N, \quad \dot{x}_s = 0 \quad \text{and} \quad \ddot{x}_s < 0, \tag{2.68}$$

or

$$x_d = -\mu N, \quad \dot{x}_s = 0 \quad \text{and} \quad \ddot{x}_s > 0. \tag{2.69}$$

Now, assuming that the entire period waveform of the guessed nonlinear displacement $x_s(t_1), \ldots, x_s(t_{N_T})$, is available – in other words, when the nonlinear solver calculates a new approximate solution and when this guessed solution is transported into the time domain by discrete fast Fourier transforms – the friction force can be iteratively evaluated as follows:

1. *Choice of initial conditions*. For the first iteration at $t = t_1$, the initial conditions regarding the state of the damper must be selected. Selecting the position of the

damper such as $x_d = 0$ and assuming that the damper is in the stick state ensures that the friction laws are satisfied and that the initial tangential effort is zero.

2. *Procedure for the* i-th *step*, $i > 1$. One assumes that between the time steps t_{i-1} and t_i the damper is in the stick state (irrespectively of its actual state at t_{i-1}). This means that if this assumption is valid the position of the damper at t_i should be

$$x_d(t_i) = x_d(t_{i-1}) + (x_s(t_i) - x_s(t_{i-1})), \tag{2.70}$$

since in the stick state the damper follows the displacement of the structure. Now, a simple examination of the value of the tangential force $kx_d(t_i)$ helps assess the validity of the initial assumption:

- If $\|kx(t_i)\| > \mu N$, then the assumption was not valid, and therefore the damper is in the slip state at t_i, and the displacement and force values are:

$$x_d(t_i) = \mu N/k \quad \text{and} \quad T(t_i) = -\mu N \quad \text{if} \quad x_s(t_i) > x_s(t_{i-1}), \tag{2.71}$$

or

$$x_d(t_i) = -\mu N/k \quad \text{and} \quad T(t_i) = \mu N \quad \text{if} \quad x_s(t_i) < x_s(t_{i-1}). \tag{2.72}$$

- If $\|kx(t_i)\| \leq \mu N$, then the assumption was valid, and the contact force is defined by:

$$T(t_i) = -kx_d(t_i). \tag{2.73}$$

3. *Repeat until a steady state is reached by the damper DOF*. This time marching procedure needs to be repeated until at most the $2N_t$-th step (that is, over at most two periods of the excitation applied to the structure), or until the displacement of the damper DOF (and therefore the contact force) reaches a periodic state.

This time-marching procedure takes advantage of the simple form of the state and transition equations to substitute the integration of the equations of motion of the damper by a simple analysis of the contact force and of the direction of motion of the DOF of the structure, a substitution which is only made possible by the 1-D character of the relative motion between the damper and the structure. The calculation of the contact effort is therefore extremely fast and efficient, a noteworthy advantage when, for instance, the analysis of complex structures with a large number of dampers attached is performed[2].

2.5.2 Time-integration procedure

When the models of dampers are more elaborate, the calculation of the contact efforts in the time domain needs to follow a less simplified time-integration procedure. In general, the absence of a known direction of friction (in the case of contact not restricted to a 1-D relative motion of the structure and the damper), or the presence of a variable normal contact load (produced by the normal component of the displacement of the structure) makes the motion of the contact point difficult to analyze with a simple time-marching procedure. Instead, the exact state equations describing the behavior of the damper need to be carefully integrated, while monitoring the mathematical transition criteria between these states.

The need for a precise integration of the equations of motion (as well as the need for an accurate evaluation of the mathematical criteria governing the state transitions) means that the discrete, time domain representation $[\mathbf{u}_{q,t_i}^{(k)}, i = 1, \ldots, N_t]$ of the nonlinear interface

[2]Two precautions need to be taken with this method. The first one is that the size of the step in the time domain should be small enough to prevent the occurrence of two state transitions or more between two consecutive points in time. Selecting a high value for N_t, such as 512 or 1024 is usually more than enough to avoid this rare problem. The second one concerns the calculation of the contact effort when the damper is always stuck and do not slip. In this case, the initial conditions presented here lead to a contact force which is not centered on 0 – that is, the Fourier transform of the force exhibits on a non-zero constant coefficient. In this case, the constant Fourier coefficient can be forced to zero before forming the set of nonlinear equations in the frequency domain.

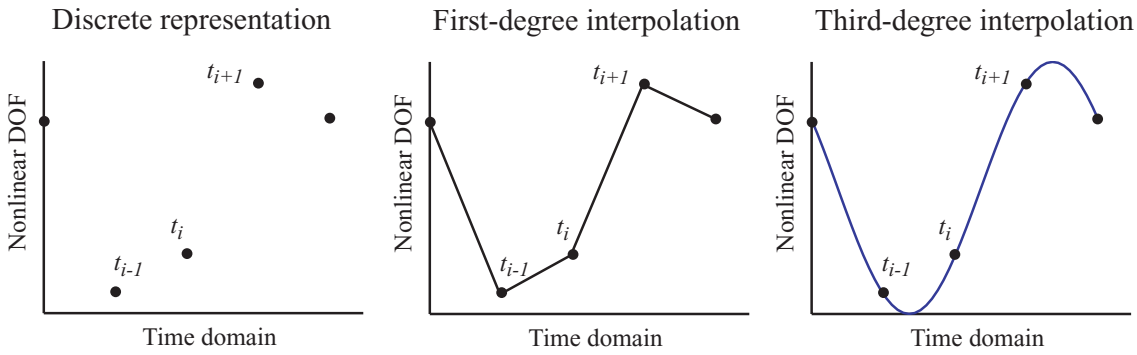

Figure 2.5: Examples of polynomial interpolation of the discrete values provided by the nonlinear solver to represent the time-domain, periodic waveforms of the nonlinear DOFs of the structure. The advantage of a third degree polynomial interpolation of these discrete values is the ability to represent their derivative as a smooth, continuous function over the entire period of motion.

DOFs presented in Fig. 2.3 is no longer adapted. More often than not, the integration of the equations of motion requires a step size much smaller than the time increment used by the Fourier transforms. Moreover, the fact that the state transitions usually occur at times different than the N_t fixed sample points used in these transforms mean than a different approach is required.

This need for precision can however be achieved by substituting the discrete representation $[\mathbf{u}_{q,t_i}^{(k)}, i = 1, \ldots, N_t]$ of the nonlinear structure DOFs by an equivalent interpolation function, so that $\mathbf{u}_q^{(k)}(t)$ can be evaluated for any time $0 < t < 2\pi/\omega$, where ω is the period of the excitation applied to the structure. As seen on Fig. 2.5, a simple third degree polynomial approximation of the discrete values provided by the nonlinear solver ensures a smooth and continuous representation of their first derivative over the entire period of motion. This important characteristic makes the numerical and computational analysis of the equations of motion of the damper much easier to handle.

The general case of a damper that models a three-dimensional (3-D) friction interface illustrates the principles of such a time-integration analysis. Figure 2.6 depicts such a 3-D

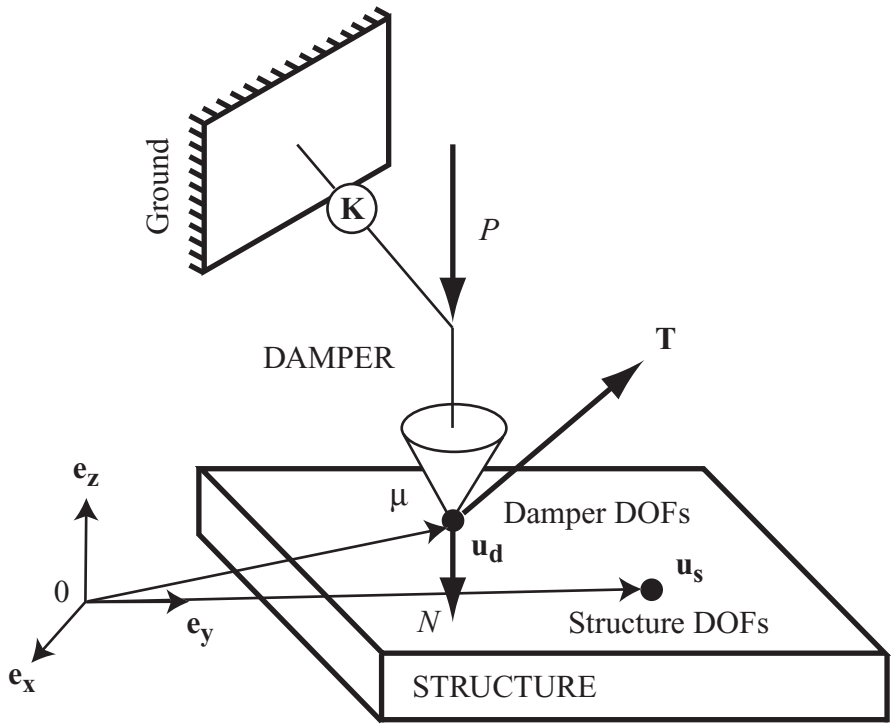

Figure 2.6: Model of 3-D friction damper. The damper is characterized by a 3-by-3 stiffness matrix $\mathbf{K}$, a constant normal load P and a friction coefficient μ. The forces transmitted to the structure by the damper are the variable normal contact force N, which is a function of the motion of the damper and of P, and the tangential component $\mathbf{T}$. The motion of the contact point is described by $\mathbf{u_d} = (x_d, y_d, z_d)$, while the motion of the structure is represented by $\mathbf{u_s} = (x_s, y_s, z_s)$.

friction damper and its interaction with the structure. The position of the contact point ($\mathbf{u_d}$), and the position of the node of the FE model of the structure at which the contact forces are applied ($\mathbf{u_s}$) are described by three coordinates each. This allows for the most general relation between the damper and the structure: the tangential friction forces are within a plane of constant orientation, and the normal load varies – and possibly vanishes if the damper separates from the structure.

Considering the reference frame $(0, \mathbf{e_x}, \mathbf{e_y}, \mathbf{e_z})$, this friction interface is fully described by:

- The displacement of the contact point: $\mathbf{u_d} = (x_d, y_d, z_d)$,

- The displacement of the node of the structure: $\mathbf{u_s} = (x_s, y_s, z_s)$,
- The contact forces applied by the damper to the structure: $\mathbf{F_{nl}} = (T_x, T_y, N)$,
- The constant load that represents the centrifugal effects (or any other constant force) applied to the damper: $\mathbf{P} = (0, 0, P)$,
- The friction coefficient μ,
- The stiffness matrix of the damper:

$$\mathbf{K} = \begin{bmatrix} k_{xx} & k_{xy} & k_{xz} \\ k_{xy} & k_{yy} & k_{yz} \\ k_{xz} & k_{yz} & k_{zz} \end{bmatrix}. \tag{2.74}$$

Although the general form of $\mathbf{K}$ is presented here, it has been noted by Cho and Barber [109, 110] that many stability problems occur when the tangential and normal components of the motion of the contact point are coupled through the corresponding terms of the stiffness matrix. In particular, the unicity of the response of the damper for a given input displacement of the structure is not always guaranteed. This can lead to serious numerical difficulties when analyzing the response of the damper, and it is therefore preferable to describe the damper by a simplified stiffness matrix where normal and tangential components are decoupled:

$$\mathbf{K} = \begin{bmatrix} k_{xx} & k_{xy} & 0 \\ k_{xy} & k_{yy} & 0 \\ 0 & 0 & k_{zz} \end{bmatrix}. \tag{2.75}$$

Depending on the motion of the structure, the damper can be in three distinct states: stick, slip, and separation. These states are governed by the following equations:

- *Stick state*. In this state the motion of the damper follows the motion of the structure, which means that

$$\dot{x}_d = \dot{x}_s, \tag{2.76}$$

$$\dot{y}_d = \dot{y}_s, \tag{2.77}$$

$$z_d = z_s, \tag{2.78}$$

and the contact forces applied to the structure are given by:

$$T_x = -k_{xx}x_d - k_{xy}y_d, \tag{2.79}$$

$$T_y = -k_{xy}x_d - k_{yy}y_d, \tag{2.80}$$

$$N = -k_{zz}z_d + P. \tag{2.81}$$

- *Slip state*. In the slip state, the normal contact load applied to the structure as well as the normal component of the motion of the damper are governed by the same equations as in the stick state:

$$z_d = z_s, \tag{2.82}$$

$$N = -k_{zz}z_d + P. \tag{2.83}$$

The direction of the tangential contact force is dictated by the relative slip motion of the damper and the structure, while its norm is a function of the normal load. The state equation for the tangential component of the motion of the damper is an algebraic differential equation that expresses the quasi-static equilibrium of the damper:

$$\begin{bmatrix} k_{xx} & k_{xy} \\ k_{xy} & k_{yy} \end{bmatrix} \begin{bmatrix} x_d \\ y_d \end{bmatrix} = -\frac{\mu N}{\sqrt{(\dot{x}_d - \dot{x}_s)^2 + (\dot{y}_d - \dot{y}_s)^2}} \begin{bmatrix} \dot{x}_d - \dot{x}_s \\ \dot{y}_d - \dot{y}_s \end{bmatrix}, \tag{2.84}$$

which simply indicates that the restoring force due do the stiffness of the damper is equal (in norm) to the normal contact force and opposed (in direction) to the relative slip between the damper and the structure. Finally, the tangential forces applied by the damper to the structure are expressed as in the stick state:

$$T_x = -k_{xx}x_d - k_{xy}y_d, \tag{2.85}$$

$$T_y = -k_{xy}x_d - k_{yy}y_d. \tag{2.86}$$

- *Separation state*. When the damper and the structure are no longer in contact, the state equations are trivially written as:

$$x_d = 0, \tag{2.87}$$

$$y_d = 0, \tag{2.88}$$

$$z_d = P/k_{zz}, \tag{2.89}$$

$$\tag{2.90}$$

and the contact forces are

$$T_x = 0, \tag{2.91}$$

$$T_y = 0, \tag{2.92}$$

$$N = 0. \tag{2.93}$$

The description of this 3-D model of damper is completed by the criteria that describe the mathematical conditions required for a state transition. There are six possible transitions: separation-to-stick, separation-to-slip, stick-to-slip, stick-to-separation, slip-to-stick and slip-to-separation:

- *separation-to-stick transition*. This transition is characterized by the fact that normal

contact between the damper and the platform resumes in a sustained fashion, that is,

$$z_s = P/k_{zz} \quad \text{and} \quad \dot{z}_s > 0. \tag{2.94}$$

These conditions are necessary but not sufficient to validate the separation-to-stick transition: additionally, in order to maintain successfully the stick state at the moment of transition, it is also necessary to compare the relative rate of increase of both the tangential and normal components of the contact force, which is expressed by the condition

$$\mu \frac{\mathrm{d}}{\mathrm{d}t}\|N\| > \frac{\mathrm{d}}{\mathrm{d}t}\|\mathbf{T}\| \quad \text{at the instant of transition,} \tag{2.95}$$

where the derivatives of $\|N\|$ and $\|\mathbf{T}\|$ are calculated using the stick state assumption.

- *separation-to-slip transition*. This transition is also characterized by the fact that normal contact resumes in a sustained fashion

$$z_s = P/k_{zz} \quad \text{and} \quad \dot{z}_s > 0, \tag{2.96}$$

but this time the rate of increase of the norm of the tangential force (assuming a stick state) should be greater than that of the norm of the normal force times μ:

$$\mu \frac{\mathrm{d}}{\mathrm{d}t}\|N\| \leq \frac{\mathrm{d}}{\mathrm{d}t}\|\mathbf{T}\| \quad \text{at the instant of transition,} \tag{2.97}$$

where the derivatives of $\|N\|$ and $\|\mathbf{T}\|$ are calculated using the stick state assumption.

- *stick-to-slip transition*. The stick-to-slip transition is reached when the norm of the tangential contact force equals the norm of the normal force times μ (and tends to

exceed it immediately after the transition time), which translates into these conditions:

$$\mu|N| = \|\mathbf{T}\| \quad \text{and} \quad \mu\frac{\mathrm{d}}{\mathrm{d}t}\|N\| < \frac{\mathrm{d}}{\mathrm{d}t}\|\mathbf{T}\| \quad \text{at the instant of transition,} \tag{2.98}$$

where the derivatives of $\|N\|$ and $\|\mathbf{T}\|$ are calculated using the stick state assumption.

- *stick-to-separation transition*. The stick-to-separation transition occurs when there is a sustained loss of contact between the damper and the structure, and this transition can be described by the following equations:

$$z_s = P/k_{zz} \quad \text{and} \quad \dot{z}_s < 0. \tag{2.99}$$

- *slip-to-stick transition*. The slip-to-stick transition occurs when the relative speed velocity of the contact point with respect to the structure vanishes:

$$\dot{x}_d = \dot{x}_s \quad \text{and} \quad \dot{y}_d = \dot{y}_s. \tag{2.100}$$

Additionally, the normal and tangential components of the contact force must verify a condition stating that it is impossible for the damper to resume slipping:

$$\mu\frac{\mathrm{d}}{\mathrm{d}t}\|N\| > \frac{\mathrm{d}}{\mathrm{d}t}\|\mathbf{T}\| \quad \text{at the instant of transition.} \tag{2.101}$$

- *slip-to-separation transition*. The slip-to-separation transition is identical to the stick-to-separation transition:

$$z_s = P/k_{zz} \quad \text{and} \quad \dot{z}_s < 0. \tag{2.102}$$

The calculation of the contact force applied by the damper to the structure can be performed by carefully integrating the state equations described above, while monitoring

all the possible transition criteria. The resulting numerical algorithm that performs such a calculation can become very complicated, as great care need to be taken regarding the appropriate detection of the transitions. This is true in particular for Eq. 2.84, which is a set of algebraic differential equations for x_d and y_d representing the motion of the contact point in the slip state. After each state transition, the proper initial conditions for the integration of the equations of motion corresponding to the next state need also to be precisely determined. The integration of the equations of motion needs to be done – just as in the case of a time-marching procedure – over several periods of motion, until the steady state of the damper is reached.

This time-integration approach is very effective to analyze the behavior of particularly complicated models of dampers. It is however computationally more demanding than the simpler time-marching procedure.

2.5.3 Damper models

The time-marching and time-integration procedures described in the previous sections can be applied to model many different types of nonlinear forces. Table 2.2 lists example damper models that have been modeled using one of these approaches. Although the previous section illustrates the time-domain methods for models of dampers that connect the ground to the structure, models of dampers that interact with two elastic structures (or two components of the same elastic structure) can be easily deduced from these ground-to-structure damper models, by considering the relative displacement of the structure DOFs instead of their absolute values.

2.5.4 Special case of cyclic symmetry

When modeling friction dampers that act on cyclic assemblies, a special situation arises when these dampers straddle two adjacent cyclic sectors of such structures, as shown on

Model of damper	**Time-domain procedure**
1-D, ground-to-structure cubic spring	Time-marching procedure
1-D, structure-to-structure cubic spring for cyclic or non-cyclic structures	Time-marching procedure
1-D, ground-to-structure linear spring stop with gap	Time-marching procedure
1-D, structure-to-structure linear spring stop with gap for cyclic or non-cyclic structures	Time-marching procedure
1-D, ground-to-structure friction damper with constant normal load	Time-marching procedure
1-D, structure-to-structure friction damper with constant normal load, for cyclic or non-cyclic structures	Time-marching procedure
1-D, ground-to-structure friction damper with variable normal load	Time-marching procedure or time-integration procedure
1-D, structure-to-structure friction damper with variable normal load, for cyclic or non-cyclic structures	Time-marching procedure or time-integration procedure
3-D, ground-to-structure friction damper with variable normal load	Time-integration procedure
3-D, structure-to-structure friction damper with variable normal load, for cyclic or non-cyclic structures	Time-integration procedure

Table 2.2: List of damper models and other nonlinear forces that can be analyzed with the methodology presented in this chapter. This list could be easily extended to include many other displacement-dependent nonlinearities, such as for instance linear or nonlinear dashpots.

Fig. 2.7. This configuration is typical of bladed disk assemblies which feature under-platform friction dampers: friction dampers of the same physical characteristics are appended to the bladed disk, and therefore the overall cyclic symmetry of the system is preserved. As a consequence, the theoretical results obtained in section 2.3 are still valid, that is, the forced response of the entire cyclic structure can be deduced from the study of the reference cyclic sector.

This also means that the nonlinear forces acting on the structure can only be derived from the motion of the nonlinear DOFs that belong to the reference sector, since only these DOFs are featured in the set of nonlinear equations that govern the forced response

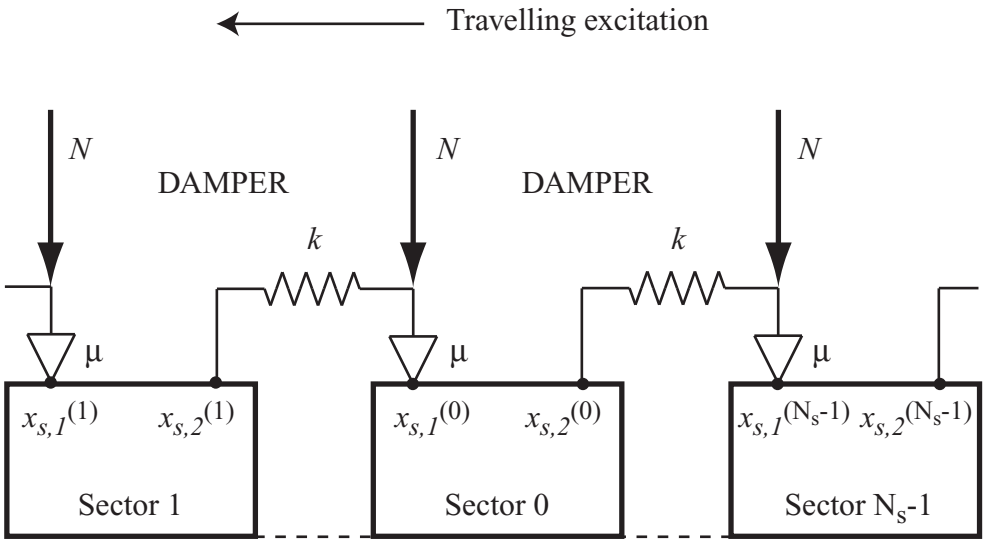

Figure 2.7: Simplified representation of a cyclic structure which features friction dampers straddling adjacent sectors of the assembly. Since all the the dampers have the same characteristics, the cyclic symmetry of the system is preserved. The cyclic sectors may or may not be elastically coupled – the later case being typical of an industrial bladed disk structure.

of the full assembly. In the simple example shown in Fig. 2.7, which features a series of 1D, structure-to-structure dampers with constant normal load, each cyclic sector has only two nonlinear DOFs. Let $x_{s,1}^{(0)}$ and $x_{s,2}^{(0)}$ represent the two nonlinear DOFs associated to the reference sector, and let $f_{nl,1}^{(0)}$ and $f_{nl,2}^{(0)}$ denote the respective nonlinear contact forces applied by the dampers. Because of the geometry of the assembly, $f_{nl,1}^{(0)}$ is obviously a function of the displacement of the two nonlinear DOFs $x_{s,1}^{(0)}$ and $x_{s,2}^{(1)}$. Now, using the phase property obtained in section 2.3, the following relations can be written:

$$f_{nl,2}^{(1)}(t) = f_{nl,2}^{(0)}(t - \phi_t), \quad \text{and} \tag{2.103}$$

$$x_{s,2}^{(1)}(t) = x_{s,2}^{(0)}(t - \phi_t). \tag{2.104}$$

Therefore, the nonlinear force $f_{nl,1}^{(0)}$(t) can be deduced from $x_{s,1}^{(0)}(t)$ and $x_{s,2}^{(0)}(t - \phi_t)$, that is, from two quantities directly derived from the information available for the reference sector of the cyclic assembly. These calculations of the nonlinear forces can be made

by a time-marching or time-integration procedure similar to that used for the non-cyclic systems. The workflow of the HFT method is therefore slightly altered to take into account this particular property of structures with cyclic symmetry:

1. A guess of the Fourier coefficients of the nonlinear DOFs $x_{s,1}^{(0)}$ and $x_{s,2}^{(0)}$ is provided by the nonlinear solver.

2. Inverse Fast Fourier transforms are applied to these coefficients to calculate the time domain, periodic waveforms of the displacement of $x_{s,1}^{(0)}$ and $x_{s,2}^{(0)}$ over a period of motion.

3. The periodic waveform of $x_{s,2}^{(0)}$ is shifted in time with a phase ϕ_t so as to obtain the periodic waveform of $x_{s,2}^{(1)}$.

4. Using a time-marching or a time-integration procedure, the time domain, periodic waveforms of the nonlinear forces $f_{nl,1}^{(0)}$ and $f_{nl,2}^{(1)}$ are deduced from that of $x_{s,2}^{(1)}$ and $x_{s,1}^{(0)}$.

5. The periodic waveform of $f_{nl,2}^{(1)}$ is shifted in time with a phase $-\phi_t$ so as to obtain the periodic waveform of $f_{nl,2}^{(0)}$.

6. Fast Fourier transforms are applied to the time-domain representation of $f_{nl,1}^{(0)}$ and $f_{nl,2}^{(0)}$. The corresponding Fourier coefficients help build the set of nonlinear equations that describe the forced response of the structure, and depending on the convergence towards the solution of this system, a new guess may be provided and this algorithm starts a new iteration.

This approach can be generalized to any kind of displacement-dependent nonlinearity or friction dampers that involve nonlinear DOFs that belong to adjacent sectors of the same cyclic structure.

2.6 Conclusion

A comprehensive theoretical analysis as well as several extensions and generalizations of the Hybrid Frequency Time domain method have been presented. A new method of reduction of the equations of motion of the nonlinear DOFs of systems with friction dampers has been introduced. It allows the study of stuctures represented by reduced order-models of relatively high size. These reduced-order models feature a high number of normal modes of vibration and a large number of physical DOFs. Therefore, they offer a better approximation of the dynamics of the structure, and they are of greater interest for parametric studies aimed at optimizing the characteristics and configurations of the dampers.

Another significant extension to the HFT method was the exact derivation of the equations of motion for flexible, cyclic structures subject to linear and nonlinear, displacement-dependent forces. It allows one to take into account the elastic coupling existing between the sectors of the structure. A special relation between the temporal harmonics and the spatial harmonics of the response is exhibited.

In addition, the principles governing the modeling of friction dampers as well as the modeling of other types of displacement-dependent nonlinearities were introduced with two example of friction dampers, including one which features a 3-D contact interface. Finally, a detailed analysis of the methods allowing the calculation of the nonlinear forces in the time domain – a requirement of the HFT method – was presented.

Sample results obtained with these extensions to the HFT method are presented in the next chapter.

CHAPTER III

SELECTED RESULTS

3.1 Introduction

In this chapter, the method presented in Chapter I for the Hybrid Frequency-Time domain analysis of the forced response of elastic structures with attached friction dampers is applied to several nonlinear systems. The forced response of simple stand-alone structures, as well as the case of structures with cyclic symmetry or mistuning is considered. The models of dampers selected for these studies include simple 1-D friction dampers as well as more elaborate 3-D models that allow for variable normal load and friction with a direction that is not fixed in space. The results obtained illustrate the complicated features exhibited by the forced response of such systems. The need to approximate the dynamics of friction-damped structures with a large number of harmonics in the HFT method is evidenced by the complexity of the periodic waveforms representing the contact efforts at the structure-damper interfaces.

3.2 Forced response of a beam with a 3-D friction damper with constant normal load

The dynamics of a simple beam with an attached 3-D damper is considered in this section. The response of the system is obtained for two types of external forcing.

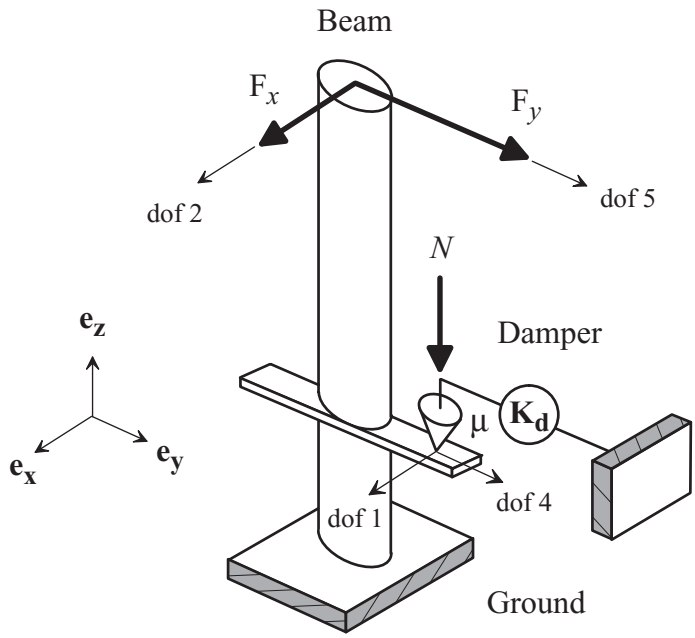

Figure 3.1: Simple beam model with a friction damper attached.

3.2.1 Model description

The friction-damped system considered is a 6-DOF, symmetric, cantilevered beam shown in Fig. 3.1. Since this model takes into account transverse vibrations in the $\mathbf{e_x}$ and $\mathbf{e_y}$ directions and ignores the normal component of the vibration of the beam, the friction point on the platform has a planar trajectory. The beam is 1.33 m long and the friction point is located at 0.318 m from the clamped end.

The first DOF of the beam is the $\mathbf{e_x}$ component of the displacement of the friction point on the platform, and the fourth one corresponds to the $\mathbf{e_y}$ component of the same point. The second and the fifth DOFs correspond to the displacement of the tip of the beam, respectively, in the $\mathbf{e_x}$ and $\mathbf{e_y}$ directions. Finally, the third and sixth DOF represent the modal coordinates associated to the first bending modes of the beam in the $\mathbf{e_x}$ and $\mathbf{e_y}$ directions. The mass, stiffness and damping properties of the beam are presented in Table 3.1.

The model of friction damper selected for this study is a simple ground-to-structure,

$$\mathbf{M} = \begin{bmatrix} 6.679 & 1.021 & 0.634 & 0 & 0 & 0 \\ 1.021 & 1.222 & 0.232 & 0 & 0 & 0 \\ 0.634 & 0.232 & 0.122 & 0 & 0 & 0 \\ 0 & 0 & 0 & 6.679 & 1.021 & 0.634 \\ 0 & 0 & 0 & 1.021 & 1.222 & 0.232 \\ 0 & 0 & 0 & 0.634 & 0.232 & 0.122 \end{bmatrix} \text{ kg.}$$

$$\mathbf{K} = 10^4 \begin{bmatrix} 443 & -37.7 & 0 & 0 & 0 & 0 \\ -37.7 & 6.96 & 0 & 0 & 0 & 0 \\ 0 & 0 & 18.5 & 0 & 0 & 0 \\ 0 & 0 & 0 & 443 & -37.7 & 0 \\ 0 & 0 & 0 & -37.7 & 6.96 & 0 \\ 0 & 0 & 0 & 0 & 0 & 18.5 \end{bmatrix} \text{ N.m}^{-1}.$$

$$\mathbf{C} = \alpha\mathbf{K} + \beta\mathbf{M}, \quad \text{where} \quad \alpha = 2.6 \cdot 10^{-5} \text{ s and } \beta = 7.49 \text{ s}^{-1}.$$

Table 3.1: Mass, stiffness and damping matrices of the beam studied in section 3.2.

3-D model where the normal load is constant, due to the absence of normal DOFs in the model of the beam. The coefficient of friction of the contact interface is $\mu = 1$, and the normal load ensuring contact between the damper and the platform of the beam is $N = 250$ N. The stiffness matrix of the damper is

$$[K] = \begin{bmatrix} 2.0 \cdot 10^7 & 0 \\ 0 & 2.0 \cdot 10^7 \end{bmatrix} \text{ N.m}^{-1}.$$

3.2.2 First case study

For this first case, the excitation applied to the beam is chosen so as to produce a true two-dimensional motion of the beam:

$$F_x = 20 \text{ N}$$

$$F_y = 15 \text{ N}$$

The results of this calculation are presented in Figs. 3.2, 3.3, 3.4, and 3.5, which depict the frequency response of the beam at the tip and damper locations, along the $\mathbf{e_x}$ and $\mathbf{e_y}$

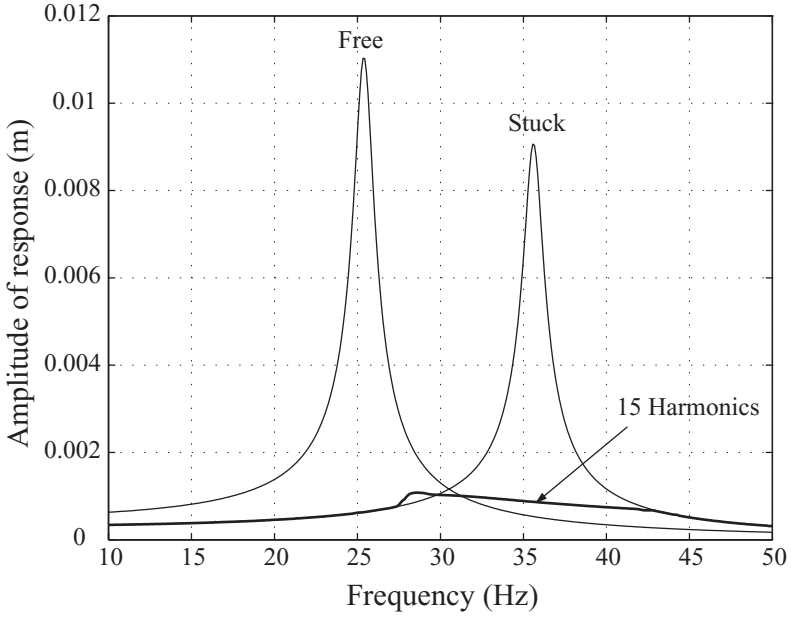

Figure 3.2: Free, stuck and stick-slip forced responses of the $\mathbf{e_x}$ component of the tip of the beam, in the first case study.

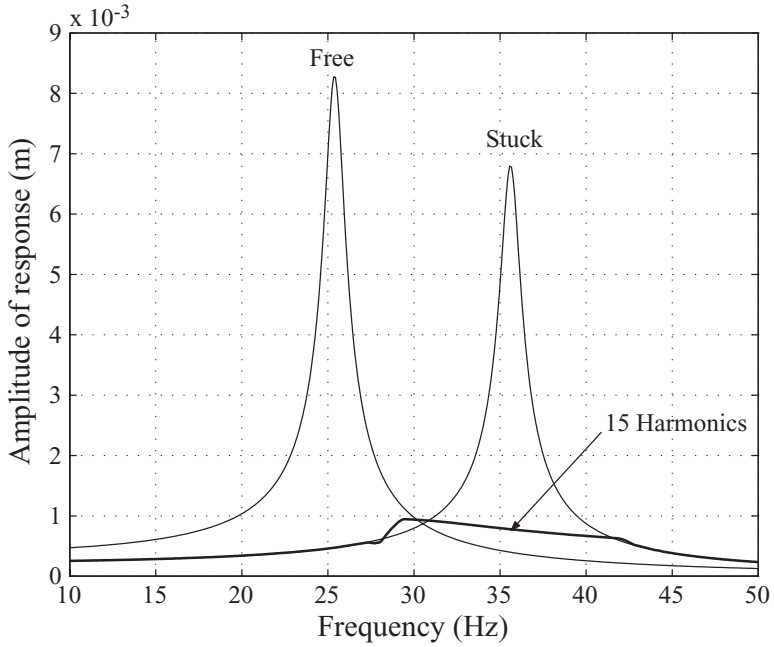

Figure 3.3: Free, stuck and stick-slip forced responses of the $\mathbf{e_y}$ component of the tip of the beam, in the first case study.

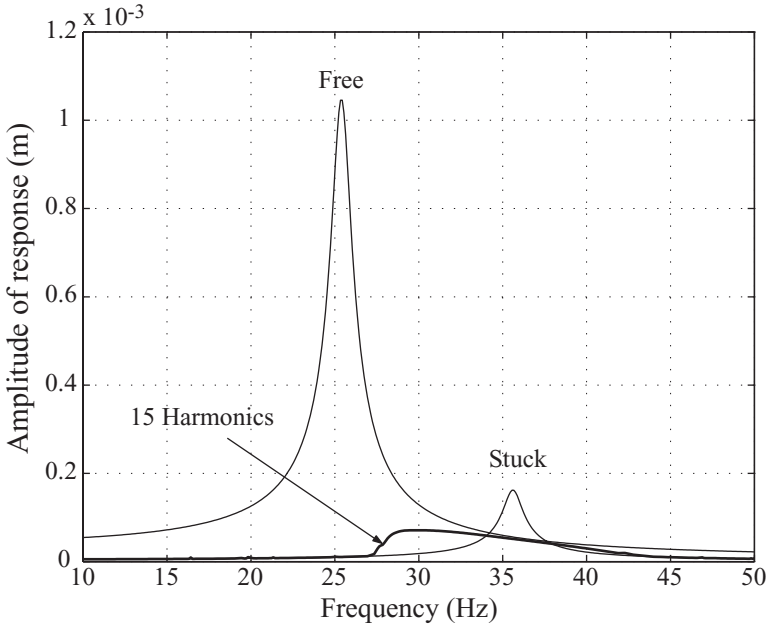

Figure 3.4: Free, stuck and stick-slip forced responses of the $\mathbf{e_x}$ component of the contact point, in the first case study.

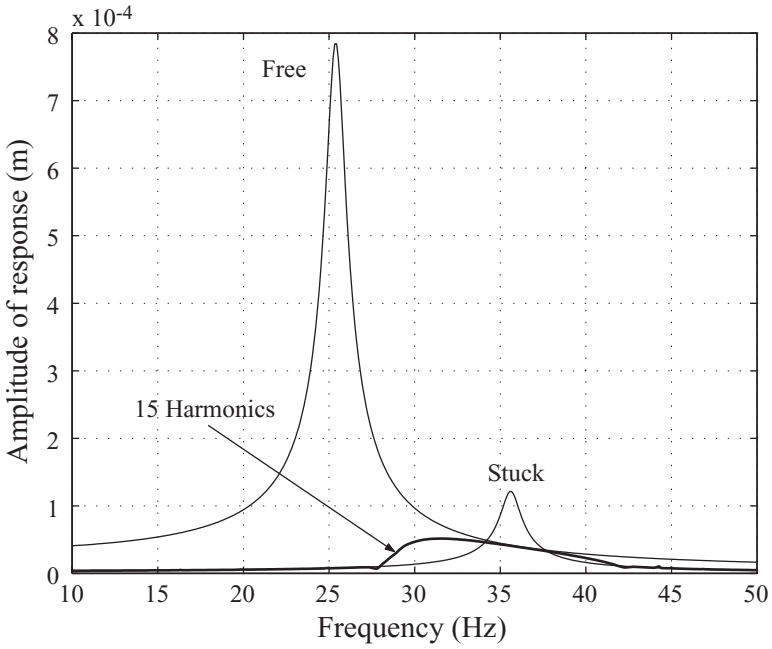

Figure 3.5: Free, stuck and stick-slip forced responses of the $\mathbf{e_y}$ component of the contact point, in the first case study.

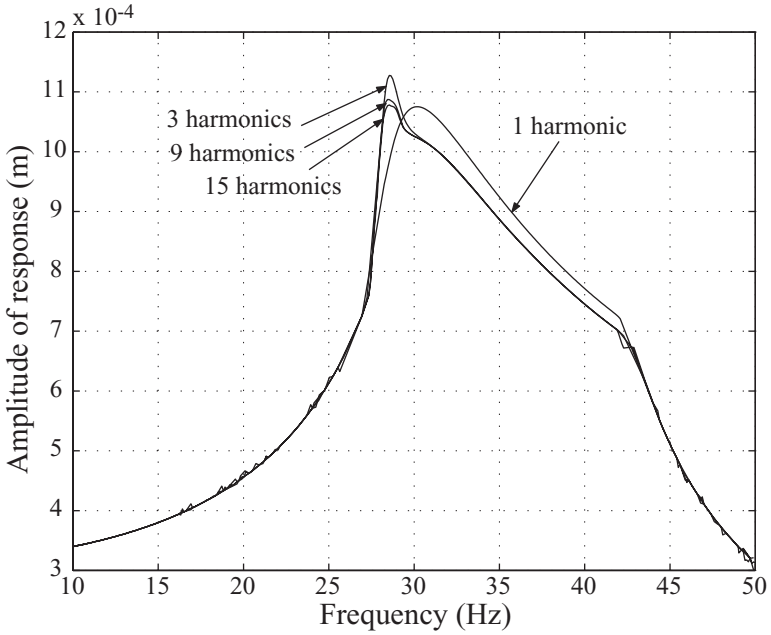

Figure 3.6: Influence of the number of harmonics on the forced response of the beam, in the first case study.

directions, when 15 harmonics are kept. The two linear responses (when the damper is fully stuck, or fully free) are also included. The stick-slip response of the beam features an overall 90% reduction of amplitude of motion at the tip with respect to the free response, and an average 94% reduction of amplitude of motion at the damper location. The influence of the number of harmonics is presented in Fig. 3.6, which shows the nonlinear forced responses of the beam obtained with 1, 3, 9 and 15 harmonics. The converged response is reached very quickly: it seems that in this case three harmonics are sufficient to describe accurately the dynamics of the beam. The various results presented hereafter are however calculated with 15 harmonics, which corresponds to the number of harmonics of the reference, converged solution.

In order to assess the increase of accuracy derived from the use of a 3-D model of damper over a simpler 1-D model, the forced response of the beam with a 1-D friction damper attached is calculated. Figure 3.7 shows a comparison of the effects of the 1-D

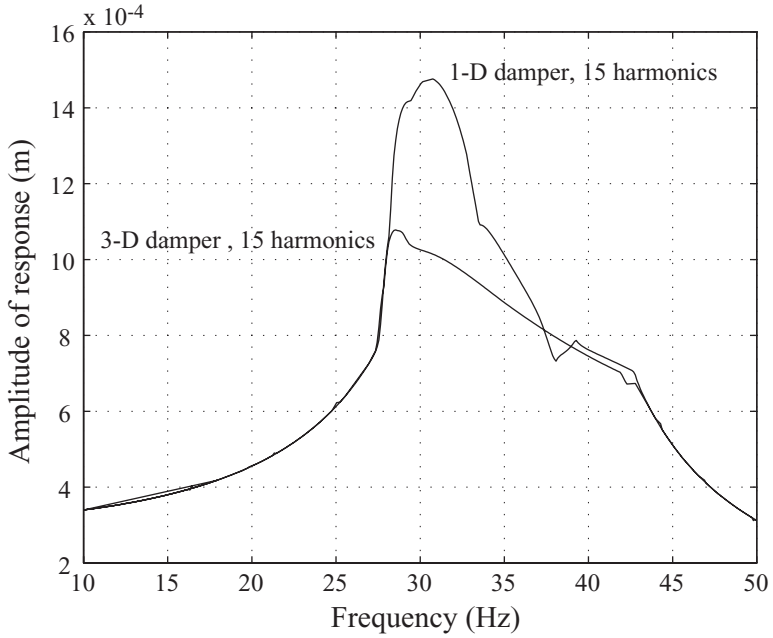

Figure 3.7: Comparison of the effects of a 1-D damper and a 3-D damper on the forced response of the beam, in the first case study.

damper and the 3-D damper on the beam response. The 1-D damper is chosen to act on the first DOF of the system, in the $\mathbf{e_x}$ direction, which corresponds to the direction exhibiting the largest amplitude of response. Its stiffness is $2.0 \cdot 10^7$N.m^{-1}, its coefficient of friction is 1.0 and the value of the normal load applied to it is 250N. The same number of harmonics (i.e., 15) is kept for this comparison. The results show the effect of the coupling of the $\mathbf{e_x}$ and $\mathbf{e_y}$ motions of the beam due to the 3-D damper: when a simple 1-D damper is used, it cannot capture the correct response of the beam, leading to a large overestimate of the maximum response of the system.

The analysis of the behavior of the 3-D damper is presented in the Figs. 3.8 and 3.9. Figure 3.8 shows the percentage of slip time of the damper over one period of motion, for the complete range of frequencies computed. Interestingly, most of the nonlinear frequencies computed feature a 100% slipping time, that is, the contact point is in constant motion on the plateform of the beam: from 27 Hz up to 42 Hz, the damper is always slipping,

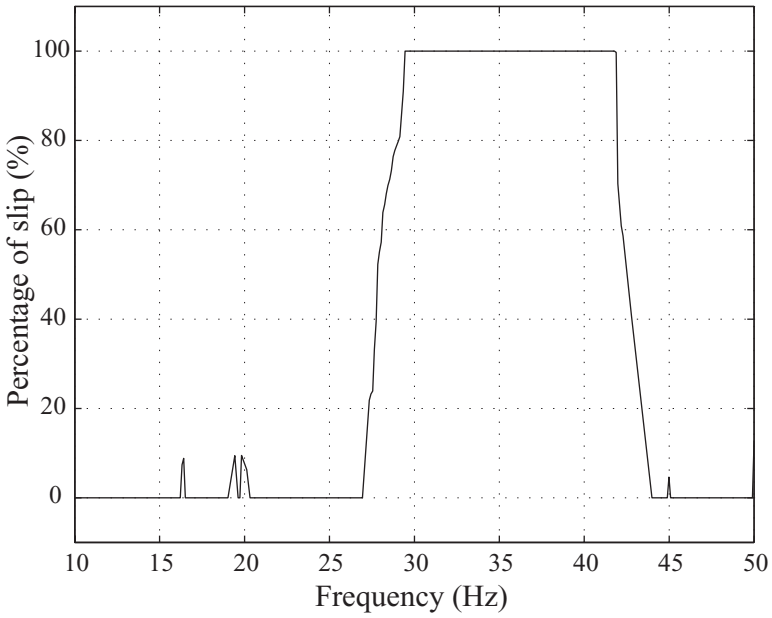

Figure 3.8: Percentage of slip time of the 3-D damper over one period of motion, for the entire frequency range considered in the first case study.

and no stick-slip phenomenon is observed. The plot in Figure 3.9 describes the state of the damper at a frequency near the resonant peak, and as mentioned above the damper is always slipping over the period of motion simulated. This behavior is also clearly depicted in Fig. 3.10, which shows the motion of the 3-D damper and the motion of the platform at 32.9 Hz in the friction plane. At this frequency the damper is always slipping. Since its stiffness matrix is symmetric with identical stiffnesses in both directions, the motion of the contact point must be a circle. This is due to the fact that the norm of the friction force – which depends on the position of the damper –, must be equal to the product of the normal load and the friction coefficient – which is constant in this study. This is confirmed by the trajectory of the damper. One should also note that the motion of the platform is almost an ellipse: this is a consequence of the fact that in this study the number of harmonics required to accurately describe the response of the system is relatively small.

The Figs. 3.11 and 3.12 further depicts the low-harmonic content of the response. The time histories of the nonlinear force at the same frequency of 32.9 Hz are shown in the

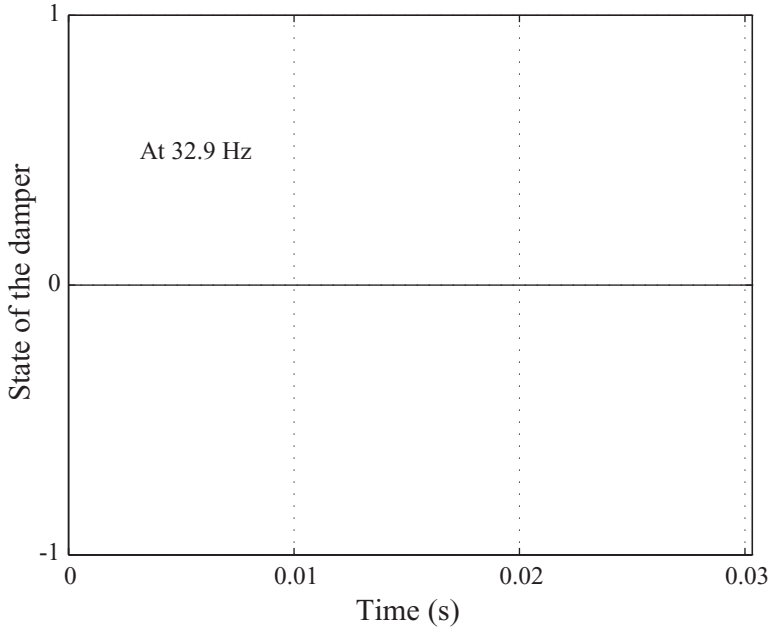

Figure 3.9: Time history of the state of the damper over one period of motion at 32.9 Hz obtained in the first case study. The convention used to represent the state of the damper is that -1 corresponds to stick and 0 corresponds to slip.

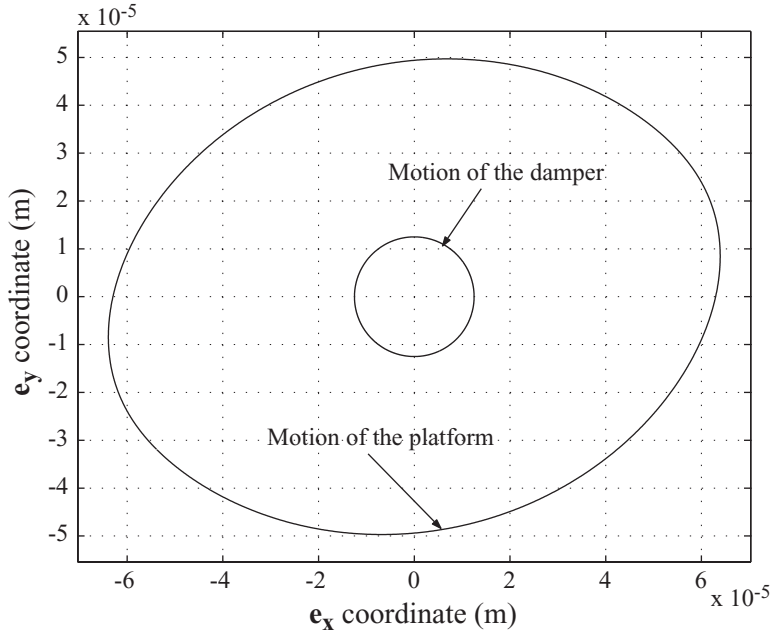

Figure 3.10: Motion of the beam and motion of the contact point at 32.9 Hz obtained in the first case study.

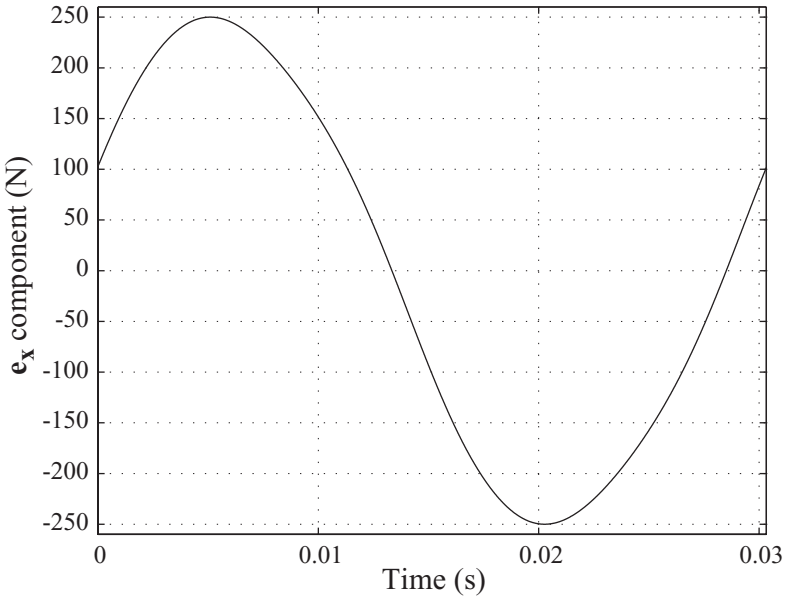

Figure 3.11: Time history of the $\mathbf{e_x}$ component of the friction force obtained at 32.9 Hz in the first case study.

$\mathbf{e_x}$ and $\mathbf{e_y}$ directions. The two components of the friction force oscillate between the maximum absolute value allowed (250 N) in an almost harmonic behavior. Since no slip-to-stick or stick-to-slip transitions occur, the system is not really perturbed by a sudden change of behavior of the damper, and the nonlinear friction force is rather smooth.

3.2.3 Second case study

The excitation considered in this second study is chosen so as to produce a highly asymmetric system response in the $\mathbf{e_x}$ and $\mathbf{e_y}$ directions. Whereas previously the tip excitation had the same order of magnitude in the $\mathbf{e_x}$ and $\mathbf{e_y}$ directions, the values chosen here reflect a preponderant direction of excitation:

$$F_x = 20 \text{ N}$$

$$F_y = 2 \text{ N}$$

The plot in Fig. 3.13 shows the frequency response of the beam when an increasing

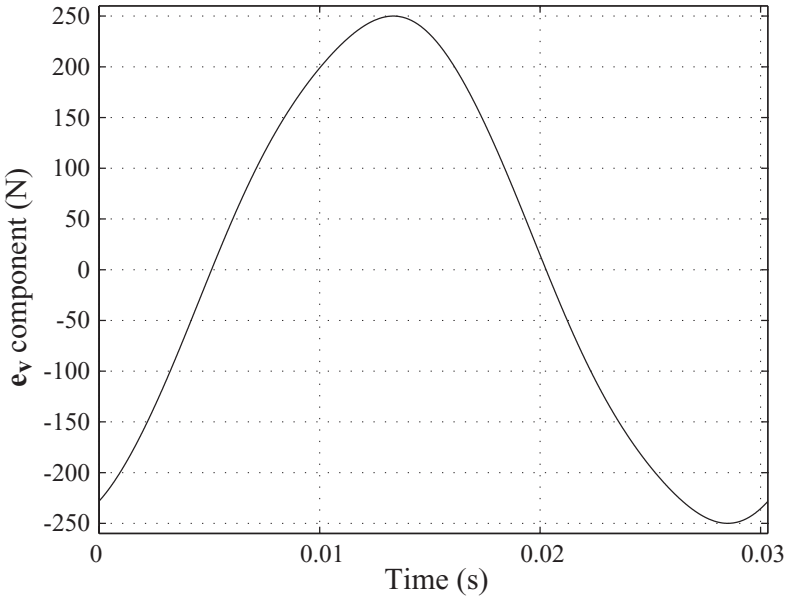

Figure 3.12: Time history of the $\mathbf{e_y}$ component of the friction force obtained at 32.9 Hz in the first case study.

number of harmonics is retained to describe the dynamics of the system. Only the $\mathbf{e_x}$ component of the response, which corresponds to the primary direction of the excitation, is presented here. The difference with the previous case study is striking: whereas 3 harmonics were sufficient in the previous study, the calculations made with the strongly non-symmetric forcing show that at least 15 harmonics are required to capture the converged solution with the same accuracy. Figure 3.14 shows that for the excitation considered, the behavior of the 3-D damper converges to that of an equivalent 1-D damper. This 1-D equivalent damper has the same physical properties as that of the damper used previously. The agreement between the responses obtained with the 1-D and 3-D dampers is very good. It shows that for a ratio F_x/F_y equal to 10, the coupling of the two directions of vibration due to the 3-D damper is negligible.

In the rest of the calculations presented here, a 21-harmonic approximation is used. It corresponds to the converged, reference solution beyond which no noticeable improvement

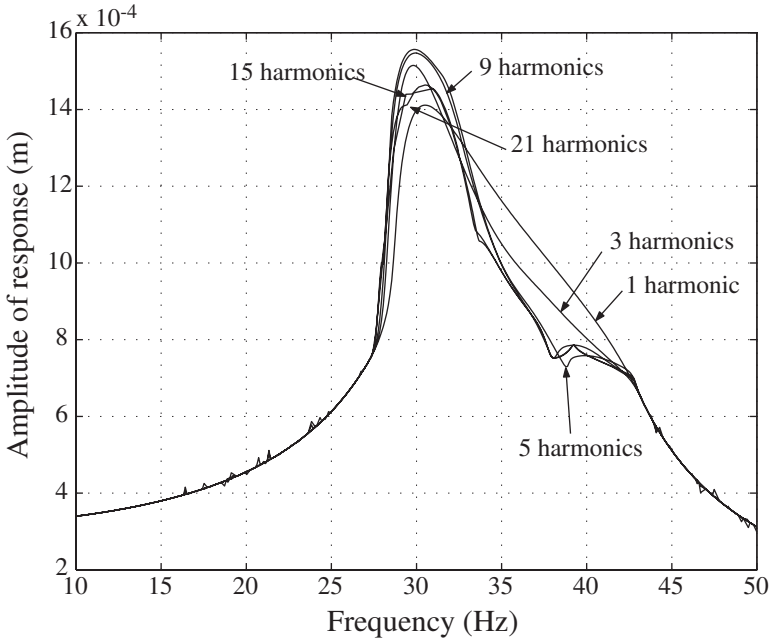

Figure 3.13: Influence of the number of harmonics on the forced response of the beam, in the second case study.

of the accuracy of the response with respect to the number of harmonics can be detected.

Unlike the previous case, the behavior of the damper presented here shows that the percentage of slipping time during a period of motion is never 100 %. The damper experiences a typical stick-slip behavior over most of the frequency range, except when the amplitude of the response of the beam is too low to prevent the damper from sticking to the platform all the time. This is well illustrated in Fig. 3.15, which describes the time history of the state of the damper near the nonlinear resonant frequency, at 32.9 Hz. This plot highlights the complex stick-slip behavior of the damper: the state of the damper alternates 12 times during one period of motion, with some of the slipping phases being very short.

These alternating stick/slip phases lead to a very complex motion of the contact point between the damper and the platform. Figure 3.16 depicts the trajectory of the beam and of the damper. The path followed by the contact point is very complicated. The time history

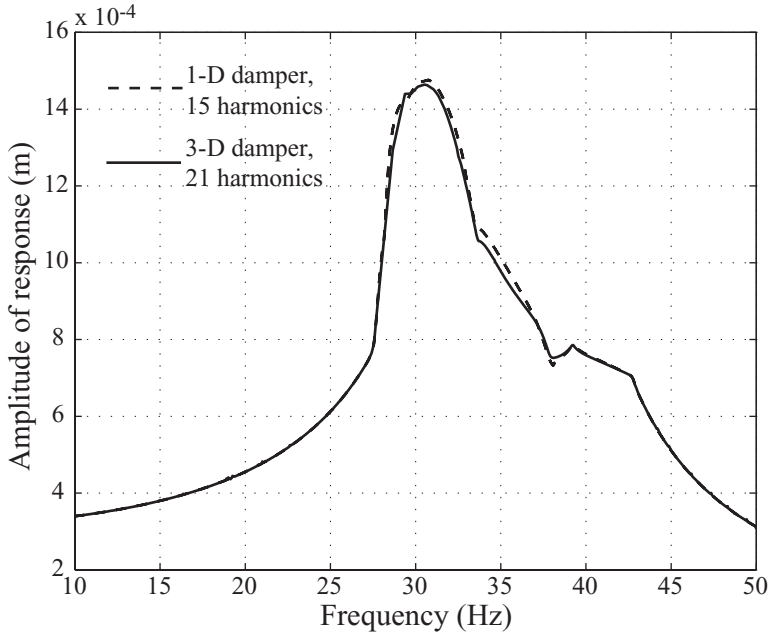

Figure 3.14: Comparison of the effects of a 1-D damper and a 3-D damper on the forced response of the beam, in the second case study.

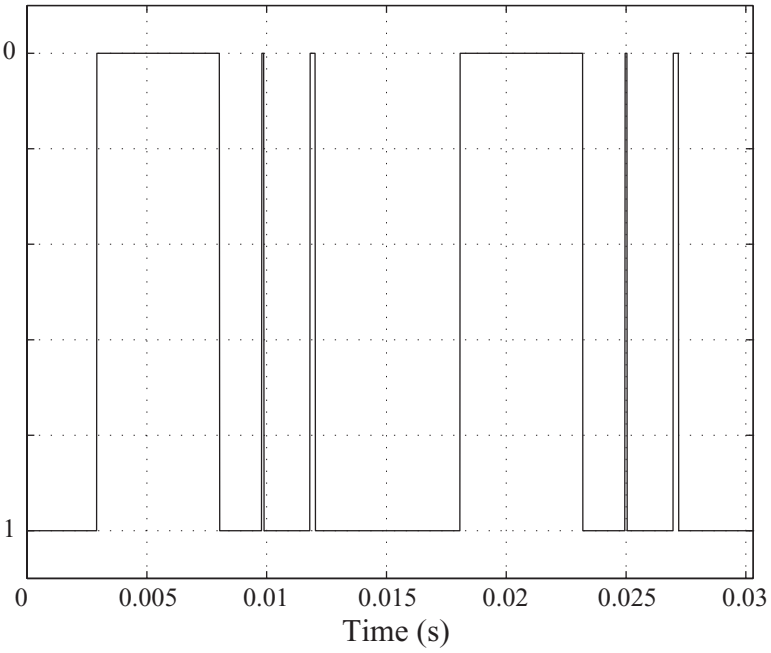

Figure 3.15: Time history of the state of the damper over one period of motion at 32.9 Hz obtained in the second case study. The convention used to represent the state of the damper is that -1 corresponds to stick and 0 corresponds to slip.

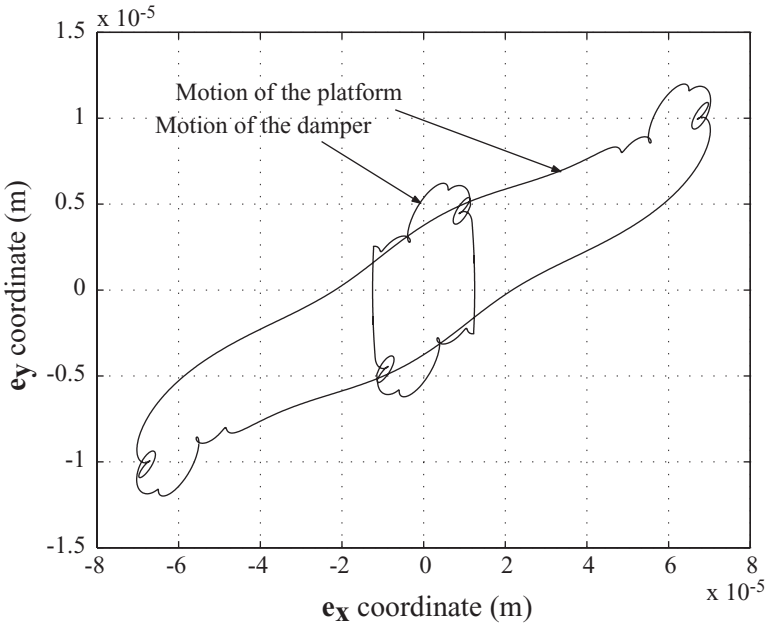

Figure 3.16: Motion of the beam and motion of the contact point at 32.9 Hz obtained in the second case study.

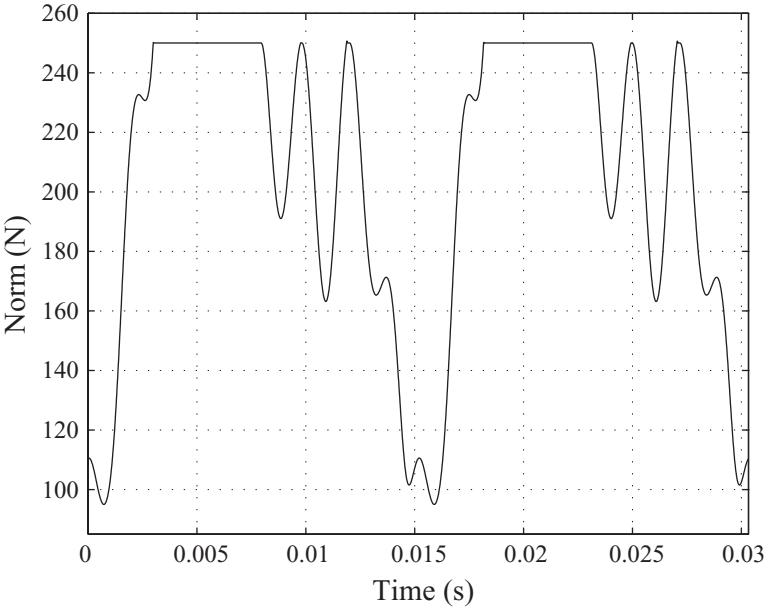

Figure 3.17: Time history of norm of the contact force, obtained at 32.9 Hz in the second case study.

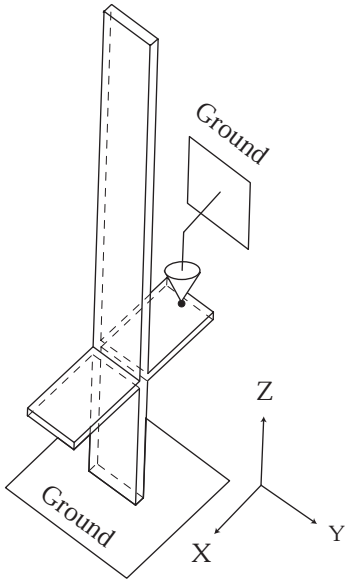

Length = 1.0 m
Width = 0.08 m
Thickness = 0.02 m
Young's modulus = 2.0 10^{11} Pa
Poisson ratio = 0.3
Density = 7600 kg/m^3

The platforms are located at one fourth of the beam, and are 0.10 m long.

The friction point is centered at 0.02 m of the free edge of the platform

Figure 3.18: Model of cantilevered beam with attached friction damper allowing for variable normal load.

of the norm of the contact force, presented in Fig. 3.17, also exhibits a similar complexity. The slip phases experienced by the damper are clearly indicated by the norm of the contact force being equal to 250 N.

3.3 Forced response of a beam subject to friction with variable normal load

The second application of the HFT method consists in the analysis of the forced response of a beam with a 3-D damper attached, when the physical parameters of the beam as well as the characteristics of the damper allow for variable normal load. This cantilevered beam – fully described in Fig. 3.18 – is excited at its tip by a harmonic force of amplitude 100 N in the X direction. The platform of the beam is subject to the action of a friction damper.

The model of friction damper considered allows for both tangential (along the X direction) and normal (along the Z direction) motion. It is characterized by its tangential stiffness k_t and its normal stiffness k_n. In this example, $k_t = k_n = 2 \times 10^7$ N.m^{-1}. The

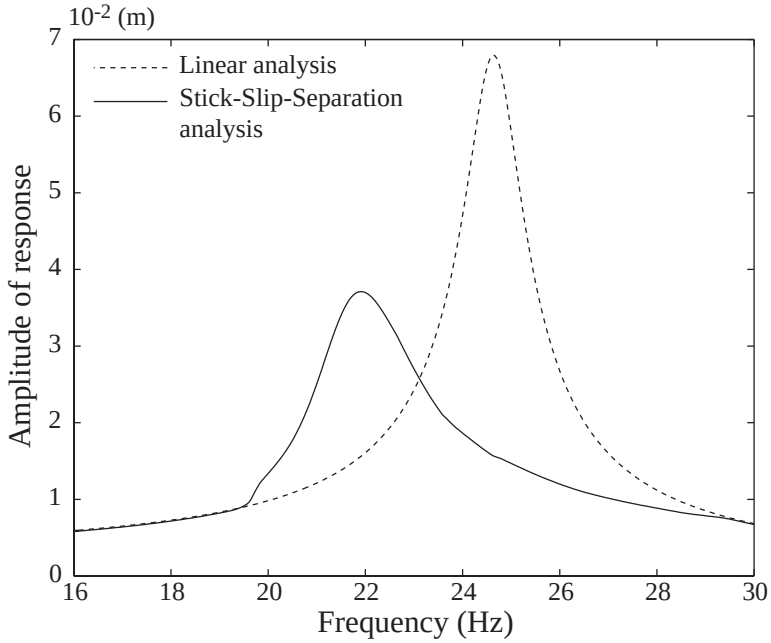

Figure 3.19: Linear and nonlinear forced responses of the cantilevered beam presented in Fig. 3.18.

flexibility of the damper in the Z direction implies that any normal motion of the platform produces a variation of the normal load applied by the damper to the platform. Also, when the displacement of the platform is zero in the Z direction, the normal contact force exerted by the damper on the platform is chosen to be equal to 2000 N.

The beam is condensed out using the Craig-Bampton component mode synthesis. The 19-DOF reduced-order model obtained is made of (1) the X and Z DOFs associated to the node of the tip where the blade is excited, (2) the X and Z DOFs associated to the friction point, and (3), 15 modal coordinates corresponding to the normal modes of vibration of the blade when the physical DOFs mentioned above are fixed.

For this system, the nonlinear analysis is carried out with the harmonics 0, 1, 2, ..., 11, corresponding to a converged solution. Two forced responses observed at the tip of the blade are described in Fig. 3.19. The first one corresponds to the mono-harmonic, linear case where the friction damper is always attached to the platform, that is, its action on

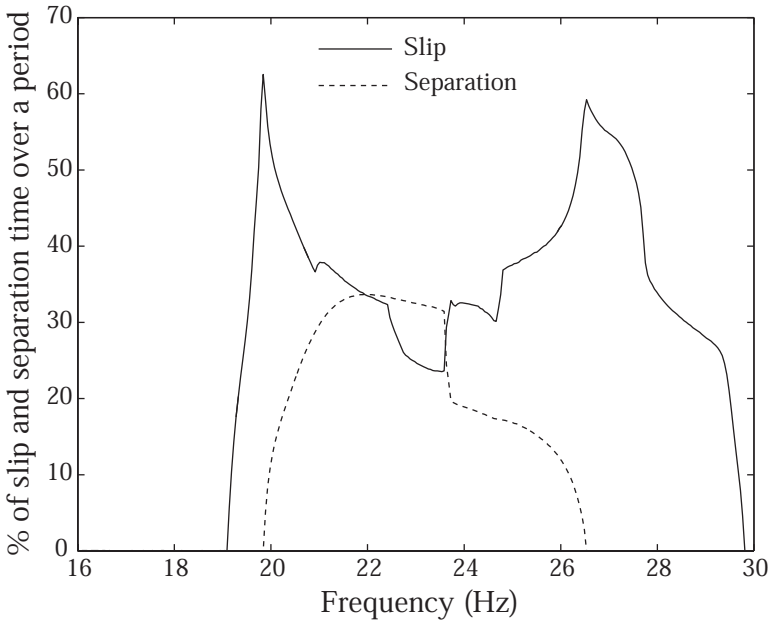

Figure 3.20: Percentage of slip time and separation time over a period of motion of the platform.

the blade is analog to the effect of an additional stiffness. The second forced response corresponds to the nonlinear case where the damper can alternate stick, slip and separation phases over a period of motion. It coincides with the linear response for the lowest amplitudes of motions, since the tangential motion of the platform at these low response levels is not large enough to make the damper slip.

As shown in Fig. 3.20, there exists a large range of frequencies for which the behavior of the damper is highly nonlinear. Near the resonant peak of the nonlinear response, around 22 Hz, the damper spends 30% of the period of motion in the slip state, and also 30% of the period in the separation state where it is no longer in contact with the platform. This is further illustrated in Fig. 3.21 where the time histories of the tangential and normal contact forces, calculated at 22 Hz, show the complexity of the interaction between the damper and the platform.

Despite the strong nonlinearity exhibited by this friction-damped structure, the Hybrid Frequency-Time domain method is able to calculate the solution of the nonlinear system

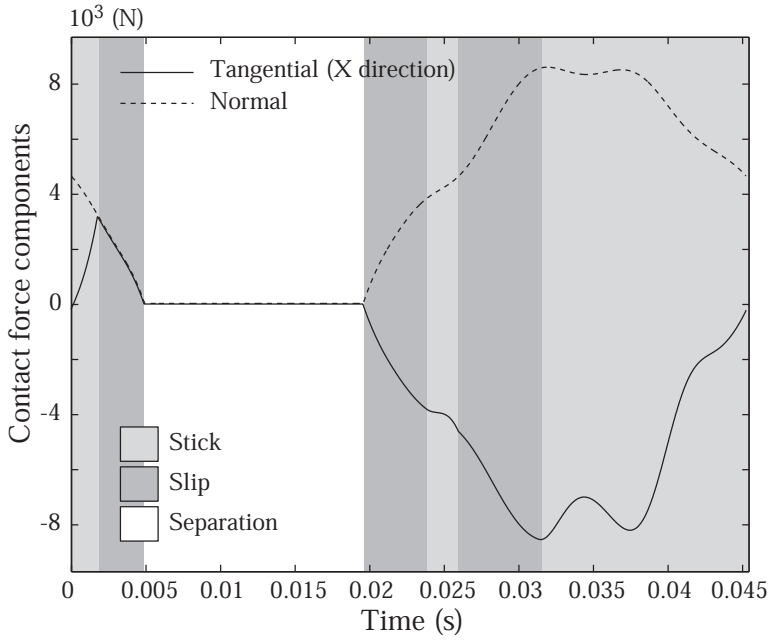

Figure 3.21: Time histories of the tangential and normal components of the contact force at 22 Hz.

over the selected range of frequencies without being hindered by convergence problems. The combination of the HFT method and the hybrid Powell algorithm seems therefore effectively adapted to the study of the dynamics of systems featuring complex nonlinear contact forces.

3.4 Forced response of a simple model of mistuned structure

In this example, a structure made of 108 beams with 108 ground-to-blade friction dampers is considered. The forced response of a system of 36 beams with similar characteristics has been studied by Nacivet *et al.* [92, 93]. As partially depicted in Fig. 3.22, the beams of this system are attached to a fixed, rigid support. The mass and stiffness matrices of the i-th beam are defined as:

$$\mathbf{M}_i = \mathbf{M}$$

$$\mathbf{K}_i = \delta_i \mathbf{K},$$

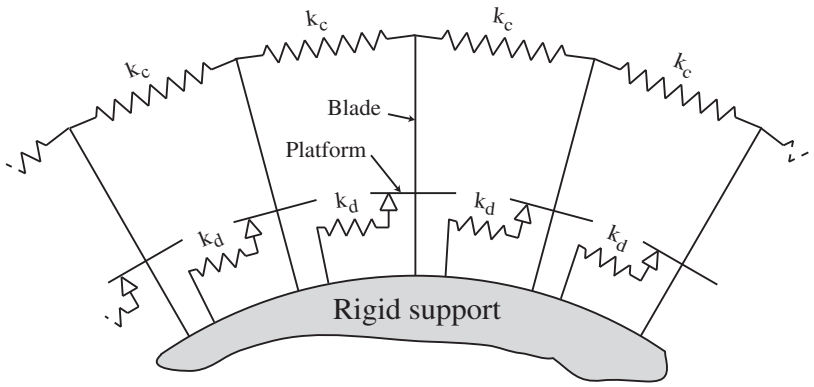

Figure 3.22: Partial view of a simple model of bladed disk assembly.

where $\mathbf{M}$ and $\mathbf{K}$ are 3-by-3 matrices provided by SNECMA, which correspond to a reduced-order model of blade described in Berthillier *et al* [57]. The mistuning coefficients δ_i follow a normal distribution centered at 1 with a standard deviation of 7%.

A stiffness k_c of 4.5×10^3 N couples the tips of two adjacent beams. This stiffness can be interpreted as the flexibility of the disk or as a shroud for more realistic bladed-disk assemblies.

Each beam is subject to the action of a ground-to-blade friction damper, and all the dampers share the same characteristics. They are modeled as simple hysteretic dampers of stiffness $k_d = 2.4 \times 10^7$ N.m^{-1}. They follow the law of dry friction of Coulomb, with a friction coefficient of 1. The contact point at the platform/damper interface is allowed to move along one direction, and the dampers are pressed under the platforms with a constant normal load of 250 N. Therefore, the dampers exert a nonlinear friction force on only one DOF of each of the beams.

Finally, the tips of the beams are subject to a mono-harmonic traveling excitation of amplitude 20 N with an engine order of 5.

The forced response of the structure is depicted in Fig. 3.23. It shows the strong localization of the energy due to the mistuning. The characteristics of the set of equations solved by the HFT method are given below:

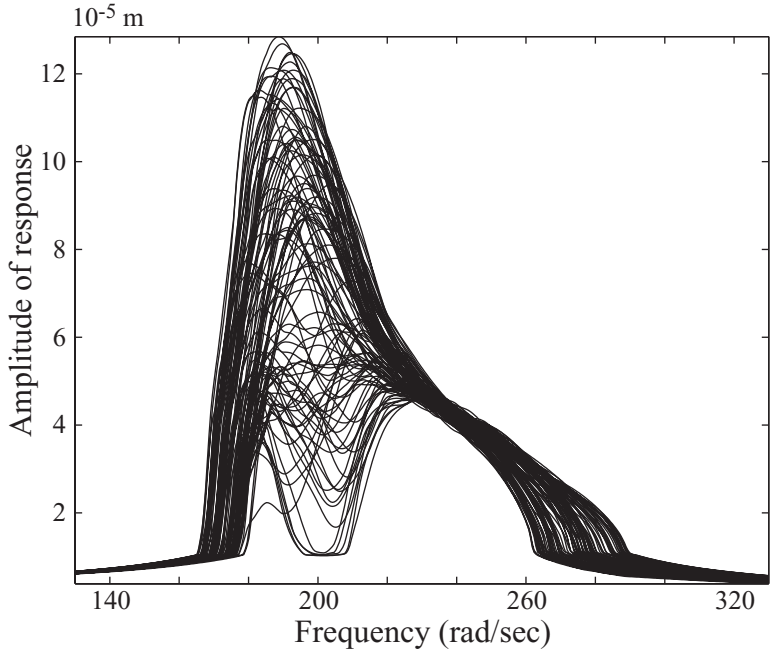

Figure 3.23: Forced response of the nonlinear friction DOFs of a 7% mistuned, 108 beam assembly. The response of the structure is approximated with the harmonics 1, 3, 5, . . ., 21.

- The structure is represented by 324 DOFs, among which 108 are nonlinear.
- The forced response of the system has been calculated with the harmonics 1, 3, 5, 7,. . ., 19 and 21, since it can be proven that the even harmonics of the friction forces are exactly zero for the type of nonlinearity considered here. Therefore, the motion of each DOF is represented by 22 real coefficients.

As a consequence, the dynamics of the structure is represented by 7128 harmonic coefficients, which lead to a reduced nonlinear system of 2376 unknowns, corresponding to the harmonic coefficients of the nonlinear DOFs only.

A Gateway computer with a 2 GHz Pentium IV processor has been used to calculate this forced response. The CPU time required to solve the nonlinear system near the resonant peak at 200 rad.s^{-1} is 110 seconds. At the same frequency, the CPU time dedicated to the condensation of the system on the nonlinear DOFs represents about 1.5 second. This

means that the number of linear DOFs of the structure could be greatly increased without penalizing the CPU time required to solve the nonlinear system. In particular, a greater number of normal modes could be included in the reduced-order models that represent the beams so as to increase the accuracy of the calculation.

This study shows that the HFT method is applicable to the calculation of the forced response of systems having a large number of nonlinear friction DOFs, without sacrificing the number of harmonics retained in the analysis and the accuracy of the results.

3.5 Forced response of a simple model of tuned (cyclic) structure

The characteristics of the structure presented in the previous example are now slightly modified: The number of beams of the assembly is reduced to 36, and the mistuning coefficients δ_i are all set to 0, so that the structure is spatially cyclic. Therefore, the cyclic symmetry theory developed in Chapter I can be directly applied to this structure. The properties of the dampers as well as the value of the inter-sector elastic coupling remain unchanged.

The forced response of the structure is studied for two different excitations. The first excitation is a traveling wave of engine order $e_o = 4$, which rotates with the angular velocity Ω. It is approximated by a series of three spatial harmonics of cyclicity e_o, $2e_o$ and $3e_o$. As these waves rotate, they excite the reference sector of the structure at the pulsations ω, 2ω and 3ω, where $\omega = e_o\Omega$. The first linear excitation applied to the tip of the beam of the reference sector is therefore defined as:

$$\begin{aligned} f_l^1(t) = \; & 20\cos(\omega t) + 15\sin(2\omega t) \\ & + 4\cos(3\omega t) + 3\sin(3\omega t) \end{aligned}$$

One should note that the amplitudes of the second and third harmonic waves are designed so that they correspond respectively to 75% and 25% of the amplitude of the fun-

damental wave. These values are common in turbomachinery applications.

The second excitation studied is simply the mono-harmonic approximation of the first one, that is:

$$f_l^2(t) = 20\cos(\omega t).$$

For these two excitations, the forced responses of the friction DOF of the reference sector have been computed with the harmonics 0, 1, 2, . . ., 20 and 21. The comparison of these two responses is shown in Fig. 3.24. It illustrates the dramatic change of behavior of the system when one neglects to take into account all the harmonics of the linear excitation.

When subject to a mono-harmonic excitation, the structure exhibits a response with only one resonant peak, around 200 rad/s. When subject to the three-harmonic excitation, a second resonant peak appears around 100 rad/s. This peak is due to the presence of the second spatial harmonic of engine order $2e_o$, which excites the reference sector at twice the frequency of the fundamental temporal harmonic. One should also expect a third resonant peak around 70 rad/s; however, the amplitude of the third harmonic of the excitation is not large enough to produce a significant contribution in the response, and the response of the structure at this frequency is largely dominated by the second component of the excitation.

Figure 3.25 shows the time history of the friction force applied to the nonlinear DOF of the reference sector. The highly nonlinear character of the friction force is obvious, as the damper switches from the stick state to the slip state twice over a period of motion. The Fourier harmonics of the friction force corresponding to this time history are presented in Fig. 3.26. They show that, although the fundamental harmonic is dominant, neglecting the other harmonics would lead to a significant loss of accuracy.

Finally, the correspondence between the temporal harmonics of the force applied to the reference sector and the spatial harmonics exhibited by the response of the complete structure shows that only 9 spatial modes of vibration are present.

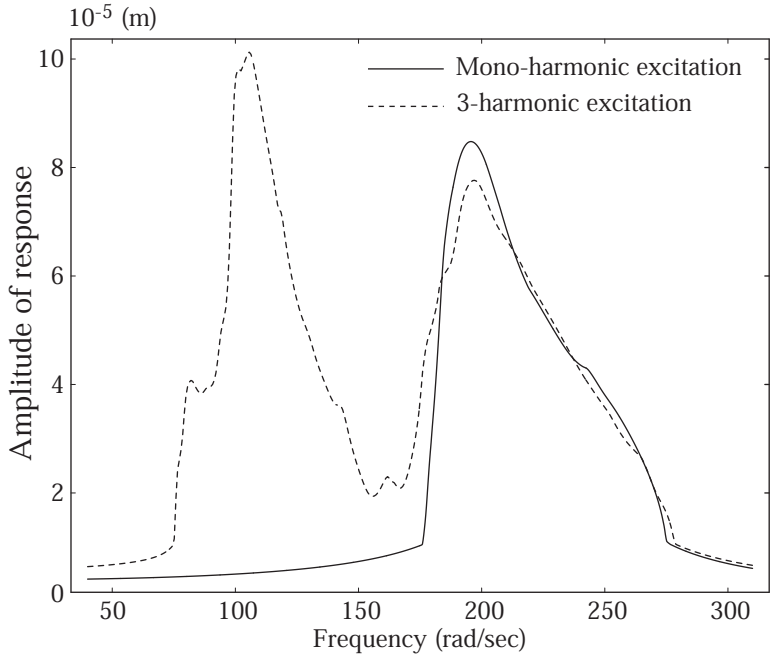

Figure 3.24: Forced response of the nonlinear friction DOF of the reference sector of a 36-beam cyclic assembly. 21 harmonics are retained to describe the dynamics of the structure.

Since the cyclic symmetry theory allows one to deduce the dynamics of the structure from the study of the response of the 3-DOF reference sector, the CPU time associated with solving the nonlinear set of equations of motion is extremely small. In this example, at 200 rad.s^{-1}, this CPU time is 0.04s. This must be compared with the CPU time required to study the response of the complete structure without using its property of cyclic symmetry: in this case, the solution at the same frequency is obtained in 65s.

3.6 Intentional friction damper mistuning

The effect of blade mistuning on bladed-disk dynamics as been extensively investigated in the field of turbomachinery applications. In particular, a well known consequence of mistuning is the localization of the vibrational energy to a few blades, which can double or triple the amplitude of the response of some blades. This effect can be quantified by defining two quantities, as follows:

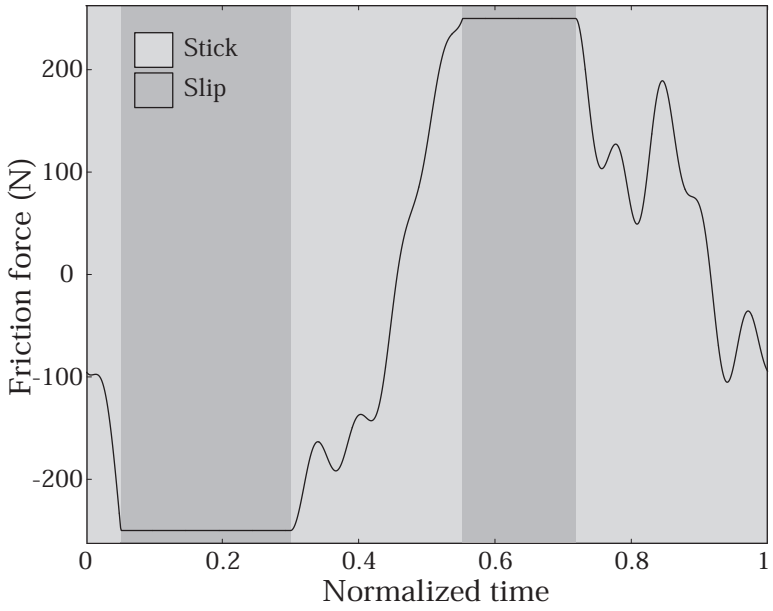

Figure 3.25: Time history of the friction force applied to the nonlinear DOF of the reference sector at 200 rad.s^{-1}.

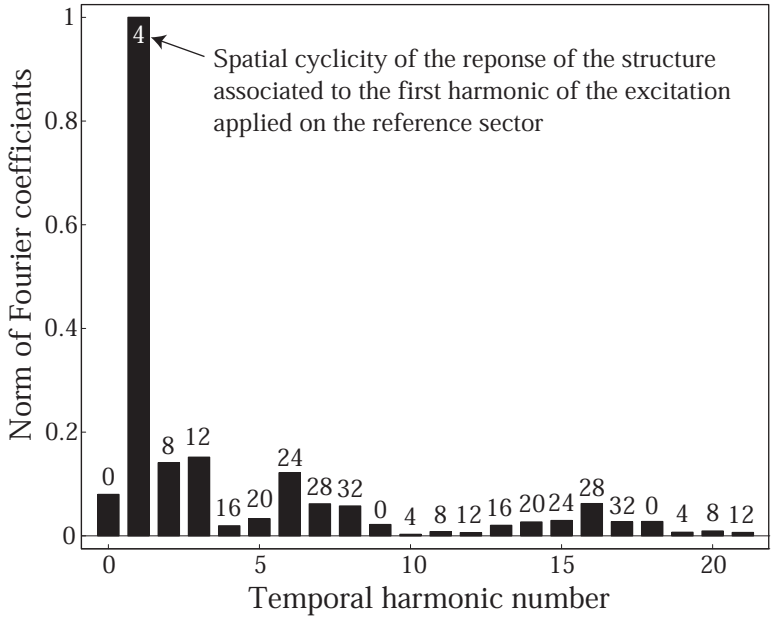

Figure 3.26: Temporal harmonics of the nonlinear force applied to the reference sector, with the corresponding spatial harmonics exhibited by the response of the structure.

- The amplification factor, A_f, defined as $A_f = \max_i \left\{ \frac{u_i}{u_{tuned}},\ i = 1, N \right\}$, where N is the number of sectors of the bladed disk, u_{tuned} the amplitude of the response of the tuned system, and u_i the amplitude of the response of the i-th sector in the mistuned case.

- The dispersion factor, D_f, defined as $D_f = \max_{i,j} \left\{ \frac{u_i - u_j}{u_{tuned}},\ i, j = 1, N \right\}$

Under certain conditions, mistuned systems may feature values of A_f as high as 300%, and the consequence of high amplification factors can be dramatic, leading to accelerated fatigue and possibly to premature blade failure. Moreover, localization can take place for very small values of mistuning, and is present despite the use of high precision machining for the blades. As a consequence, minimizing the effects of small, unavoidable mistuning is of great importance to increase the reliability of these turbomachinery structures. Among the ideas proposed to reduce or at least control these dramatic effects, the introduction of *intentional* blade mistuning in the design of blade assemblies has been considered by Castanier and Pierre [111], among others. Intentional mistuning can be achieved by introducing a relatively simple pattern for the blade properties, for example with two of three types of different blades. However promising, these techniques have the considerable drawback of requiring distinct designs for the blades, which can be costly to implement.

More recently, Petrov and Ewins [98] have presented the idea that the mistuning of the physical characteristics of the dampers can also be modeled and analyzed, and that in some cases specific mistuning design patterns applied to the dampers could bring benefits to the dispersion of the individual forced reponse of the blades of a mistuned bladed disk assembly. The idea that the mistuning pattern of a set of dampers can be optimized to minimize the dispersion of the response of the blades of a structure of known mistuning

characteristics has however not been explored.

This section briefly illustrates the benefits that can be derived from the HFT method's speed and robustness for this new concept of intentionally optimizing the mistuning of dampers so as to match it to the mistuning of the bladed disk assembly.

3.6.1 System investigated

The dynamics of a simple 10-blade assembly is investigated. The blade model used is a 3-DOF beam which stiffness and mass matrices $\mathbf{M}$ and $\mathbf{K}$ as well as the viscous damping matrix $\mathbf{C} = \alpha\mathbf{K} + \beta\mathbf{M}$ are similar to that of the cyclic structure described above. The disk is modeled by springs of stiffness $k_c = 5.10^5$ N.m^{-1}, which couple adjacent beams. Each beam is subject to the action of a ground-to-blade, 1-D damper. The system is excited at the tip of each beam by a $20N$, engine order 2 forcing.

This optimization is conducted by retaining only one harmonic of the temporal response of the structure. A 7 % random blade mistuning is introduced by randomly perturbing the stiffness of the springs that connect the adjacent sectors of the assembly. Figure 3.27 shows the frequency response of the blade assembly, both without friction dampers and with a set of identical dampers. When the system is not friction damped, the amplification and dispersion factors are found to be $A_f = 14\,\%$ and $D_f = 51\,\%$.

In this example, a 83 % reduction of the largest blade amplitude is observed when identical friction dampers are used.

3.6.2 Optimization problem and results

The objective of the optimization process is to find a spatial configuration of (non-identical) friction dampers, which leads to a reduction in both the largest blade amplitude (similar to that previously observed) and the dispersion of blade amplitudes.

The design variables are the ten values of the stiffness of the dampers and the ten values

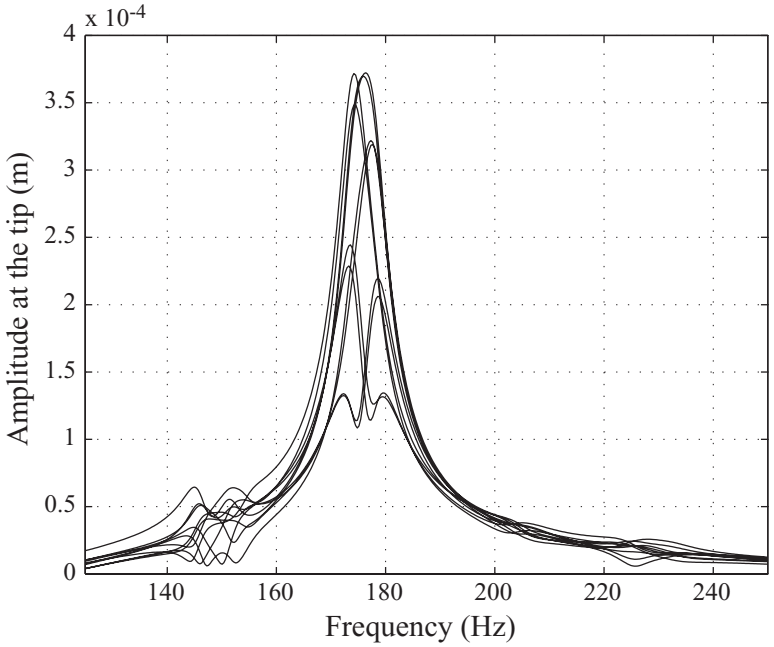

Figure 3.27: Linear forced response of the mistuned system without friction dampers.

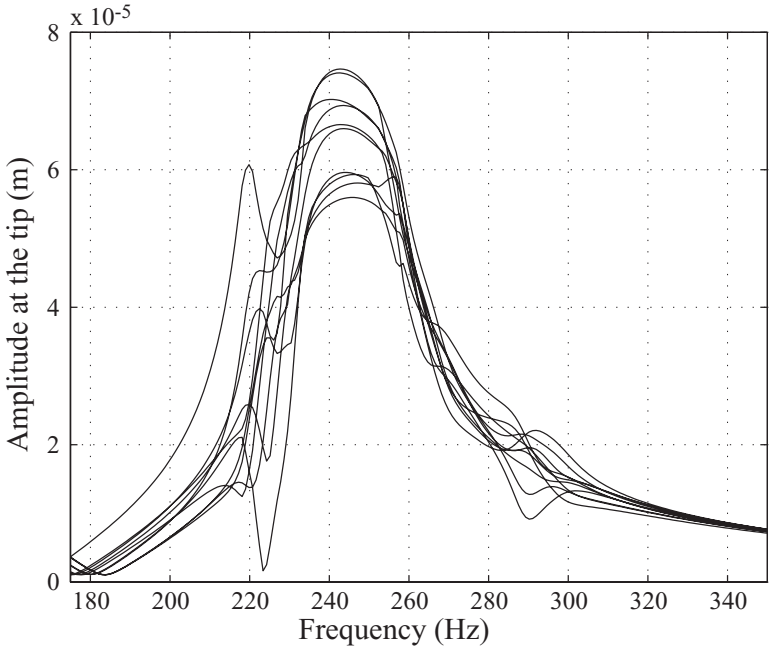

Figure 3.28: Nonlinear forced response of the mistuned, friction-damped system with identical dampers of characteristics [stiffness $k = 2\ 10^6$ N.m^{-1}, normal load $N = 200$ N].

of the normal loads. Thus, the optimization problem can be stated as:

$$\begin{aligned}
&\text{Find:} && \min_{N_i,k_i}\left\{\sum_{j=1}^{10}\left(\max_{\omega}\{u_j\}-u^{\star}\right)^2,\ i=1\ldots10\right\}\\
&\text{Such that:} && N_{min}<N_i<N_{max},\ i=1\ldots10\\
& && k_{min}<k<k_{max},\ i=1\ldots10\\
& && \omega_1<\omega<\omega_2\\
&\text{Where:} && u^{\star}\text{ is the response of the tuned, uniformly damped system.}
\end{aligned}$$

The upper and lower bounds of the 20 design variables are chosen such that large variations about their nominal, tuned values are allowed.

The optimal configuration found for the friction dampers is described in Table 3.2, and the corresponding mistuned, friction-damped frequency response of the assembly is shown in Fig. 3.29. The dispersion of the resonant blade amplitudes is considerably reduced, without lessening the positive effect of friction damping on the largest blade amplitude. The magnification and dispersion factors in the optimal case are:

$$A_{f,optimum}=0.6\ \%\quad\text{and}\quad D_{f,optimum}=1.1\ \%$$

These results prove that the initial concept is valid: non-identical friction dampers can be used to simultaneously reduce blade amplitudes *and* counteract the effects of blade mistuning. In other words, once the mistuning pattern of a bladed disk assembly is identified, an associated optimized set of friction dampers can be calculated. Thus, critical applications requiring a perfectly tuned bladed disk assembly could take advantage of this cost-effective design strategy which do not require different blades designs.

Initial solution	Converged solution	Initial solution	Converged solution
$k_1 = 200$ N.m^{-1}	$k_1^\star = 213.3421$ N.m^{-1}	$N_1 = 200$ N	$N_1^\star = 227.8156$ N
$k_2 = 200$ N.m^{-1}	$k_2^\star = 211.4026$ N.m^{-1}	$N_2 = 200$ N	$N_2^\star = 189.6255$ N
$k_3 = 200$ N.m^{-1}	$k_3^\star = 179.5341$ N.m^{-1}	$N_3 = 200$ N	$N_3^\star = 233.7462$ N
$k_4 = 200$ N.m^{-1}	$k_4^\star = 216.5225$ N.m^{-1}	$N_4 = 200$ N	$N_4^\star = 203.1638$ N
$k_5 = 200$ N.m^{-1}	$k_5^\star = 170.8149$ N.m^{-1}	$N_5 = 200$ N	$N_5^\star = 204.2310$ N
$k_6 = 200$ N.m^{-1}	$k_6^\star = 228.4019$ N.m^{-1}	$N_6 = 200$ N	$N_6^\star = 175.7614$ N
$k_7 = 200$ N.m^{-1}	$k_7^\star = 185.3555$ N.m^{-1}	$N_7 = 200$ N	$N_7^\star = 200.2310$ N
$k_8 = 200$ N.m^{-1}	$k_8^\star = 191.9482$ N.m^{-1}	$N_8 = 200$ N	$N_8^\star = 240.1072$ N
$k_9 = 200$ N.m^{-1}	$k_9^\star = 213.1507$N.m^{-1}	$N_9 = 200$ N	$N_9^\star = 203.4475$N
$k_{10} = 200$ N.m^{-1}	$k_{10}^\star = 195.1022$ N.m^{-1}	$N_{10} = 200$ N	$N_{10}^\star = 207.7661$ N

Table 3.2: Converged values of the design variables. Left: optimal damper stiffnesses. Right: optimal normal loads.

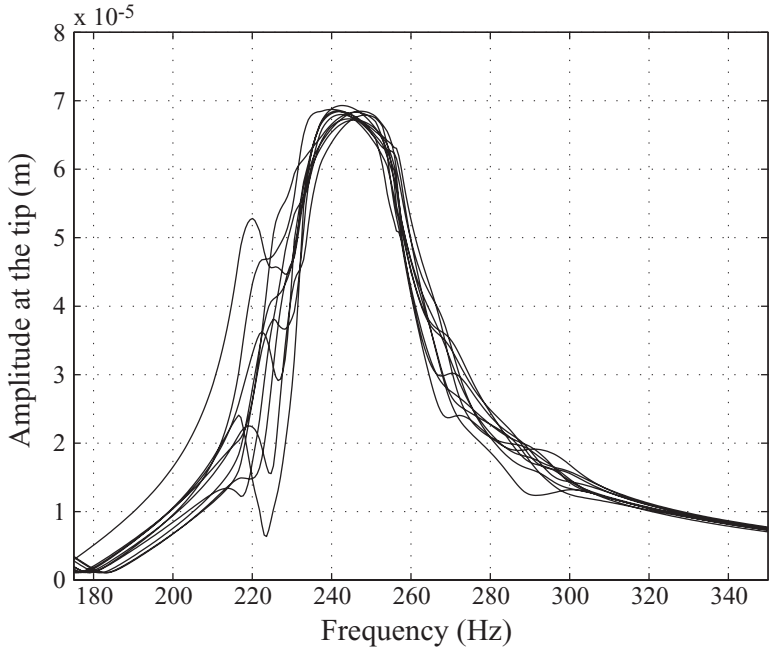

Figure 3.29: Frequency response of the mistuned assembly with the optimal set of friction dampers.

3.7 Conclusion

A selection of results for the nonlinear behavior of various structures with friction dampers attached has been presented. The forced responses of simple systems with 1-D as well as 3-D dampers have been investigated, in the case of constant and variable normal contact efforts. The examples considered were chosen so as to represent the three possible types of configuration for friction-damped structures, namely (1) stand-alone assemblies with a limited number of contact interfaces; (2) structures with cyclic symmetry; (3) mistuned (that is, non-cyclic) assemblies with a very large number of friction dampers.

The Hybrid Frequency-Time domain method has been applied very successfully to these nonlinear systems. It has been shown that the complex dynamics of these systems can be analyzed very accurately and at a very low computational cost. The time histories of the periodic waveforms of the contact forces obtained show very clearly that the dynamics of such systems can only be captured accurately if a large number of harmonics is retained.

Finally, the efficiency and speed of the method allows one to conduct parametric studies to determine the optimal design and characteristics the friction dampers, even for complex configurations.

CHAPTER IV

HYBRID FREQUENCY-TIME DOMAIN METHOD FOR THE FORCED VIBRATION OF ELASTIC STRUCTURES WITH DIRECT FRICTION AND INTERMITTENT CONTACT

4.1 Introduction

The study of the dynamics of structures subjected to periodic excitations and nonlinear contact forces, such as those stemming from friction or impact phenomena, is a complex theoretical and numerical endeavor. In particular, the direct methods of time integration of the equations of motion are often hampered by (1) the complexity of these nonlinearities, which requires one to select extremely small time steps, and (2), the very low amount of damping encountered in most industrial structures – especially in turbomachinery applications – which requires one to integrate the equations of motion over a very long period of time until any transient behavior dies out. In order to circumvent these problems, approximate methods of analysis have been regularly proposed over the past 25 years, and among them the Harmonic Balance Method (HBM) introduced by Nayfeh and Mook [20] has proven to be particularly suited for the study of the dynamics of structures with nonlinear damping. As mentioned in the literature review in Chapter I, recent multi-harmonic, alternating time-domain techniques derived from the HBM have made the study of complex

nonlinear structures possible with a very high accuracy.

Still, most of the works found in the literature have focused on nonlinearities that stem from operators which are modeled independently from the structure they are applied to, such as the flexible friction dampers found in the context of turbomachines. The case of nonlinearities resulting from interactions between the structure and an infinitely rigid obstacle, as well as the case of nonlinearities stemming from the reciprocal interactions of two contacting parts of the same structure, have received little attention in comparison.

The direct friction interaction that may occur between two parts of the same bladed disk assembly has been studied in the case of shroud-to-shroud contact by mono-harmonic approximations, by Srinivasan and Cutts [32], Griffin and Sinha [40], and Yang *et al.* [79]. The introduction of multi-harmonic methods suited for this type of analysis is relatively new and parallels the development of this dissertation work: multi-harmonic analysis of shroud-to-shroud contact or platform-to-platform contact have been recently proposed by Chen *et al.* [90], Nacivet *et al.* [93] and Petrov *et al.* [95–98]. The most advanced applications of such methods have been dedicated to the analysis of the dovetail root attachement of the disk-blade interface, as featured in works by Petrov and Ewins [102, 103], Nacivet [99], and Charleux *et al.* [100, 101].

In this chapter, a new multi-harmonic method derived from the Hybrid Frequency Time (HFT) domain method presented earlier in this dissertation is proposed for the analysis of the periodic forced response of systems with impact and friction between some of their components. This new method is adapted to the study of systems that do not require the modeling of friction dampers as external, nonlinear operators. The nonlinear boundary conditions at the contact interfaces are calculated in the time domain, and the presence of the Fourier coefficients of the nonlinear forces in the frequency-domain nonlinear equations is not necessary anymore. A robust solution algorithm is developed so as to form in

the frequency domain a new set of nonlinear equations which involve the displacements of the nonlinear degrees of freedom only. It is shown that the system formed of these new equations possesses better numerical properties than those obtained when traditional HFT techniques are used.

A brief introductory example highlights the theoretical difficulties encountered when the traditional HFT method is used to study structures with direct contact interactions between some of their parts. Then, the method of analysis is presented from both the frequency-domain and the time-domain points of view. Finally, the dynamics of simple systems are investigated so as to illustrate the capabilities of the new method.

4.2 Introductory example

The notation conventions, as well as the nomenclature of the variables used for the theoretical development of the method presented herein are summarized in table 4.1.

4.2.1 Intrinsic limitation of the HFT method

The Hybrid Frequency-Time (HFT) domain method presented in chapter II is adapted to the study of the periodic response of nonlinear systems where the nonlinear force can be explicitly expressed as a function of the displacement of its degrees of freedom (DOFs). A very simple illustration of such systems is presented in Fig. 4.1. For this spring-mass example subjected to a periodic linear excitation F and impacting an elastic stop, the nonlinear force $F_{nl}[x]$ can be expressed as[1]:

$$\begin{aligned} &\textbf{a.} \quad \text{if } x(t) \leq g,\ F_{nl}[x](t) = 0 \\ &\textbf{b.} \quad \text{if } x(t) > g,\ F_{nl}[x](t) = -k^*(x(t) - g), \end{aligned} \tag{4.1}$$

[1]The operator notation $F_{nl}[x]$ is adopted so as to highlight the fact that although the nonlinear force depends on the displacement x only, the value of the nonlinear force at time t do not necessarily depend on the value $x(t)$ only. For instance, in the case of a hysteretic nonlinearity such as Coulomb friction, the value of the nonlinear force at t depends on $x(t)$ *and* on the state (stick or slip) of the system at the same time. Therefore, F_{nl} must be interpreted as a functional of x, and $F_{nl}[x]$ as a function of t.

General variables	
t	time
ω, T	frequency and period of excitation
n_h	number of harmonics
n_t	number of sampling points in the time domain, over a period of motion
Variables used for the example systems	
x, x_1, x_2	degrees of freedom (DOFs)
m, m_1, m_2	mass coefficients
c, c_1, c_2	viscous damping coefficients
k, k_1, k_2	stiffness coefficients
F, F_1, F_2	linear excitation
F_{nl}	nonlinear impact or friction force
x^*	additional nonlinear DOF
k^*	nonlinear interface stiffness
g	clearance
N	normal load
μ	friction coefficient
Variables describing general structures	
$\mathbf{x}, \mathbf{u}$	DOFs (before and after change of coordinates)
$\mathbf{M}, \mathbf{K}, \mathbf{C}$	mass, stiffness and viscous damping matrices
$\mathbf{f}_l$	linear, external forces
$\mathbf{f}_{nl}$	nonlinear impact or friction forces
$\mathbf{x}^*$	additional nonlinear DOFs
$\mathbf{x}^{*,bc}$	additional nonlinear DOFs which respect exactly the nonlinear boundary conditions
k^*	nonlinear interface stiffness coefficient
$\mathbf{P}$	matrix of change of coordinates
$\mathbf{I}$	identity matrix
$\mathbf{\Lambda}$	linear part of the jacobian of system of nonlinear, frequency-domain equations
Subscripts, superscripts and accents	
k	harmonic number
g	ground contacting DOFs
m, s	master and slave DOFs
l	linear DOFs
c	contact DOFs
$\tilde{}$	accent used to specify augmented variables that take into account the additional nonlinear DOFs

Table 4.1: Nomenclature. Roman letters represent scalar variables (F, t, etc.). Bold-faced, lower-case letters represent vector variables ($\mathbf{x}$, $\mathbf{u}$, etc.). Bold-faced, capital letters represent matrices ($\mathbf{M}$, $\mathbf{K}$, $\mathbf{C}$, etc.). Underlined letters represent complex variables.

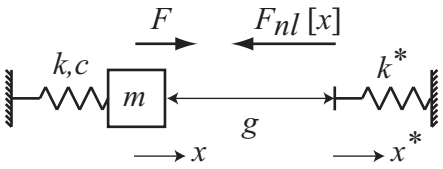

Figure 4.1: Simple system with external, displacement-dependent nonlinear force.

where g corresponds to the initial clearance and k^* is the stiffness of the elastic obstacle.

In Eq. (4.1) the nonlinear force is defined for any possible value of x. This of crucial importance for the HFT method, since it is based on successive evaluations over a period of motion of $F_{nl}[x]$ for iteratively guessed values of x which do not necessarily represent the exact dynamics of the system. That is, the two sides of the equation of motion

$$m\ddot{x}(t) + c\dot{x}(t) + kx(t) - F(t) = F_{nl}[x](t) \tag{4.2}$$

are evaluated for guessed, periodic time histories of x until the agreement between the two sides is sufficient – this being determined by comparing the Fourier coefficients of the periodic time histories representing each side of Eq. (4.2).

Because of this requirement, the HFT method is not directly applicable to the study of systems where a nonlinear force can be defined for certain values of x only. This happens for instance when the elastic structure interacts with an infinitely stiff obstacle, as shown in Fig. 4.2. Here, the nonlinearity defining the contact interaction between the mass and the obstacle can be characterized by:

$$\begin{aligned}
&\textbf{a.} \quad \text{if } x(t) \leq g,\ F_{nl}[x](t) = 0 \\
&\textbf{b.} \quad x(t) > g \text{ has no physical meaning} \\
&\textbf{c.} \quad \dot{x}(t^+_{impact}) = -\dot{x}(t^-_{impact}) \text{ when purely} \\
&\qquad\quad \text{elastic impact occurs at } t_{impact}.
\end{aligned} \tag{4.3}$$

Although the system is described by a simple equation of motion,

$$m\ddot{x}(t) + c\dot{x}(t) + kx(t) - F(t) = 0, \tag{4.4}$$

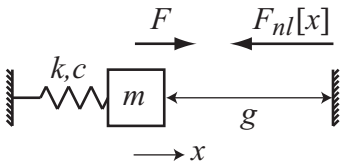

Figure 4.2: Simple system impacting an infinitely stiff obstacle.

its dynamics can become very complex as Eq. (4.4) must be verified on contiguous time domains satisfying the initial conditions (b) and (c) when impacts occur. Therefore, the nonlinear behavior of the system does not stem from the presence of a nonlinear term in the equation of motions: it depends only on kinematics conditions applied to the displacement x. As a consequence, the absence of an explicit nonlinear force $F_{nl}[x]$ in Eq. (4.4) hinders the direct application of the HFT method to the study of such systems.

One should also note that the same kind of limitation holds for structures directly rubbing on infinitely stiff obstacles.

4.2.2 Overview of the proposed approach

In order to extend the applicability of the HFT method to systems with elastic impact or Coulomb friction, a simple modification is proposed. Since the behavior of the system presented in Fig. 4.1 must converge towards the behavior of the system presented in Fig. 4.2 when the stiffness of the elastic stop tends towards infinity, the method of analysis introduced hereafter adds to the system's DOF x an additional, artificial DOF x^* associated with a stiffness k^*, whose value is iteratively increased towards infinity. In other words, the goal of the method is to study systems with nonlinearities of decreasing flexibility until they converge towards the actual system interacting with infinitely stiff obstacles.

As mentioned above, the HFT method is readily applicable to systems similar to the one depicted in Fig. 4.1. However, strong numerical difficulties arise when the stiffness k^* of the elastic stop increases and reaches values several orders of magnitude higher

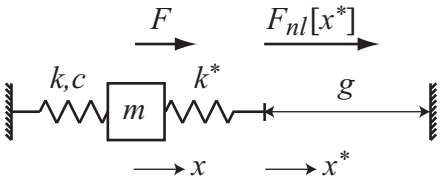

Figure 4.3: New equivalent nonlinear system adopted in the proposed approach.

that the stiffness k of the system itself, that is, values required to accurately capture the behavior of a system impacting an infinitely stiff obstacle. Because of this, the dynamics of the system – described by the frequency-domain representation of Eq. (4.2) – cannot be solved numerically in most cases. Among the main reasons behind these difficulties, one should mention the fact that as the additional stiffness k^* increases, (1) the nonlinear force $F_{nl}[x]$ resembles more a dirac impulse, which is very hard to accurately represent by a truncated Fourier series, and (2), the right-hand side of Eq. (4.2) becomes very sensitive to small variations of x, which makes the nonlinear system representing Eq. (4.2) in the frequency domain unstable.

In order to circumvent the difficulties stemming from the Fourier representation of the nonlinear contact forces, the system is augmented with an additional DOF and an additional stiffness in a way that differs slightly from the previous approach discussed, as depicted in Fig. 4.3. Again, as k^* increases towards infinity, the behavior of this new system converges towards the behavior of the system presented in Fig. 4.2.

Now, although a nonlinear contact force $F_{nl}[x^*]$ can still be defined as required by the regular HFT method, the equations of motions are solved in a way that directly enforces the nonlinear kinematic contact conditions, instead of deducing them from the effect of the nonlinear contact force. In other words, instead of iteratively adjusting the value of x so as to make x and $F_{nl}[x]$ satisfy Eq. (4.2) – which in this case would raise the same kind of numerical difficulties as the ones mentioned above – a new equation that does not

involve the nonlinear force is solved in the frequency domain. The generation of this new equation can be outlined as follows:

1. The frequency-domain, Fourier coefficients of the periodic time history of the additional DOF x^* are guessed. This step can be performed arbitrarily during the first iteration of the solution process, otherwise the Fourier coefficients are usually generated by taking into account the convergence history observed at previous iterations. One should note that this guess is not subject to kinematic constraints, that is, x^* can be generated without respecting the boundary conditions. This means that in the example presented above, it is possible for x^* to reach values greater than the clearance g.

2. The frequency-domain, Fourier coefficients of the periodic time histories of the linear DOF of the system x are deduced from those of x^*. As further explained in the following section of this chapter, this step involves only trivial linear calculations and it is a natural consequence of the frequency-domain representation of the equations of motion of the system.

3. The time history of x is deduced from the coefficients obtained at step (2) by an Inverse Fast Fourier Transform (IFFT).

4. Taking into account the time history of x *and* the nonlinear boundary conditions, a new time history of x^* is calculated. Let $x^{*,bc}$ denote this new time history, where the superscript bc stands for "boundary conditions".

5. The frequency domain, Fourier coefficients of $x^{*,bc}$ are computed by applying a Fast Fourier Transform (FFT) to the corresponding time history calculated at step (4).

6. The equation to be solved can now be formed: it is the frequency domain representation of the equality

$$x^* = x^{*,bc}, \tag{4.5}$$

that is, it consists in comparing the values of the Fourier coefficients calculated previously for x^* and $x^{*,bc}$. If this equation is not satisfactorily satisfied, the nonlinear algorithm used to solve it generates a better guess for the Fourier coefficients of x^*, and restarts at step (1).

When convergence is achieved, x^* tends towards $x^{*,bc}$, which always satisfies the boundary conditions; x^* might still violate these nonlinear boundary conditions, however, the amplitude of these violations is directly controlled by the degree of precision requested for solving Eq. (4.5) and can be made as small as desired.

Since the displacement of the structure always has better continuity and derivability properties than the acceleration and the nonlinear force, Eq. (4.5) is much easier to handle on a numerical point of view than Eq. (4.2). That is, the set of nonlinear equations made of the Fourier coefficients of x^* and $x^{*,bc}$ representing Eq. (4.5) in the frequency domain is more stable than the set of equations representing Eq. (4.2) when the unmodified HFT method is considered, as illustrated later in this chapter.

The following section extends these introductory concepts and remarks to the case of elastic structures experiencing intermittent contact and friction, these nonlinear interactions occurring either between adjacent components of the structure or between the structure and an infinitely rigid obstacle.

4.3 Method of analysis

4.3.1 Time domain equations of motion

The general equations of motion of an elastic structure are expressed as

$$\mathbf{M}\ddot{\mathbf{x}}(t) + \mathbf{C}\dot{\mathbf{x}}(t) + \mathbf{K}\mathbf{x}(t) = \mathbf{f}_l(t) + \mathbf{f}_{nl}[\mathbf{x}](t), \tag{4.6}$$

where $\mathbf{M}$, $\mathbf{C}$ and $\mathbf{K}$ are respectively its mass, damping and stiffness matrices; $\mathbf{f}_l$ represents a periodic, external excitation which is linear, that is, it does not depend on the response of the structure it is applied to; and $\mathbf{f}_{nl}[\mathbf{x}]$ represents the nonlinear contact forces that stem from the motion of the structure. The work presented herein limits its scope to the case of localized nonlinear contact forces representing Coulomb friction and purely elastic impact interactions, but the method of analysis presented hereafter is readily applicable to other kinds of displacement-dependent nonlinearities.

Since the nonlinearities considered in this chapter are localized, the degrees of freedom of the structure can be re-ordered as

$$\mathbf{x}(t) = \begin{bmatrix} \mathbf{x}^g(t) \\ \mathbf{x}^m(t) \\ \mathbf{x}^s(t) \\ \mathbf{x}^l(t) \end{bmatrix}, \tag{4.7}$$

where each of these groups of DOFs corresponds to a specific type of nonlinear interaction:

- $\mathbf{x}^g$ represents the DOFs contacting an infinitely rigid surface, referred to hereafter as *ground*. The ground can be viewed as a very stiff obstacle the elastic structure might contact while vibrating.

- $\mathbf{x}^m$ and $\mathbf{x}^s$ correspond to the vectors of DOFs that contact each other directly, that is, they represent pairs of *master* and *slave* DOFs of the structure. For instance,

they might represent DOFs of two adjacent components of the structure which are separated by a clearance but which might contact each other when the system is excited.

- $\mathbf{x}^l$ represents all the other DOFs of the structure. Since the contact interactions considered here necessarily fall into one of the previous two categories, $\mathbf{x}^l$ contains linear DOFs only.

Therefore, considering this ordering of the structure DOFs, and taking into account the law of action and reaction for the pairs of master and slave DOFs, the vector of the nonlinear forces can be written as

$$\mathbf{f}_{nl}[\mathbf{x}](t) = \begin{bmatrix} \mathbf{f}_{nl}^g[\mathbf{x}^g](t) \\ \mathbf{f}_{nl}^m[\mathbf{x}^m - \mathbf{x}^s](t) \\ -\mathbf{f}_{nl}^m[\mathbf{x}^m - \mathbf{x}^s](t) \\ \mathbf{0} \end{bmatrix}. \tag{4.8}$$

In order to simplify the analysis, a trivial transformation is applied to the equations of motion of the structure so as to transform the pairs of master and slave DOFs into equivalent ground-contacting DOFs. Defining the transformation matrix

$$\mathbf{P} = \frac{1}{2} \begin{bmatrix} 2\,\mathbf{I}^g & \mathbf{0} & \mathbf{0} & \mathbf{0} \\ \mathbf{0} & \mathbf{I}^m & \mathbf{I}^m & \mathbf{0} \\ \mathbf{0} & -\mathbf{I}^m & \mathbf{I}^m & \mathbf{0} \\ \mathbf{0} & \mathbf{0} & \mathbf{0} & 2\,\mathbf{I}^l \end{bmatrix}, \tag{4.9}$$

and introducing a new set of DOFs $\mathbf{u}$ that represents the relative displacement of the master

DOFs $\mathbf{x}^m$ with respect to the slave DOFs $\mathbf{x}^s$,

$$\mathbf{u}(t) = \begin{bmatrix} \mathbf{u}^g(t) \\ \mathbf{u}^m(t) \\ \mathbf{u}^s(t) \\ \mathbf{u}^l(t) \end{bmatrix} = \mathbf{P}^{-1}\mathbf{x}(t) = \begin{bmatrix} \mathbf{x}^g(t) \\ \mathbf{x}^m(t) - \mathbf{x}^s(t) \\ \mathbf{x}^m(t) + \mathbf{x}^s(t) \\ \mathbf{x}^l(t) \end{bmatrix}, \tag{4.10}$$

Eq. (4.6) becomes

$$\mathbf{P}^{-1}\,\mathbf{MP}\begin{bmatrix} \ddot{\mathbf{u}}^g(t) \\ \ddot{\mathbf{u}}^m(t) \\ \ddot{\mathbf{u}}^s(t) \\ \ddot{\mathbf{u}}^l(t) \end{bmatrix} + \mathbf{P}^{-1}\,\mathbf{CP}\begin{bmatrix} \dot{\mathbf{u}}^g(t) \\ \dot{\mathbf{u}}^m(t) \\ \dot{\mathbf{u}}^s(t) \\ \dot{\mathbf{u}}^l(t) \end{bmatrix} + \mathbf{P}^{-1}\,\mathbf{KP}\begin{bmatrix} \mathbf{u}^g(t) \\ \mathbf{u}^m(t) \\ \mathbf{u}^s(t) \\ \mathbf{u}^l(t) \end{bmatrix} = \mathbf{P}^{-1}\,\mathbf{f}_l(t) + \begin{bmatrix} \mathbf{f}_{nl}^g[\mathbf{u}^g](t) \\ 2\cdot\mathbf{f}_{nl}^m[\mathbf{u}^m](t) \\ \mathbf{0} \\ \mathbf{0} \end{bmatrix}. \tag{4.11}$$

This change of coordinates eliminates the need of distinguishing the ground-contacting DOFs from the pairs of contacting master and slave DOFs, as the expressions of the nonlinear forces acting on $\mathbf{u}^g$ and $\mathbf{u}^m$ take similar forms. Furthermore, since there are no longer nonlinear contact forces acting on $\mathbf{u}^s$, the size of the nonlinear system is reduced, which yields substantial benefits in terms of the numerical handling of these equations.

Thus, the study of the dynamics of a structure featuring these two types of DOFs can be reduced to the study of an equivalent structure featuring ground-contacting DOFs only, where relative DOFs displacement are substituted to the original pairs of contacting DOFs. Therefore, the equations of motion of such a structure can always be written – without loss

of generality – in the following form[2],

$$\begin{bmatrix} \mathbf{M}^{cc} & \mathbf{M}^{cl} \\ \mathbf{M}^{lc} & \mathbf{M}^{ll} \end{bmatrix} \begin{bmatrix} \ddot{\mathbf{x}}^c(t) \\ \ddot{\mathbf{x}}^l(t) \end{bmatrix} + \begin{bmatrix} \mathbf{C}^{cc} & \mathbf{C}^{cl} \\ \mathbf{C}^{lc} & \mathbf{C}^{ll} \end{bmatrix} \begin{bmatrix} \dot{\mathbf{x}}^c(t) \\ \dot{\mathbf{x}}^l(t) \end{bmatrix} + \begin{bmatrix} \mathbf{K}^{cc} & \mathbf{K}^{cl} \\ \mathbf{K}^{lc} & \mathbf{K}^{ll} \end{bmatrix} \begin{bmatrix} \mathbf{x}^c(t) \\ \mathbf{x}^l(t) \end{bmatrix} = \begin{bmatrix} \mathbf{f}_l^c(t) \\ \mathbf{f}_l^l(t) \end{bmatrix} + \begin{bmatrix} \mathbf{f}_{nl}^c[\mathbf{x}^c](t) \\ \mathbf{0} \end{bmatrix}, \quad (4.12)$$

where $\mathbf{x}^c$ represents the vector of the nonlinear, ground-contacting DOFs – possibly obtained with the aforementioned change of coordinates –, and $\mathbf{x}^l$ is the vector of the linear DOFs.

4.3.2 Augmented equations of motion

In order to handle the nonlinear contact interactions – now reduced to interactions of the structure-to-ground type –, the degrees of freedom of the system are augmented by a set of additional DOFs, $\mathbf{x}^*$, as discussed in the introductory example:

$$\tilde{\mathbf{x}}(t) = \begin{bmatrix} \mathbf{x}^*(t) \\ \mathbf{x}^c(t) \\ \mathbf{x}^l(t) \end{bmatrix}. \quad (4.13)$$

The vector $\mathbf{x}^*$ of the additional DOFs has the same size as $\mathbf{x}^c$, since the additional DOFs are uniquely associated with each of the contact DOFs. The equations of motion of the augmented system are now

$$\tilde{\mathbf{M}}\ddot{\tilde{\mathbf{x}}}(t) + \tilde{\mathbf{C}}\dot{\tilde{\mathbf{x}}}(t) + \tilde{\mathbf{K}}\tilde{\mathbf{x}}(t) = \tilde{\mathbf{f}}_l(t) + \tilde{\mathbf{f}}_{nl}[\tilde{\mathbf{x}}](t) \quad (4.14)$$

where the new mass and damping matrices are simply filled with extra zeros

$$\tilde{\mathbf{M}} = \begin{bmatrix} \mathbf{0} & \mathbf{0} & \mathbf{0} \\ \mathbf{0} & \mathbf{M}^{cc} & \mathbf{M}^{cl} \\ \mathbf{0} & \mathbf{M}^{lc} & \mathbf{M}^{ll} \end{bmatrix}, \ \tilde{\mathbf{C}} = \begin{bmatrix} \mathbf{0} & \mathbf{0} & \mathbf{0} \\ \mathbf{0} & \mathbf{C}^{cc} & \mathbf{C}^{cl} \\ \mathbf{0} & \mathbf{C}^{lc} & \mathbf{C}^{ll} \end{bmatrix}, \quad (4.15)$$

[2]Note that for the sake of generality the DOFs of the structure are referred to as $\mathbf{x}$ again, instead of $\mathbf{u}$.

and where the stiffness matrix is augmented so as to take into account the additional stiffnesses associated with the DOFs grouped in $\mathbf{x}^*$:

$$\tilde{\mathbf{K}} = \begin{bmatrix} k^*\mathbf{I}^c & -k^*\mathbf{I}^c & \mathbf{0} \\ -k^*\mathbf{I}^c & \mathbf{K}^{cc} + k^*\mathbf{I}^c & \mathbf{K}^{cl} \\ \mathbf{0} & \mathbf{K}^{lc} & \mathbf{K}^{ll} \end{bmatrix}. \tag{4.16}$$

Similarly, the expressions of the linear and nonlinear forces are modified so as to accommodate the new DOFs:

$$\tilde{\mathbf{f}}_l(t) = \begin{bmatrix} \mathbf{0} \\ \mathbf{f}_l^c(t) \\ \mathbf{f}_l^l(t) \end{bmatrix}, \; \tilde{\mathbf{f}}_{nl}(t) = \begin{bmatrix} \mathbf{f}_{nl}^*[\mathbf{x}^*](t) \\ \mathbf{0} \\ \mathbf{0} \end{bmatrix}. \tag{4.17}$$

One should note that the nonlinearities due to the contact interactions are transferred from the original contact DOFs $\mathbf{x}^c$ to the additional DOFs $\mathbf{x}^*$.

These modifications yield equations of motions for $\mathbf{x}^*$ that correspond to the quasi-static equilibrium

$$k^*(\mathbf{x}^*(t) - \mathbf{x}^c(t)) = \mathbf{f}_{nl}^*[\mathbf{x}^*](t) \tag{4.18}$$

from which it can be deduced that, as the values of the stiffnesses k^* tend towards infinity, the additional DOFs $\mathbf{x}^*$ and the original contact DOFs $\mathbf{x}^c$ converge towards each other:

$$\mathbf{x}^*(t) \xrightarrow[k^* \to \infty]{} \mathbf{x}^c(t). \tag{4.19}$$

Therefore, the nonlinear contact force deduced from the displacement of $\mathbf{x}^*$ tends towards the actual contact force that would be applied to the DOFs $\mathbf{x}^c$ should the system interact directly with the ground:

$$\mathbf{f}_{nl}^*[\mathbf{x}^*](t) \xrightarrow[k^* \to \infty]{} \mathbf{f}_{nl}^c[\mathbf{x}^c](t). \tag{4.20}$$

In other words, the dynamics of the augmented system tends toward the dynamics of the original ground-contacting structure as the value of the stiffness increases.

4.3.3 Frequency-domain equations of motion

Now that the equivalence of the dynamics of the augmented and original systems has been established when k^* tends towards infinity, the equations of motion of the augmented system can be expressed in the frequency domain. When the steady-state response of the structure is assumed to be periodic, the displacement $\tilde{\mathbf{x}}$ and the linear force $\tilde{\mathbf{f}}_l$ can be written as Fourier series of harmonic functions. Assuming that keeping n_h harmonics guarantees an accurate approximation of the dynamics of the structure, they can be expressed as:

$$\tilde{\mathbf{x}}(t) = \text{Re}\left(\sum_{k=0}^{n_h} \begin{bmatrix} \underline{\mathbf{x}}_k^* \\ \underline{\mathbf{x}}_k^c \\ \underline{\mathbf{x}}_k^l \end{bmatrix} e^{\underline{j}k\omega t}\right), \tag{4.21}$$

$$\tilde{\mathbf{f}}_l(t) = \text{Re}\left(\sum_{k=0}^{n_h} \begin{bmatrix} \mathbf{0} \\ \underline{\mathbf{f}}_{l,k}^c \\ \underline{\mathbf{f}}_{l,k}^l \end{bmatrix} e^{\underline{j}k\omega t}\right). \tag{4.22}$$

Similarly, the nonlinear forces acting on the augmented system can be written as:

$$\tilde{\mathbf{f}}_{nl}^*[\mathbf{x}^*](t) = \text{Re}\left(\sum_{k=0}^{n_h} \begin{bmatrix} \underline{\mathbf{f}}_{nl,k}^*(\underline{\mathbf{x}}_0^*, \dots \underline{\mathbf{x}}_{n_h}^*) \\ \mathbf{0} \\ \mathbf{0} \end{bmatrix} e^{\underline{j}k\omega t}\right). \tag{4.23}$$

Now, applying the Harmonic Balance Method to Eq. (4.14) yields a set of n_h complex, nonlinear, coupled equations:

$$\begin{bmatrix} \underline{\mathbf{\Lambda}}_k^{*,*} & \underline{\mathbf{\Lambda}}_k^{*,c} & \underline{\mathbf{\Lambda}}_k^{*,l} \\ \underline{\mathbf{\Lambda}}_k^{c,*} & \underline{\mathbf{\Lambda}}_k^{c,c} & \underline{\mathbf{\Lambda}}_k^{c,l} \\ \underline{\mathbf{\Lambda}}_k^{l,*} & \underline{\mathbf{\Lambda}}_k^{l,c} & \underline{\mathbf{\Lambda}}_k^{l,l} \end{bmatrix} \begin{bmatrix} \underline{\mathbf{x}}_k^* \\ \underline{\mathbf{x}}_k^c \\ \underline{\mathbf{x}}_k^l \end{bmatrix} - \begin{bmatrix} \mathbf{0} \\ \underline{\mathbf{f}}_{l,k}^c \\ \underline{\mathbf{f}}_{l,k}^l \end{bmatrix} = \begin{bmatrix} \underline{\mathbf{f}}_{nl,k}^*(\underline{\mathbf{x}}_0^*, \dots \underline{\mathbf{x}}_{n_h}^*) \\ \mathbf{0} \\ \mathbf{0} \end{bmatrix} \tag{4.24}$$

where the (l, c) block of the linear part of the jacobian of this system of equations is defined as:

$$\underline{\mathbf{\Lambda}}_k^{l,c} = -(k\omega)^2 \mathbf{M}^{l,c} + \underline{j}k\omega \mathbf{C}^{l,c} + \mathbf{K}^{l,c}, \tag{4.25}$$

with similar expressions for $\underline{\mathbf{\Lambda}}_k^{l,l}$, $\underline{\mathbf{\Lambda}}_k^{l,*}$ etc.

4.3.4 Solution algorithm

As briefly explained in the introductory example, the algorithm used to solve the nonlinear dynamics of the system is based on both the frequency-domain and the time-domain representations of Eq. (4.24).

When the traditional HFT method is used, Eq. (4.24) is the set of nonlinear equations being directly solved. This requires extracting the Fourier coefficients of the nonlinear forces (the right-hand side of Eq. (4.24)) from the calculation of its time history in the time domain; the right-hand side of Eq. (4.24) is indeed the frequency-domain representation of the nonlinearities applied to the structure.

The modification of the HFT proposed here pushes even further the dichotomies that can be defined between the linear and nonlinear parts of the system and the frequency and time domains of analysis. It is based on a new nonlinear equation that stems from (1) the study of the linear dynamics of the system in the frequency domain – the left-hand side of Eq. (4.24) –, and (2) a strict enforcement in the time domain of the nonlinear boundary conditions – the time domain representation of the right-hand side of Eq. (4.24).

The solution algorithm unfolds as follows:

1. An initial value is given to k^*. At the beginning of the algorithm, this value can be chosen to be very low so as to "soften" the nonlinearity and avoid possible numerical convergence problems.

2. The frequency-domain, Fourier coefficients of the nonlinear additional DOFs $\mathbf{x}^*$ are guessed.

   When this is done for the first time, an arbitrary guess must be provided. In particular, if k^* is very small, it makes sense to choose for $\mathbf{x}^*$ the linear solution obtained

when the nonlinearities are not taken into account, since it is necessarily very close from the solution sought.

Otherwise, a guess that takes into account the evolution of the convergence over the previous iterations is automatically provided by the nonlinear solver. A modified version of the hybrid Powell algorithm [107, 108] has been found to produce excellent results in terms of speed and convergence qualities.

Finally, one should note that no constraints are placed upon the generation of the guess $\mathbf{x}^*$. In particular, these coefficients can lead to time histories of the nonlinear displacements that violate the nonlinear boundary conditions associated with non-penetration or Coulomb friction. However, these violations are expected to become smaller as the algorithm makes these guesses converge towards displacements that respect the boundary conditions.

3. The frequency-domain, Fourier coefficients of the periodic time histories of the linear DOFs $\mathbf{x}^c$ and $\mathbf{x}^l$ are deduced from those of $\mathbf{x}^*$. This is done by substituting the coefficients $\underline{\mathbf{x}}_k^*$ into the subsets of equations of Eq. (4.24) which are associated with the coefficients $\underline{\mathbf{x}}_k^c$ and $\underline{\mathbf{x}}_k^l$:

$$\begin{bmatrix} \underline{\mathbf{x}}_k^c \\ \underline{\mathbf{x}}_k^l \end{bmatrix} = \begin{bmatrix} \underline{\mathbf{\Lambda}}_k^{c,c} & \underline{\mathbf{\Lambda}}_k^{c,l} \\ \underline{\mathbf{\Lambda}}_k^{l,c} & \underline{\mathbf{\Lambda}}_k^{l,l} \end{bmatrix}^{-1} \begin{bmatrix} \underline{\mathbf{f}}_{l,k}^c - \underline{\mathbf{\Lambda}}_k^{c,*} \underline{\mathbf{x}}_k^* \\ \underline{\mathbf{f}}_{l,k}^l - \underline{\mathbf{\Lambda}}_k^{l,*} \underline{\mathbf{x}}_k^* \end{bmatrix}. \tag{4.26}$$

As a physical interpretation of this step, one can observe that the Fourier coefficients $\underline{\mathbf{x}}_k^c$ and $\underline{\mathbf{x}}_k^l$ correspond to the motion of the linear part of the structure when the linear force and the displacements at the nonlinear interface are imposed.

4. The time histories of the original contact DOFs $\mathbf{x}^c$ are deduced from the coefficients obtained at the previous step by IFFTs.

5. Now, quasi-static calculations are performed in the time domain to find the time histories of $\mathbf{x}^{*,bc}$ that are compatible with (1) the imposed time histories of $\mathbf{x}^{c}$ obtained at the previous step, and (2) the nonlinear boundary conditions[3].

6. The Fourier coefficients $\underline{\mathbf{x}}_k^{*,bc}$ describing the time histories of $\mathbf{x}^{*,bc}$ calculated above are obtained by FFT.

7. The nonlinear equations to be solved can now be formed. They are functions of the nonlinear unknowns $\underline{\mathbf{x}}_k^{*}$, and are expressed as:

$$\mathcal{F}_k(\underline{\mathbf{x}}_0^{*}, \ldots, \underline{\mathbf{x}}_{n_h}^{*}) = \underline{\mathbf{x}}_k^{*} - \underline{\mathbf{x}}_k^{*,bc} = \mathbf{0} \tag{4.27}$$

   As stated previously, these equations do not involve the nonlinear forces. Actually, the calculation of the nonlinear forces is not necessary with this approach, which emphasises the effects of the nonlinearities on the displacement of the boundary DOFs only.

   When these equations are verified, the Fourier coefficients $\underline{\mathbf{x}}_0^{*} \ldots \underline{\mathbf{x}}_{n_h}^{*}$ match exactly the coefficients $\underline{\mathbf{x}}_0^{*,bc} \ldots \underline{\mathbf{x}}_{n_h}^{*,bc}$ obtained from the time histories of the additional DOFs when the boundary conditions are enforced.

8. If these equations are not satisfied, new Fourier coefficients $\underline{\mathbf{x}}_k^{*}$ are provided by the nonlinear solver, and the algorithm restarts at step (3).

9. When convergence is reached, the value of the additional stiffness k^* is increased[4] and the algorithm restarts at step (3), unless the results obtained show that k^* has

[3] Details of these calculations for systems with impact or Coulomb friction are presented later in this chapter.

[4] A simple geometric progression can be used for k^* in most cases. The choice of the geometric ratio of the series is a trade off between speed (large ratios) and robustness (low ratios for which the solution obtained at the end of an iteration is close from the solution sought at the following iteration).

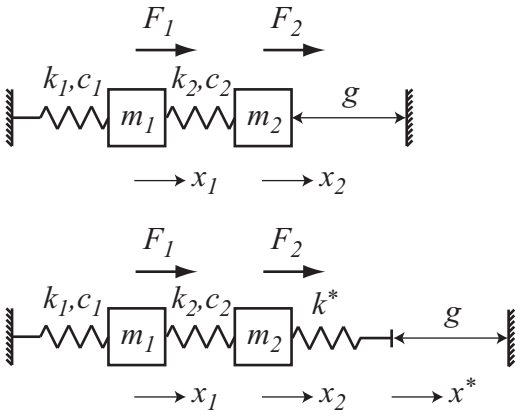

Figure 4.4: Simple two-DOF structure impacting an infinitely stiff obstacle and its equivalent, augmented representation. F_1 and F_2 are linear, periodic functions of t and represent an external excitation. g is the clearance between the DOF x_2 and the obstacle.

already reached a value high enough to consider that the dynamics of the augmented system coincides with the dynamics of the original system.

When the algorithm successfully stops, the DOFs computed in steps (1) to (9) satisfy the following relations:

- The dynamics of the linear DOFs $\mathbf{x}^c$ is consistent with the displacements of the guessed DOFs $\mathbf{x}^*$, this being a trivial consequence of Eq. (4.26).
- The displacements of the nonlinear DOFs $\mathbf{x}^{*,bc}$ are consistent with the displacements of the linear DOFs $\mathbf{x}^c$ *and* with the nonlinear boundary conditions.
- The displacements of the nonlinear DOFs $\mathbf{x}^*$ and $\mathbf{x}^{*,bc}$ are identical.
- As k^* increases towards infinity, $\mathbf{x}^c$ tends towards $\mathbf{x}^*$.

This algorithm can therefore be summarized by a double convergence:

$$\mathbf{x}^c \xrightarrow[k^* \to \infty]{} \mathbf{x}^* \xrightarrow[\text{being solved}]{\text{As Eqs. (4.27) are}} \mathbf{x}^{*,bc} \tag{4.28}$$

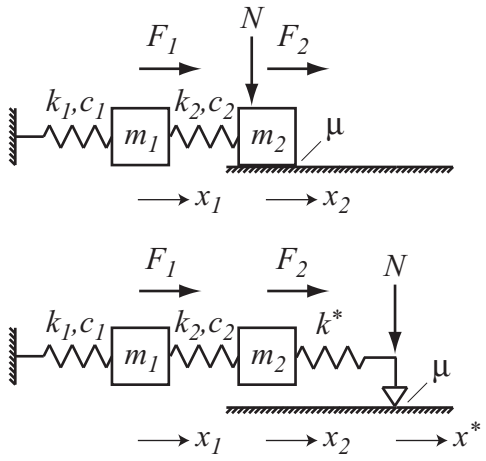

Figure 4.5: Simple two-DOF structure with friction and its equivalent, augmented representation. F_1 and F_2 are linear, periodic functions of t and represent an external excitation. N represents the normal load applied to the friction DOF, and μ is the friction coefficient of the contact interface.

The first one corresponds to the convergence of the behavior of the augmented system towards the behavior of the original system as k^* increases, and the second reflects the enforcement of the nonlinear boundary conditions applied to the additional nonlinear DOFs.

4.3.5 Time-domain treatment of the boundary conditions

A critical part of the algorithm outlined above is the calculation of the effect of the nonlinear boundary conditions on the nonlinear DOFs, performed during step 5. During this step, the time histories of the nonlinear DOFs are calculated so as to be consistent with (1) the time histories of the linear DOFs and (2), with the nonlinear boundary conditions.

The time-domain treatment of the boundary conditions is presented here for both impact and Coulomb friction. The simple systems depicted in Figs. 4.4 and 4.5 are used here to illustrate this treatment; a detailed analysis of their behavior is presented later in this chapter.

Impact against an infinitely stiff obstacle

When the algorithm enters step 5, the time histories of the linear DOFs $\mathbf{x}^c$ are known since they are deduced from the guess made on $\mathbf{x}^*$. Since they are obtained from inverse fast Fourier transforms, these time histories are represented by a finite set of values equally spaced in the time interval $[0, T]$, where T is the period of motion of the structure, given by $T = 2\pi/\omega$. For instance, assuming that the period of motion is sampled with n_t points, the time history of the DOF x_2 of the augmented system presented in Fig. 4.4 is a set of values $x_2(t_1), \ldots, x_2(t_{n_t})$, where t_i is given by:

$$t_i = \frac{T}{n_t}(i-1). \tag{4.29}$$

In this case, the time history of $x^{*,bc}$ – that is, the time history of x^* that satisfies the boundary conditions – is computed in a very simple way:

$$\begin{aligned} &\text{if } \; x^c(t_i) \leq g \;\; \text{ then } \;\; x^{*,bc}(t_i) = x^c(t_i), \\ &\text{if } \; x^c(t_i) > g \;\; \text{ then } \;\; x^{*,bc}(t_i) = g. \end{aligned} \tag{4.30}$$

The n_t discrete values $x^{*,bc}(t_1), \ldots, x^{*,bc}(t_{n_t})$ are therefore easily calculated, and step 6 of the algorithm simply consists in applying a fast Fourier transform to them in order to compute the corresponding Fourier coefficients.

Coulomb friction

The case of nonlinearities involving Coulomb friction is more complicated than the nonlinearities associated with impacts, because of the hysteretic nature of the friction forces. The calculation of the time history of $x^{*,bc}$ is therefore more algorithmic:

1. As in the previous example, the time history of the linear DOF x_2 of the augmented system shown in Fig. 4.5 is represented by a series of discrete values $x_2(t_i)$. When

$i = 1$, $x^{*,bc}(t_1)$ is chosen as follows:

$$x^{*,bc}(t_1) = x_2(t_1). \tag{4.31}$$

This ensures that the tangential component of the contact force applied to x^*, defined as

$$F_t(t_i) = k^*(x^{*,bc}(t_i) - x_2(t_i)) \tag{4.32}$$

is null. In other words, the system is forced to be in the "stick" state when $i = 1$.

2. When i is greater than 1:

   - If the system was in the "stick" state at t_{i-1}:
     - If $k^*(x^{*,bc}(t_{i-1}) - x_2(t_i)) > \mu N$, the "stick" assumption is not valid anymore, and $x^{*,bc}(t_i)$ is given by:

       $$x^{*,bc}(t_i) = x_2(t_i) + \mu N/k^*, \tag{4.33}$$

       which corresponds to a "slip" state where $\dot{x}^{*,bc} < 0$.
     - If $k^*(x^{*,bc}(t_{i-1}) - x_2(t_i)) < -\mu N$, the "stick" assumption is not valid anymore, and $x^{*,bc}(t_i)$ is given by:

       $$x^{*,bc}(t_i) = x_2(t_i) - \mu N/k^*, \tag{4.34}$$

       which corresponds to a "slip" state where $\dot{x}^{*,bc} > 0$.
     - If none of the conditions above are verified, the friction point stays in the "stick" state, i.e.:

       $$x^{*,bc}(t_i) = x^{*,bc}(t_{i-1}). \tag{4.35}$$

   - If the system was in the "slip" state at t_{i-1}:

- If $\dot{x}^{*,bc}(t_{i-1}) < 0$ and $\dot{x}_2(t_i) < 0$, the damper stays in the "slip" state, and $x^{*,bc}(t_i)$ is given by:

$$x^{*,bc}(t_i) = x_2(t_i) + \mu N/k^*. \tag{4.36}$$

- Similarly, if $\dot{x}^{*,bc}(t_{i-1}) > 0$ and $\dot{x}_2(t_i) > 0$, the damper stays in the "slip" state, and $x^{*,bc}(t_i)$ is given by:

$$x^{*,bc}(t_i) = x_2(t_i) - \mu N/k^*. \tag{4.37}$$

- Otherwise, if $\dot{x}_2$ changes its sign, i.e. $\dot{x}_2(t_{i-1}) \cdot \dot{x}_2(t_i) < 0$, the friction point switches to the "stick" state, and therefore

$$x^{*,bc}(t_i) = x^{*,bc}(t_{i-1}). \tag{4.38}$$

3. The operations described in step (2) are performed until i is equal to $2n_t$, i.e., the quasi-static calculations described above are performed over two periods of motion. This is necessary because the choice of the initial condition in step (1) leads to a transient behavior that disappears after the first period of motion: it can be shown indeed that the exact steady cycle (that is, the periodic time history of $x^{*,bc}$) is completely described by the calculations made over the second period of motion, and that this steady cycle is independent of the initial conditions imposed at the beginning of the first period of motion.

Then, the n_t discrete values $x^{*,bc}(t_{n_t+1}), \ldots, x^{*,bc}(t_{2n_t})$ are used in step (6) of the solution algorithm to compute the Fourier coefficients of the time history of $x^{*,bc}$.

4.4 Results

This section presents results obtained from the application of the modified HFT method to the study of (1) the dynamics of simple, spring-mass systems, and (2) the dynamics of

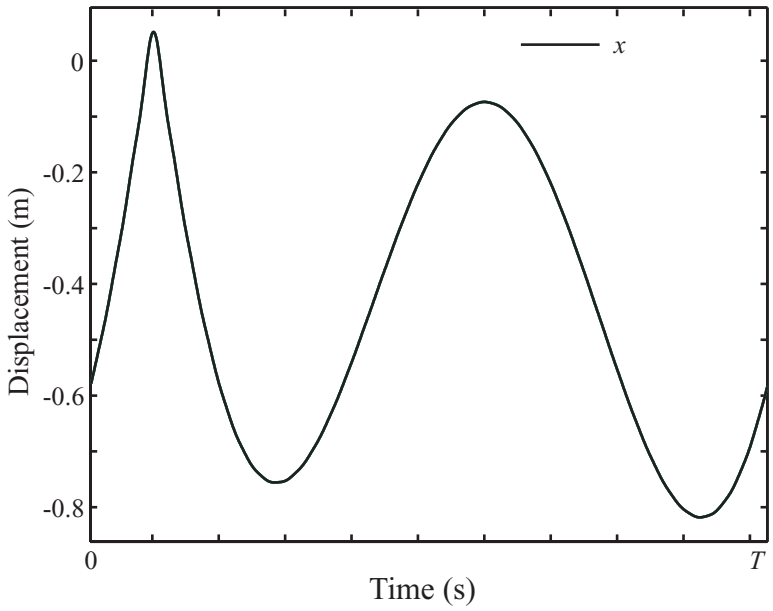

Figure 4.6: Time history over a period of motion of the nonlinear DOF x of the system presented in Fig. 4.3, at $\omega = 1$ rad/s^{-1}.

a more realistic finite element model of complex structure.

4.4.1 Simple one-DOF system with impact

A few results obtained with the simple system shown in Fig. 4.3 are presented first to illustrate the potential difficulties that arise when the traditional HFT method is used, that is, when the Fourier coefficients of the nonlinear contact force are present in the set of frequency-domain nonlinear equations.

The parameters of this simple one-DOF, spring-mass system are given as follows:

$$m = 2 \text{ kg}, \quad c = 1 \text{ kg.s}^{-1},$$

$$k = 2 \text{ N.m}^{-1}, \quad g = 0.05 \text{ m}.$$

The linear excitation applied to the mass is chosen as:

$$F(t) = 1.5\cos(\omega t) + \sin(\omega t).$$

The periodic response of the system is calculated with 100 harmonics at the frequency

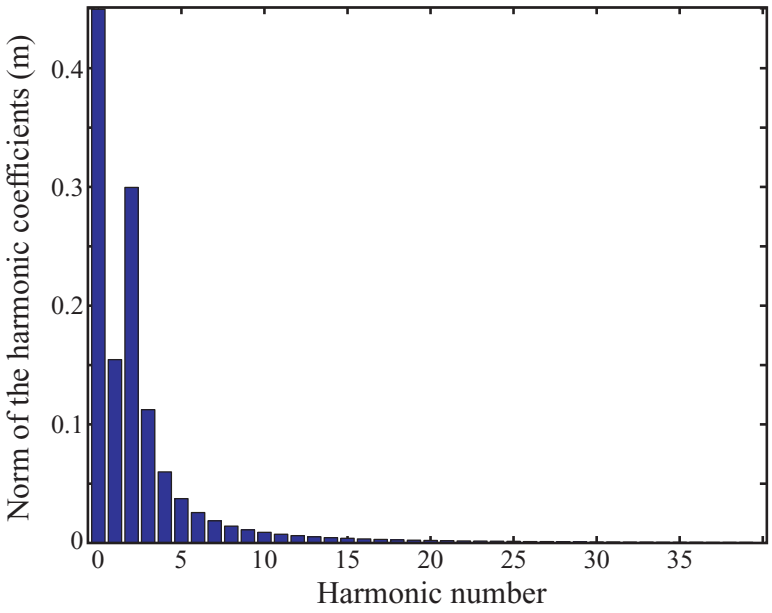

Figure 4.7: Norm of the Fourier coefficients of the nonlinear DOF x at $\omega = 1$ rad/s^{-1}.

$\omega = 1$ rad.s^{-1}. The additional stiffness k^* is set to $2.0 \cdot 10^5$ N.m^{-1}.

The time histories of the contact DOF x and the nonlinear force $F_{nl}[x]$ are presented in Figs. 4.6 and 4.8. The corresponding Fourier coefficients obtained from the FFTs applied to these time histories are shown in Figs. 4.7 and 4.9.

As expected, the nonlinear force is zero when the system does not contact the obstacle, and it looks like a dirac function when x becomes greater than g for a short period of time. Therefore, almost all the harmonics are present in its time history, as shown in Fig. 4.9. On the other hand, although the time history of x is characteristic of a system that impacts elastically a stiff obstacle – the time history features a typical symmetric kink at $t = T/10$ –, the number of harmonics necessary to approximate it accurately is rather limited: 20 harmonics seem sufficient to obtain a precise representation of x over a period of motion. For the contact force, the same number would yield a gross approximation only.

As a consequence, traditional HFT methods are hindered by the necessity to handle a very large number of harmonics to describe accurately the nonlinear contact force, whereas

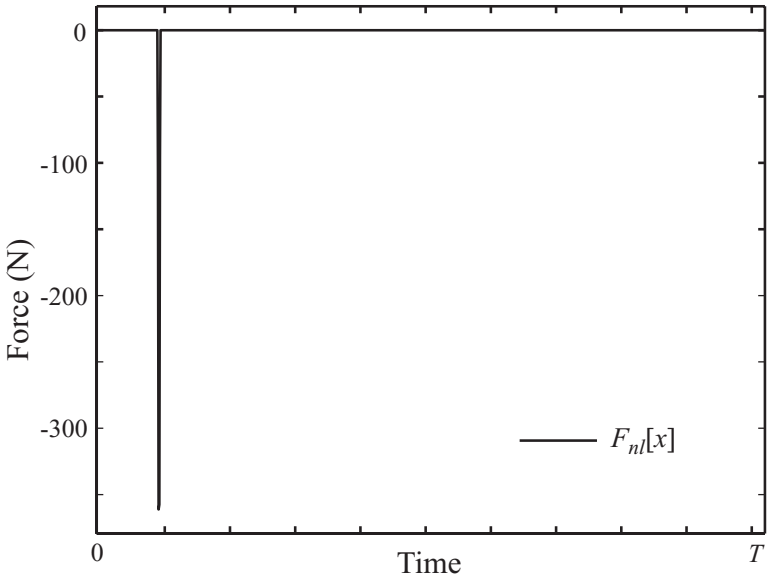

Figure 4.8: Time history over a period of motion of the nonlinear contact force $F_{nl}[x]$, at $\omega = 1$ rad/s^{-1}.

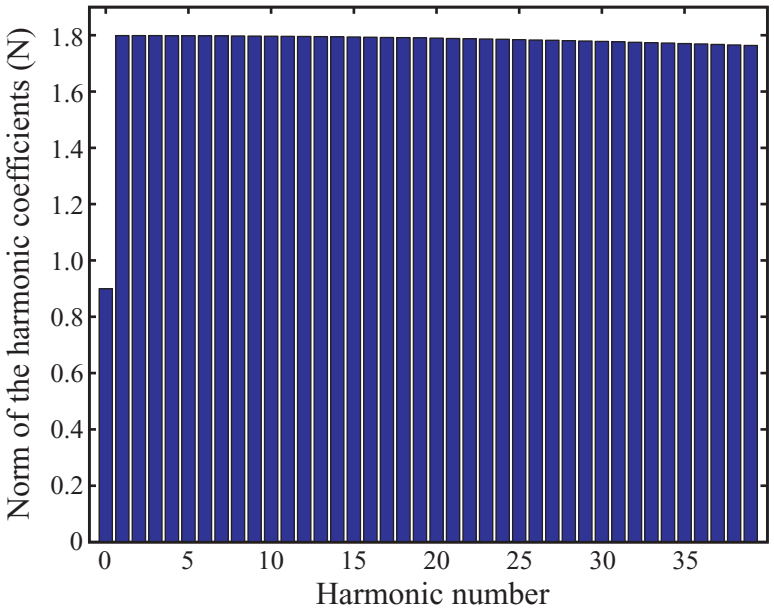

Figure 4.9: Norm of the Fourier coefficients of $F_{nl}[x]$, at $\omega =$ rad/s^{-1}.

the modified method presented here achieves the same accuracy at a lower cost, since the effect of the nonlinear boundary conditions is taken into account in the time domain only.

4.4.2 Two-DOF system with impact

A more complex, two-DOF system with impact is now studied. The system is depicted in Fig. 4.4. It consists in two spring-mass systems impacting an infinitely rigid wall. Its parameters are given as follows:

$$m_1 = m_2 = 2 \text{ kg}, \quad c_1 = c_2 = 1 \text{ kg.s}^{-1},$$
$$k_1 = k_2 = 2 \text{ N.m}^{-1}, \quad g = 0.05 \text{ m}.$$

The linear excitations applied to m_1 and m_2 are chosen as:

$$F_1(t) = 1.5\cos(\omega t) + \sin(\omega t)$$
$$F_2(t) = 0.$$

The frequency response of the system is shown in Fig. 4.10. It is calculated with 20 harmonics, and the value of the additional stiffness of the augmented system is $k^* = 2.0 \cdot 10^6$ N.m^{-1}.

The behavior exhibited is somewhat complicated. For frequencies greater than 2.4 rad.s^{-1}, the amplitude of x_2 is smaller than 0.05, that is, it is smaller than the clearance g, and therefore the system behaves linearly. Then, as ω decreases from 2.4 rad.s^{-1}, the system begins to impact the obstacle. For values close from 2.4 rad.s^{-1}, one impact per period of motion is observed. Then the number of impacts per period gradually increases as ω further decreases: at 0.2 rad.s^{-1} the time history of the contact force exhibits seven impacts, as shown in Fig. 4.11[5].

[5]Again, one should note that in the method of analysis proposed the calculation of the time history of the nonlinear force is not necessary; it is given here for illustration purposes only.

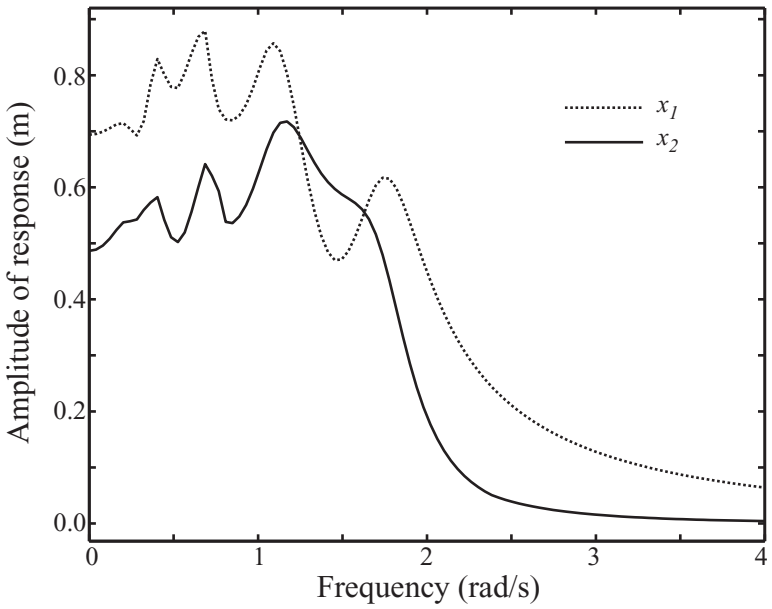

Figure 4.10: Frequency response of the DOFs of the system with impact presented in Fig. 4.4.

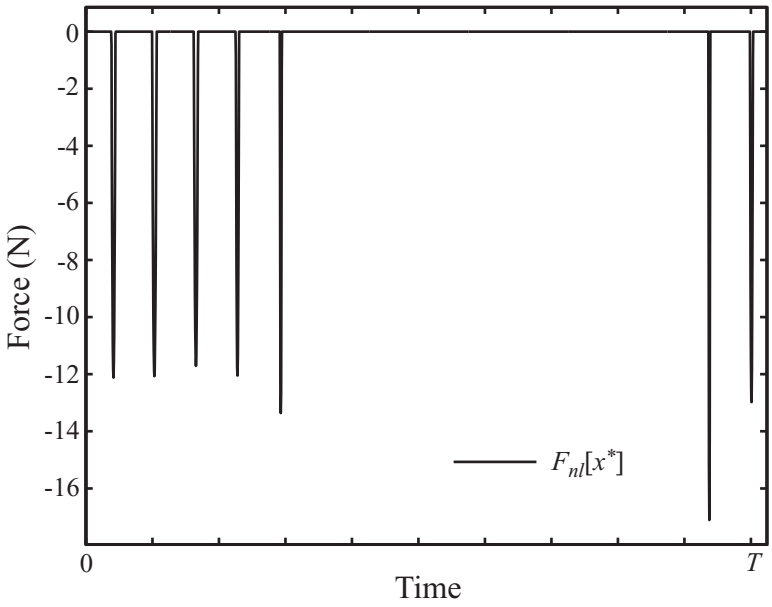

Figure 4.11: Time history of the nonlinear force applied to the two-DOF system with impact, at $\omega = 0.2$ rad.s^{-1}.

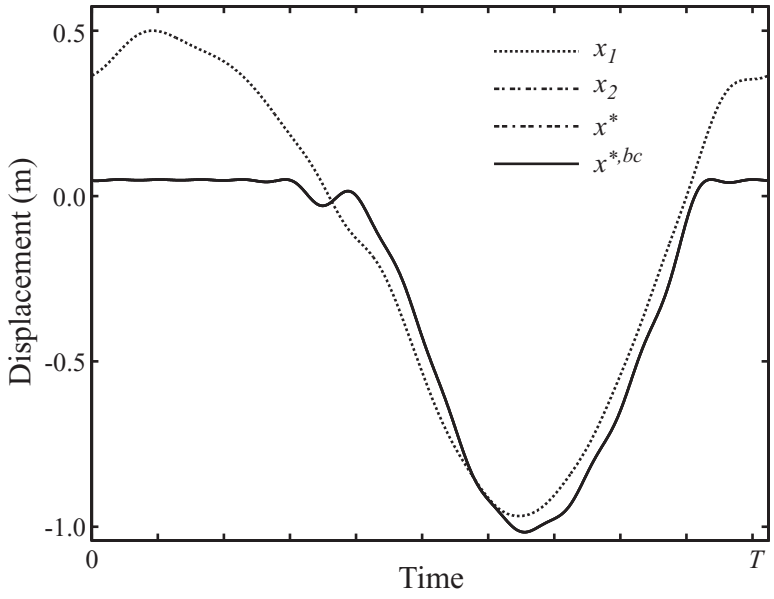

Figure 4.12: Time history of the DOFs of the system with impact presented in Fig. 4.4, at the period of excitation $\omega = 0.2$ rad.s^{-1}.

The corresponding time histories of the DOFs of the system are shown in Fig. 4.12. It is harder to deduce from this figure the number of impacts over a period of motion, but the enforcement of the nonlinear condition on the contact DOF appears very clearly.

The time histories shown in Fig. 4.12 also show clearly that for the value of k^* chosen, the DOFs x^2 and x^* behave virtually identically. In other terms, x_2 verifies the non-penetration condition. The behavior of the augmented system is therefore an accurate approximation of the behavior of the original system.

4.4.3 Two-DOF system with friction

The dynamics of the same two-DOF system is now investigated when the nonlinear force is a Coulomb friction force, as depicted in Fig. 4.5. Instead of impacting an obstacle, the DOF x_2 directly rubs onto the ground. A constant load $N = 1$ N is applied in the normal direction, and the friction coefficient chosen is $\mu = 1$. The frequency response of the system is shown in Fig. 4.13.

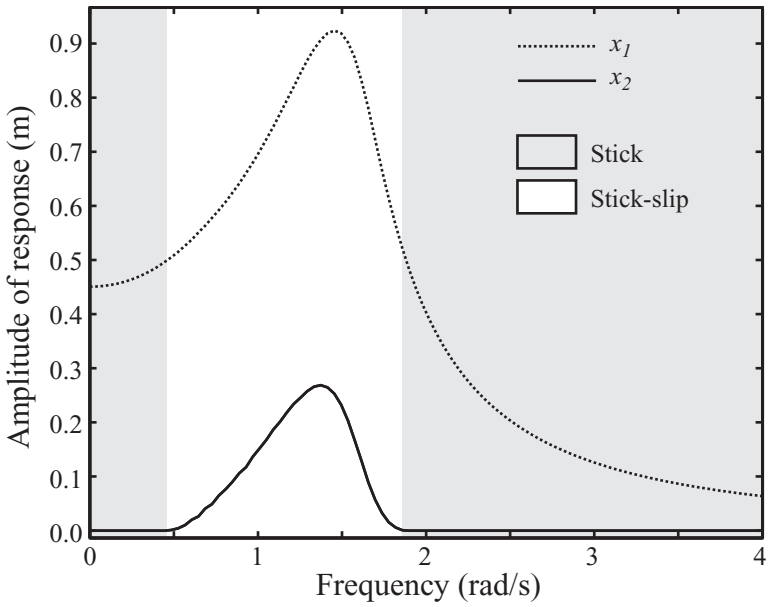

Figure 4.13: Frequency response of the DOFs of the simple system with friction of Fig. 4.5.

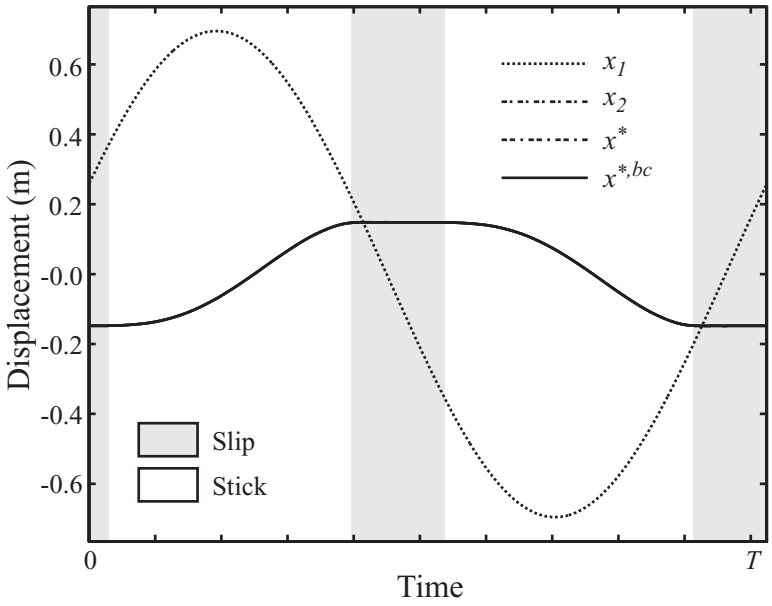

Figure 4.14: Time history of the DOFs of the two-DOF system with friction, at $\omega = 1.0$ rad.s^{-1}.

The system exhibits clearly two distinct behaviors depending on the value of ω. When $\omega < 0.5$ rad.s^{-1} or when $\omega > 1.8$ rad.s^{-1}, the amplitude of oscillation of x_1 is too small to make x_2 start slipping, and therefore x_2 is zero. When the amplitude of x_1 reaches 0.5 at $\omega = 0.5$ or 1.8 rad.s^{-1}, the slip condition $|k_2(x_2 - x_1)| = \mu N$ is verified, and x_2 experiences both stick and slip over a period of motion, as observed in Fig. 4.14.

Again, as noted for the two-DOF system with impact, the perfect agreement between x_2 and x^* justifies (a posteriori) the value chosen for k^*.

4.4.4 Study of the influence of k*

The values chosen for k^* in the two previous examples where high enough to ensure that x_2 (that is, the nonlinear DOF of the non-augmented systems) and x^* are identical. However, since the method of analysis is based on an algorithm that iteratively increases k^*, it is crucial to know the threshold above which k^* yield accurate results, so as to minimize the computational cost associated with the calculations performed at each iteration.

In this section, the dynamics of the two-DOF system with impact is investigated for various values of k^*. The periodic forced response of the system is calculated at $\omega = 1$ rad.s^{-1}, which yields one impact per period of motion, as shown in Fig. 4.15. Three kinds of calculations are presented:

- A reference calculation obtained with Mathematica by solving the exact dynamics of the non-augmented system.
- Calculations performed with 20 harmonics, with k^* varying from $2.0 \cdot 10^1$ to $2.0 \cdot 10^6$ N.
- A calculation performed with 100 harmonics, for $k^* = 2.0 \cdot 10^6$ N

The accuracy of the method is indeed a function of the number of harmonics – which

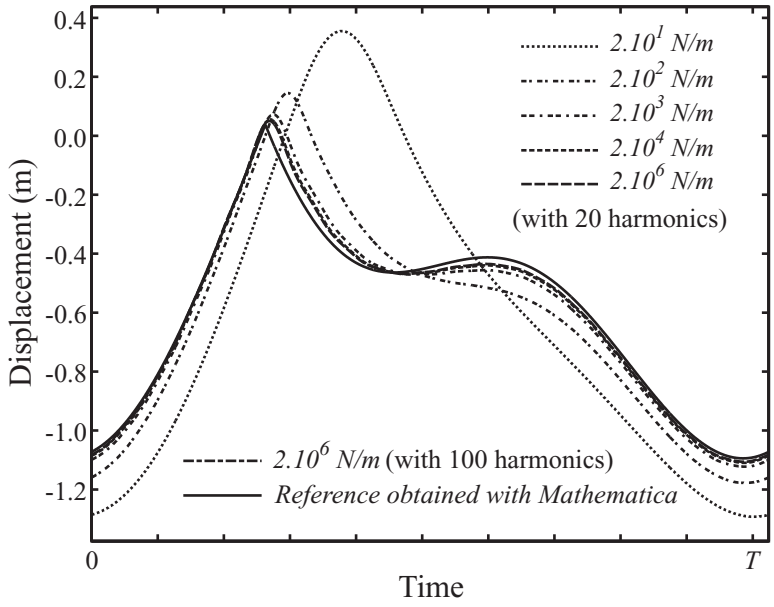

Figure 4.15: Time histories of the DOF x_2 of the two-DOF system with impact, calculated for various values of k^*. Results are presented for 20 and 100 harmonics, and compared to a reference calculation obtained with Mathematica. The time histories are computed at $\omega = 1$ rad.s^{-1}.

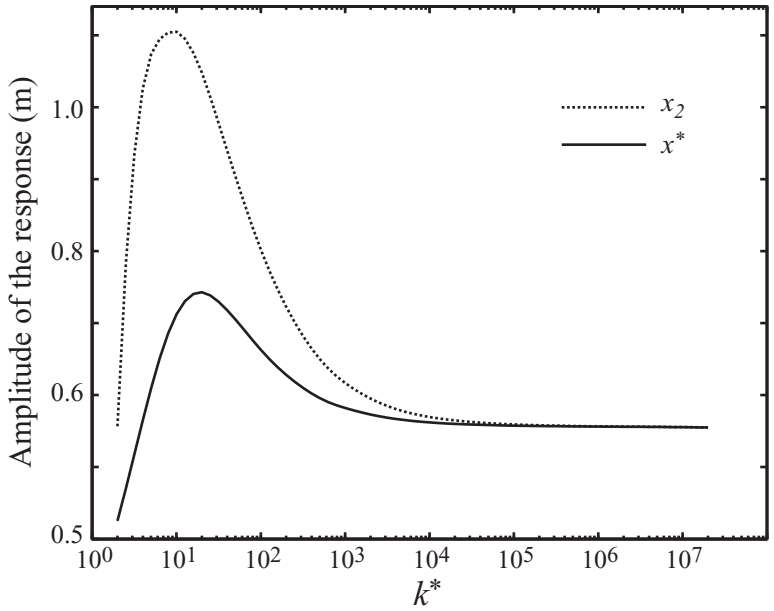

Figure 4.16: Evolution of the amplitude of response of the DOFs x_2 and x^* as a function of k^*.

controls how accurately the nonlinear DOFs respect the kinematic boundary conditions – and a function of k^*, which controls how close the dynamics of the original and augmented systems are.

The time histories of x_2 are shown in Fig. 4.15. There is an excellent agreement between the reference calculation and the results obtained with 100 harmonics and $k^* = 2.0 \cdot 10^6$ N.m^{-1}. When only 20 harmonics are used, the variations of k^* for values above $2.0 \cdot 10^4$ N.m^{-1} have a negligible impact on the evolution of the time history, and a small difference (less than 5% in amplitude) is observed with the reference calculation. As a consequence, reducing this difference requires increasing the number of harmonics and keeping the value of k^* at $2.0 \cdot 10^4$ N.m^{-1}.

The results shown in Fig. 4.16 illustrate this convergence from a different point of view. In this figure, the amplitudes of response of the DOFs x_2 and x^* are plotted as a function of k^* . In other words, Fig. 4.16 describes how the augmented system converges towards the original system as k^* increases, as opposed to the results shown in Fig. 4.15 which describe how the response of the system converges towards the exact solution.

Again, there is no noticeable difference between x_2 and x^* when k^* is greater than $2.0 \cdot 10^4$ N.m^{-1}, which seems to be the value – for this system – that provides accurate results.

4.4.5 Finite element model of two blades with impact

In this example, a more complicated structure – more representative of typical industrial systems – is considered. As shown in Fig. 4.17, it consists of two adjacent blades fixed on an elastic support. The blades have platforms which can potentially contact each other. At rest, the upper and lower platforms have a clearance of 1 mm. The overall height of the system is 0.5 m.

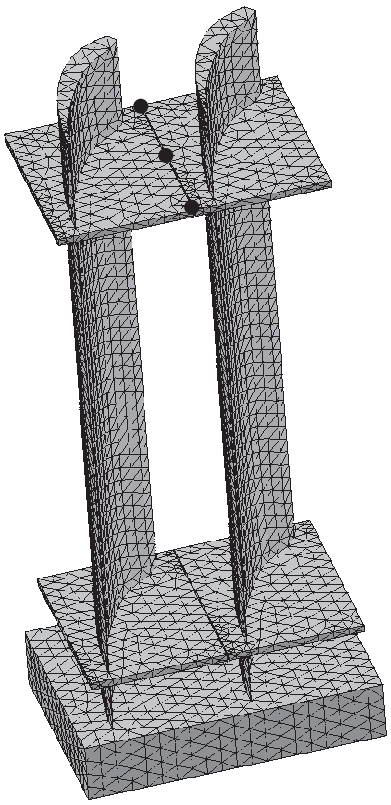

Figure 4.17: Example of realistic structure studied with the modified HFT method. Three pairs of nodes are selected on the adjacent upper-platforms of the blades. The study focuses on the nonlinear behavior of the structure when these nodes impact each other without friction.

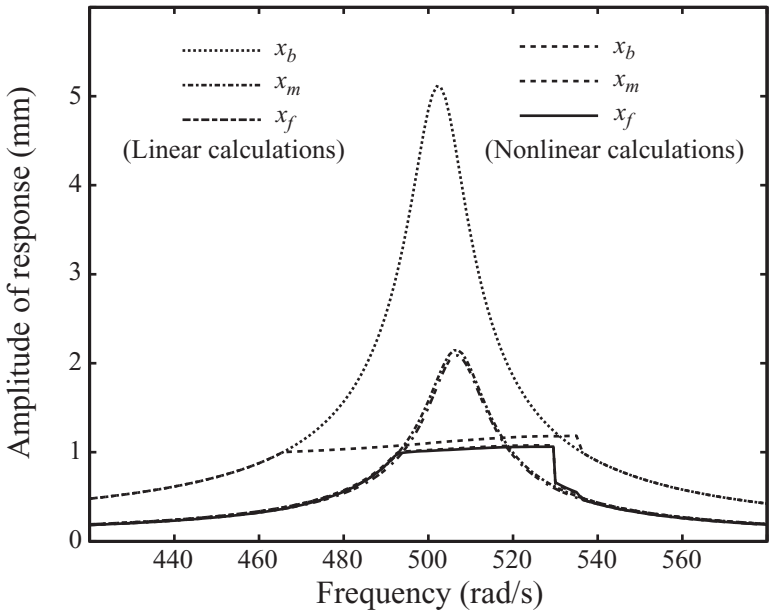

Figure 4.18: Frequency response of the realistic system presented in Fig. 4.17.

An external, linear forcing is applied to the tips of the blades, so as to make the upper platforms contact each other. The mode of vibration which is investigated corresponds to the first bending mode of the system, around $\omega = 500$ rad.s^{-1}.

Since the finite element model features more than 5000 DOFs, a reduced-order model is used for the calculations. The system is condensed out using Craig-Bampton component mode synthesis. The reduced-order model obtained is made of 18 3-DOF nodes (which include the contact DOFs and the DOFs where the linear forcing is applied, among others), and 20 modal coordinates corresponding to the normal modes of vibration of the structure when the physical DOFs mentioned above are fixed. It is assumed here that the nonlinear interactions occur at the upper platforms only and are of the impact type, that is, friction between the platforms is not considered. Three pairs of nonlinear DOFs are chosen, and a change of coordinates is performed so as to obtain the relative displacement of the DOFs of the left upper-platform with respect to the DOFs of the right upper-platform. The frequency response of the system is calculated with 20 harmonics. Following the guidelines suggested in the previous section, the value of k^* is set to $2.0 \cdot 10^8$ N.m^{-1}.

Two sets of results are presented in Fig. 4.18, where the nonlinear dynamics of the structure is compared to its dynamics when the non-penetration conditions at the platform DOFs are ignored.

As expected, when the amplitude of vibration is small, the linear and nonlinear behaviors coincide, since the platform DOFs vibrates freely without impacting each other. Then, for ω in the interval [467-538] rad.s^{-1}, the structure exhibits a strong reduction of the amplitude of motion, which is typical of such nonlinear systems.

4.5 Conclusion

A new formulation of the hybrid frequency/time domain method has been proposed in this chapter. It extends the applicability of the traditional HFT method to the study of the periodic forced response of systems with friction or intermittent contact. The nonlinearities handled by the method must be displacement-dependent, and can stem (1) from the interaction between the structure and an infinitely stiff obstacle, or (2), from the reciprocal actions of two parts of the structure contacting each other.

The method is still based on a mixed frequency-domain/time-domain representation of the equations of motion of the system. However, unlike the traditional implementation of the HFT method, it does not require the calculation of the Fourier coefficients of the nonlinear contact forces. Actually, the nonlinear equations that are solved in the frequency domain do not involve such coefficients. As a consequence, a major hindrance to the efficient numerical analysis of systems with stiff nonlinearities is overcome. The evaluation of the Fourier coefficients of the nonlinear contact forces is indeed replaced by the enforcement in the time domain of the nonlinear boundary conditions.

In addition to the fact that the nonlinear forces do not appear in the nonlinear frequency-domain equations to be solved, the advantages of the method are the following:

- The method can easily be extended to other types of displacement-dependent nonlinearities, such as elastic stops with cubic nonlinear stiffness, friction with variable normal load, etc.

- The augmented systems used by the method are trivially deduced from the original nonlinear systems.

- It is easy to assess the precision of the solution obtained with respect to the number

of harmonics retained to describe the dynamics of the system and with respect to the value of k^*.

- The nonlinear boundary conditions can be captured very accurately in the time domain.

- The method is applicable to systems with many nonlinear nodes, since the corresponding DOFs are handled independently from each other.

- Solving numerically a set of nonlinear equations always requires a relatively accurate initial guess. For complex nonlinear systems, finding such a guess can be a daunting task and a source of numerical problems. However, in the method of analysis introduced in this chapter, it is always possible to use as an initial guess the solution of the linear system (that is, the system for which the effect of the nonlinearities is ignored), and to build a series of solutions (indexed by the value of k^*) which converge more or less continuously towards the solution of the non-augmented system.

Finally, numerical examples have demonstrated the accuracy of the method as well as its applicability to realistic, industrial-like structures.

CHAPTER V

A NEW METHOD FOR THE ANALYSIS OF THE NONLINEAR DYNAMICS OF STRUCTURES WITH CRACKS

5.1 Introduction

The nonlinear dynamics of structures with cracks are examined in this chapter. Cracks are usually induced by the high-cycle fatigue that results from excessive vibration levels. Monitoring the evolution of such damaged structures requires predictive tools able to calculate accurately their behavior in the presence of the nonlinear boundary conditions that result from the repetitive opening and closing of the crack interfaces. Direct methods of analysis of the periodic forced response of such structures – such as time integration methods – are however hindered by (1) the complexity of the nonlinear contact forces at the crack interfaces, (2) the low amount of damping encountered in most industrial structures – especially in turbomachinery applications –, and (3) the size of the nonlinear systems that stem from the study of realistic structures. As a consequence, most of the methods of analysis developed for structures with cracks have been based on simplified geometries, such as the work by Shen and Pierre [112, 113] on Euler-Bernoulli beams featuring different types of cracks. Although many works have focused on such simplified systems, there are on the other hand hardly any studies available regarding the analysis of realistic

structures with cracks. This is particularly true of studies carried out without simplifying modeling assumptions and without the use of direct time-integration methods.

On the other hand, significant advances regarding the modeling and analysis of the periodic forced response of structures with displacement-dependent nonlinearities have been recently made, as mentioned in the previous chapters. These techniques have been applied to complex systems, mostly in the field of turbomachinery bladed disks, and have not been considered for the analysis of structures with cracks.

The analysis method introduced here is a modification of the multi-harmonic, hybrid frequency/time domain methods presented earlier in this dissertation. It allows for an efficient handling of arbitrary complex structures with cracks, and it can be viewed as an application of the well-known penalty method to these multi-harmonic techniques. The method is based on a frequency domain representation of the dynamics of the structure, and a time domain enforcement of the nonlinear boundary conditions.

This new method of analysis is applied here to the finite element models of two cracked beams. The accuracy of the method is first established by comparing its results with that obtained with a direct time-integration approach. Then, the influence of the method parameters on the accuracy of the prediction of the nonlinear forced response is investigated.

5.2 Theoretical analysis

5.2.1 Equations of motion in the time domain

The general equations of motion of a linear elastic structure with cracks can be expressed as

$$\mathbf{M}\ddot{\mathbf{x}}(t) + \mathbf{C}\dot{\mathbf{x}}(t) + \mathbf{K}\mathbf{x}(t) = \mathbf{f}(t) + \mathbf{f_{nl}}[\mathbf{x}](t), \tag{5.1}$$

where $\mathbf{M}$, $\mathbf{C}$ and $\mathbf{K}$ represent the mass, stiffness and damping matrices, $\mathbf{f}$ is a time-dependent forcing applied to the structure, and $\mathbf{f_{nl}}[\mathbf{x}]$ is a displacement-dependent non-

linear force. Let us assume, for the sake of clarity, that the structure features only one crack, and that this crack is modeled by two nodes potentially contacting each other as the crack opens and closes[1]. Furthermore, we assume that any friction phenomenon occurring at the crack interface can be neglected, and that only the normal displacement of these two nodes needs to be taken into account[2]. Under these assumptions, the structure features only two nonlinear degrees of freedom (DOFs), and the equations of motion can be written as:

$$\mathbf{M}\begin{bmatrix}\ddot{x}_{nl,1}(t)\\ \ddot{x}_{nl,2}(t)\\ \ddot{\mathbf{x}}_{\mathbf{l}}(t)\end{bmatrix}+\mathbf{C}\begin{bmatrix}\dot{x}_{nl,1}(t)\\ \dot{x}_{nl,2}(t)\\ \dot{\mathbf{x}}_{\mathbf{l}}(t)\end{bmatrix}+\mathbf{K}\begin{bmatrix}x_{nl,1}(t)\\ x_{nl,2}(t)\\ \mathbf{x}_{\mathbf{l}}(t)\end{bmatrix}=\mathbf{f}(t)+\begin{bmatrix}f_{nl,1}[x_{nl,1},x_{nl,2}](t)\\ f_{nl,2}[x_{nl,1},x_{nl,2}](t)\\ \mathbf{0}\end{bmatrix}, \quad (5.2)$$

where the subscript l is used for the other linear DOFs of the structure. Since the principle of action and reaction applied to the nonlinear DOFs yields

$$f_{nl,1}[x_{nl,1},x_{nl,2}](t)=-f_{nl,2}[x_{nl,1},x_{nl,2}](t), \quad (5.3)$$

performing the following change of coordinates

$$\begin{bmatrix}u_{nl}\\ v\end{bmatrix}=\frac{1}{\sqrt{2}}\begin{bmatrix}x_{nl,2}-x_{nl,1}\\ x_{nl,2}+x_{nl,1}\end{bmatrix} \quad (5.4)$$

results in eliminating one of the nonlinear DOF and retaining only the nonlinear DOF, u_{nl}, corresponding to the relative normal displacement of the crack nodes. Therefore, updating the definitions of $\mathbf{M}$, $\mathbf{C}$, $\mathbf{K}$ and $\mathbf{f}$ in the new coordinate system, the general equations of motion of the system can be written as[3]:

$$\mathbf{M}\begin{bmatrix}\ddot{u}_{nl}(t)\\ \ddot{\mathbf{u}}_{\mathbf{l}}(t)\end{bmatrix}+\mathbf{C}\begin{bmatrix}\dot{u}_{nl}(t)\\ \dot{\mathbf{u}}_{\mathbf{l}}(t)\end{bmatrix}+\mathbf{K}\begin{bmatrix}u_{nl}(t)\\ \mathbf{u}_{\mathbf{l}}(t)\end{bmatrix}=\mathbf{f}(t)-\begin{bmatrix}\sqrt{2}f_{nl,1}[x_{nl,1},x_{nl,2}](t)\\ \mathbf{0}\end{bmatrix}, \quad (5.5)$$

[1]The general case of structures with several cracks and with several nonlinear nodes is trivially deduced from the equations presented here.

[2]Taking into account the tangential friction and its possible dependence with respect to the normal relative displacement of the contacting nodes can also be easily included in the method.

[3]Underlined symbols represent complex quantities. Bold symbols denote vectors or matrices.

where $\mathbf{u_l}^T = [v\ \mathbf{x_l}^T]$ contains all the linear DOFs of the new system of equations.

The method presented in this chapter can be described as a Hybrid Time-Frequency domain version of the well-known penalty method often used in direct time integration techniques. The nonlinear force applied to the relative normal displacement is expressed as:

$$f_{nl,1}[x_{nl,1}, x_{nl,2}](t) = k^* \min[0, x_{nl,2}(t) - x_{nl,1}(t)], \tag{5.6}$$

where k^* is a coefficient that penalizes the relative normal penetration of the DOFs[4]. The nonlinear set of equations describing the motion of the system can therefore be written as:

$$\mathbf{M} \begin{bmatrix} \ddot{u}_{nl}(t) \\ \ddot{\mathbf{u}}_\mathbf{l}(t) \end{bmatrix} + \mathbf{C} \begin{bmatrix} \dot{u}_{nl}(t) \\ \dot{\mathbf{u}}_\mathbf{l}(t) \end{bmatrix} + \mathbf{K} \begin{bmatrix} u_{nl}(t) \\ \mathbf{u}_\mathbf{l}(t) \end{bmatrix} = \mathbf{f}(t) + \begin{bmatrix} f_{nl}[u_{nl}](t) \\ \mathbf{0} \end{bmatrix}, \tag{5.7}$$

where

$$f_{nl}[u_{nl}](t) = -2k^* \min[0, u_{nl}(t)]. \tag{5.8}$$

5.2.2 Equations of motion in the frequency domain

When the steady-state forced response of the system is assumed to be periodic, the displacements as well as the forces acting on the structure can be written as Fourier series of harmonic functions. Assuming that keeping N_h harmonics guarantees an accurate approximation of the dynamics of the structure, the displacements can be expressed as:

$$\begin{bmatrix} u_{nl}(t) \\ \mathbf{u}_\mathbf{l}(t) \end{bmatrix} = \mathrm{Re}\left(\sum_{k=0}^{N_h} \begin{bmatrix} \underline{u_{nl}}_k \\ \underline{\mathbf{u_l}}_k \end{bmatrix} e^{\underline{jk\omega t}} \right) \quad \text{and} \quad \mathbf{f}(t) = \mathrm{Re}\left(\sum_{k=0}^{N_h} \underline{\mathbf{f}}_k e^{\underline{jk\omega t}} \right), \tag{5.9}$$

where ω is the frequency of the periodic excitation. Similarly, the nonlinear force can be written as:

$$f_{nl}[u_{nl}](t) = \mathrm{Re}\left(\sum_{k=0}^{N_h} \underline{f_{nl}}_k [\underline{u_{nl}}_0, \ldots, \underline{u_{nl}}_{N_h}] e^{\underline{jk\omega t}} \right). \tag{5.10}$$

[4]It is assumed here that the orientation of the two nonlinear normal DOFs at the crack is such that the crack is considered open when $x_{nl,2}(t) > x_{nl,1}(t)$.

Now, applying the Harmonic Balance Method to Eq. (5.7) yields a set of $N_h + 1$ complex, nonlinear, coupled equations:

$$\begin{bmatrix} \underline{\Lambda}_k^{nl,nl} & \underline{\mathbf{\Lambda}}_k^{\mathbf{nl,l}} \\ \underline{\mathbf{\Lambda}}_k^{\mathbf{l,nl}} & \underline{\mathbf{\Lambda}}_k^{\mathbf{l,l}} \end{bmatrix} \begin{bmatrix} \underline{u_{nl}}_k \\ \underline{\mathbf{u_l}}_k \end{bmatrix} = \underline{\mathbf{f}}_k + \begin{bmatrix} \underline{f_{nl}}_k[\underline{u_{nl}}_0, \ldots, \underline{u_{nl}}_{N_h}] \\ \mathbf{0} \end{bmatrix}, \tag{5.11}$$

where the (l, l) block of the linear part of the jacobian of this system of equation is defined as:

$$\underline{\mathbf{\Lambda}}_k^{\mathbf{l,l}} = -(k\omega)^2 \mathbf{M}^{\mathbf{l,l}} + \underline{j} k\omega \mathbf{C}^{\mathbf{l,l}} + \mathbf{K}^{\mathbf{l,l}}, \tag{5.12}$$

with similar expressions for $\underline{\mathbf{\Lambda}}_k^{\mathbf{l,nl}}$, $\underline{\mathbf{\Lambda}}_k^{\mathbf{nl,l}}$ and $\underline{\Lambda}_k^{nl,nl}$. [5]

5.2.3 Solution method

The set of $N_h + 1$ coupled nonlinear equations (5.12) is solved iteratively with the following algorithm:

1. An initial value is given to the penalty coefficient k^*. The higher the value is, the greater the accuracy is. One should note however that, if iterations on the values of k^* are needed because the set of nonlinear equations cannot be solved directly for the desired value of k^* without knowing a sufficiently close guess of its solution, then a very low value can be used as a starting point, since the extreme case $k^* = 0$ corresponds to an easily solvable linear case.

2. The Fourier coefficients of the nonlinear DOF are guessed. When this is done for the first time, an arbitrary guess can be provided. However, if k^* is very small, it makes sense to choose for u_{nl} the linear solution obtained when the nonlinear boundary conditions are not taken into account. In other cases, a guess that takes into account the history of the previous guesses and the evolution of the convergence towards the

[5] This nonlinear set of equations can be further reduced so as to involve the Fourier coefficient of the nonlinear DOF only, and therefore reduce the size of the system to be solved.

solution is automatically provided by the nonlinear solver. A nonlinear solver based on a modified hybrid Powell method was found to provide the required speed and robustness necessary to handle such complicated nonlinear systems.

3. The time history of the nonlinear DOF u_{nl} is deduced from the guessed Fourier coefficients $\underline{u_{nl}}_k$ using an inverse fast Fourier transform.

4. The time history of the penalty force is deduced from the time history of u_{nl}, using Eq. (5.8).

5. A fast Fourier transform applied to the time history of the nonlinear penalty force yields the Fourier coefficients $\underline{f_{nl}}_k$.

6. Now, the residue of the nonlinear set of equations (5.12) can be evaluated, and the convergence towards its solution assessed. If these equations are not satisfied, new approximate Fourier coefficients $\underline{u_{nl}}_k$ are provided by the nonlinear solver, and the algorithm restarts at step (3).

7. When convergence is reached, the value of k^* is increased and the algorithm restarts at step (3), unless the results show that the penalty coefficient has reached a value high enough to consider that the dynamics of the system has been accurately captured.

5.3 Nonlinear dynamics of cracked beam models

In this section, the nonlinear forced responses of two models of cracked cantilevered beams are studied. The accuracy of the method is established with the first model by comparing the results with that obtained with a direct time-domain method, using the commercial code ANSYS. The second beam model is then used to assess the influence

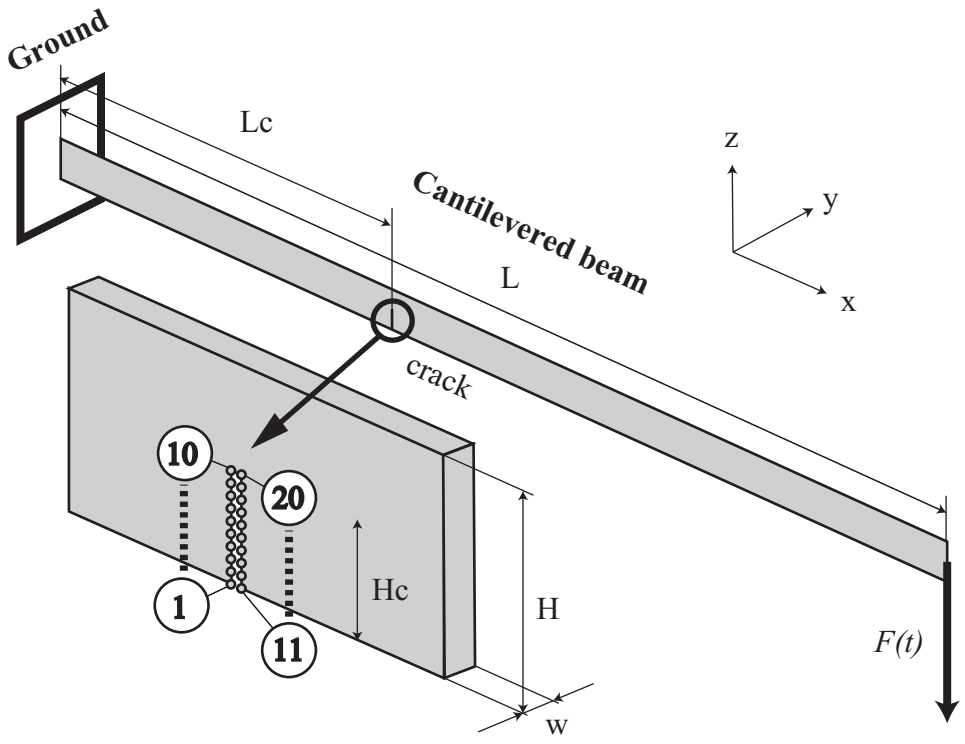

Figure 5.1: Geometric representation of the cracked cantilevered beam studied. At rest, the crack opening is zero, that is, the two interfaces of the crack contact each other.

that the numerical parameters of the analysis method have on the accuracy of the results. Finally, a simple parametric study shows the effect of the crack length on the dynamics of this beam model.

5.3.1 Reference calculation

In order to establish the accuracy of the method, a simple model of cracked cantilevered beam is studied. The physical characteristics of the beam – shown in Fig. 5.1 – are:

- The length of the beam is $L = 0.72$ m, its width is $w = 0.016$ m and its height is $H = 0.032$ m.

- The crack is located at approximately one-eighth of the length of the beam, since $L_c = 0.08$ m. The crack length in the z direction is $H_c = 0.018$ m, and the crack

spreads across the entire width of the beam in the y direction. At rest, the crack opening is zero, that is, the two interfaces of the crack contact each other.

- The material properties of the beam are $E = 206$ GPa, $\rho = 7650$ kg/m^3, and $\nu = 0.29$.

- The beam is excited by a harmonic forcing $F(t) = 1.0\cos(\omega t)$ which is applied at its tip in the z direction. The structure damping of the beam is defined by $\mathbf{C} = \alpha\mathbf{K}$, where $\alpha = 5.0 \times 10^{-4}$ s.

The cracked beam is represented by a 13000-DOF finite element (FE) model, in order to (1) capture accurately the linear behavior of the beam and (2) describe the crack with a sufficient number of nodes. Since the mode of vibration of interest is the first bending mode in the x-z plane, the FE model contains only the DOFs corresponding to these directions. As a consequence, the model of the crack is also planar and it is described by 10 pairs of nodes uniformly distributed in the z direction that can contact each other or separate, depending on the relative motion of the two faces of the crack in the x direction.

In order to alleviate the computational cost of the analysis that would stem from manipulating such a large nonlinear system, a reduced order model of the cracked beam is created. A Craig-Bampton component mode synthesis procedure is used to condense out the FE model into a 62-DOF system made of (1) 40 physical DOFs associated to the 20 nodes describing the crack, (2) two physical DOFs at the tip of the beam, where the excitation is applied, and (3) 20 modal coordinates corresponding to the normal modes of vibration of the structure when all the previous 42 physical DOFs are constrained.

The forced response of the beam is obtained by applying the method presented above to the reduced order model. In this analysis the first seven harmonics are retained and the penalty coefficient is chosen as $k^* = 1.0^9$ N.m^{-1}. The reference forced response results are

obtained by a time-integration analysis obtained with the commercial code ANSYS on the finite element model[6]. In this case, the numerical parameters used for the reference study with ANSYS allow for a maximum penetration p of 0.01, that is, the maximum penetration allowed at the nodes describing the crack is at most one-hundredth of the x dimension of the finite elements modeling the crack interface. Results with a less stringent penetration condition $p = 0.1$ are also obtained.

Figure 5.2, which depicts the forced response of the beam, shows how the results obtained with the analysis method developed in this chapter compare to the reference analysis provided by ANSYS. These results show an excellent agreement between the two methods. The comparison of the computational cost incurred when performing these two analysis show the outstanding benefits that stem from the use of the HFT method: on average, the CPU time required by ANSYS (with $p = 0.01$) to obtain the forced response for a given frequency of the interval studied is 5000 times higher than that required by the HFT method. This comparison clearly demonstrates that the exact dynamics of complicated, realistic nonlinear structures can be captured extremely accurately at a very low computational cost.

5.3.2 Influence of the parameters of the method

The accuracy of the forced response is a function of the numerical parameters that characterize the new analysis method. These parameters are listed below:

- Physical parameters
  - The number N_{cm} of component modes retained in the reduced order model. The greater N_{cm} is, the higher the accuracy of the reduced order model is.

[6]The author wishes to extend hereby his sincere gratitude to his colleague Akira Saito for his expertise and help for carrying out the time-integration analysis with ANSYS.

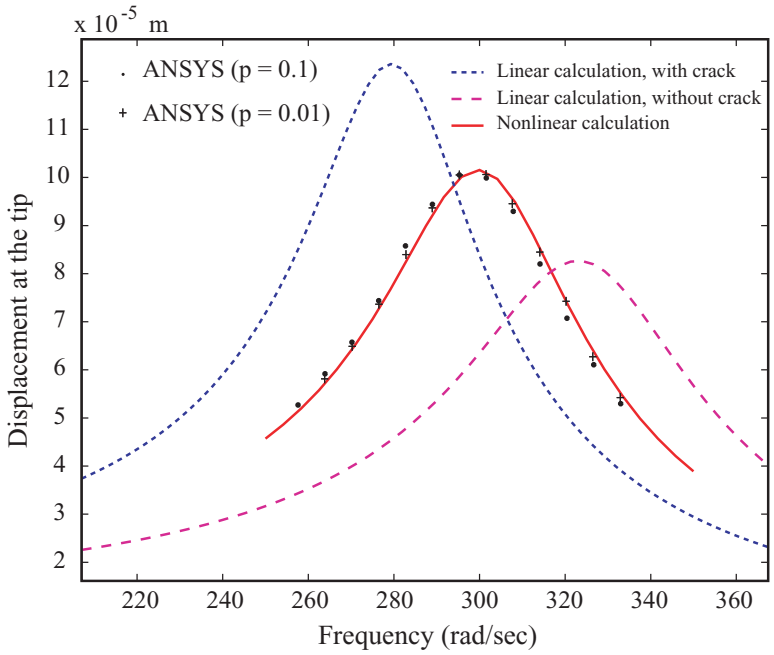

Figure 5.2: Forced response at the tip of the first model of beam studied, in the z direction. The results derived from the analysis method developed in this chapter are compared to the reference calculations obtained with ANSYS. The forced response corresponding to the two limiting linear cases – that is, (1) the linear forced response of the beam without crack, and (2) the linear forced response of the cracked beam without taking into account the nonlinear boundary conditions at the crack interface – are also presented.

  - The number of nodes N_n used to model the crack. A high number of nonlinear nodes ensures an accurate description of the local deformation of the crack interfaces.

- Numerical parameters

  - The penalty coefficient k^*, which controls the enforcement of the boundary conditions.

  - The number of the highest harmonic N_h retained to describe the dynamics of the system. For instance, if the harmonics retained are 0,1,. . . 9, then $N_h = 9$.

  - The number of sample points N_t over one period of motion used for the fast Fourier transforms.

Ideally, the method presented here allows one to capture the *exact* nonlinear dynamics of the system when all these parameters tend towards infinity. Practically, however, it is of great interest to determine realistic values that would maintain the accuracy of the predicted forced response without compromising the computational cost of solving the nonlinear equations. Since the CPU cost of the method is roughly proportional to the cube of N_h and N_n, and proportional to N_t and k^*, it is important to find optimal values of the parameters beyond which no significant improvement of the solution can be found.

A model of a cracked beam slightly different from the one studied above is used to analyze the influence of the method parameters. In particular, the structural damping of the beam is chosen to be smaller than the one used for the first study, so as to maximize the nonlinear damping effect due to the crack. The new properties of the beam are listed below:

- The length of the beam is $L = 0.99$ m, its width is $w = 0.01$ m and its height is $H = 0.04$ m.

- The crack is located at approximately one-third of the length of the beam, since $L_c = 0.38$ m. The crack length in the z direction is $H_c = 0.02,$ m, which is half the height of the beam, and the crack spreads across the entire width of the beam in the y direction. At rest, the crack opening is zero, that is, the two interfaces of the crack contact each other.

- The material properties of the beam are $E = 200$ GPa, $\rho = 7800$ kg/m^3, and $\nu = 0.3$.

- The beam is excited by a harmonic forcing $F(t) = 0.0316\cos(\omega t) + 0.0244\sin(\omega t)$ which is applied at its tip in the z direction. The structure damping of the beam is defined by $\mathbf{C} = \alpha\mathbf{K} + \beta\mathbf{M}$, where $\alpha = 1.0 \times 10^{-5}$ s and $\beta = 1.0$ s^{-1}.

$N_{cm} = 20$	$N_n = 20$	$k^* = 10^{12}$ N.m^{-1}	$N_h = 9$	$N_t = 1024$

Table 5.1: Reference calculation parameters.

This beam is represented by a finite element model featuring 21000 DOFs, and a Craig-Bampton component mode synthesis procedure yields a reduced order model featuring the same characteristics as those of the beam used for the previous calculations: the number of DOFs of the reduced order model, the number of component modes retained as well as the number of physical DOFs describing the crack interface are the same.

The accuracy of the reduced order model is first demonstrated by its capability to capture the natural frequency of the *linear* bending mode of vibration of the beam with a crack, that is, the resonant frequency obtained when the beam's stiffness is affected by the crack and when the actual nonlinear boundary conditions at the crack interface are ignored. In other words, it is the resonant frequency of the beam when the mutual penetration of the crack nodes is allowed. In this case, the reduced order model predicts with less than 0.001 percent of error the frequency obtained by conducting the modal analysis on the full FE model. This reduced order model can therefore be used with confidence for the nonlinear analysis.

The calculation of the nonlinear forced response of the beam is carried out for various parameter values. The converged calculation with the set of parameters beyond which no noticeable improvement can be observed is referred to as the *reference* calculation, which is defined by the parameters shown in table (5.1). For this calculation the crack spreads across one half of the beam's section, and 20 contact nodes are considered. Since each pair of contact nodes is associated to a nonlinear DOF corresponding to their relative motion in the x direction, and since all the harmonics from 0 to 9 are considered, the nonlinear set of equations representing the system at a given frequency is made of 190 nonlinear variables.

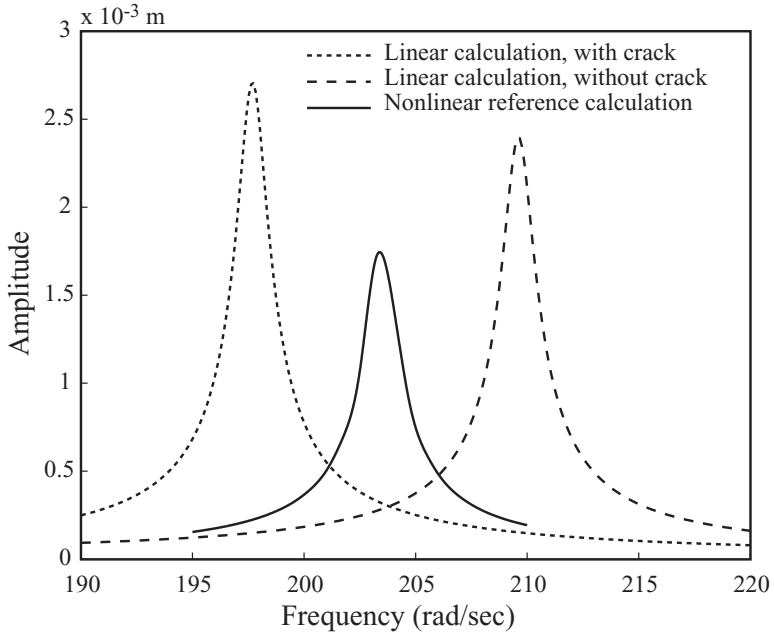

Figure 5.3: Amplitude of the forced response at the tip of the beam, in the z direction.

The frequency response curves obtained with the reference parameters are shown in Fig. (5.3). The nonlinear reference calculation exhibits a resonant peak at 203.48 rad.s^{-1}. Two linear calculations are also shown in Fig. (5.3). They correspond to the linear limiting cases obtained (1) when the beam doesn't feature a crack, and (2) when the beam does feature a crack for which the corresponding nonlinear boundary conditions are ignored, thus allowing for mutual penetration of the contacting nodes. The frequencies of the resonant peaks found for these limiting cases are respectively 209.61 rad.s^{-1} and 197.69 rad.s^{-1}. The frequency shift FS – that is, the relative variation of the resonant frequency due to the presence of the crack with respect to the natural frequency of the structurally sound beam – is -2.93 %.

The nonlinear behavior occurring at the crack interfaces is illustrated in Fig. (5.4), where the time histories of the x-component of the displacement of the contacting nodes #1 and #11 are shown. They clearly indicate that for this type of excitation and for the mode of vibration considered, the crack opens for nearly half the period of motion, and

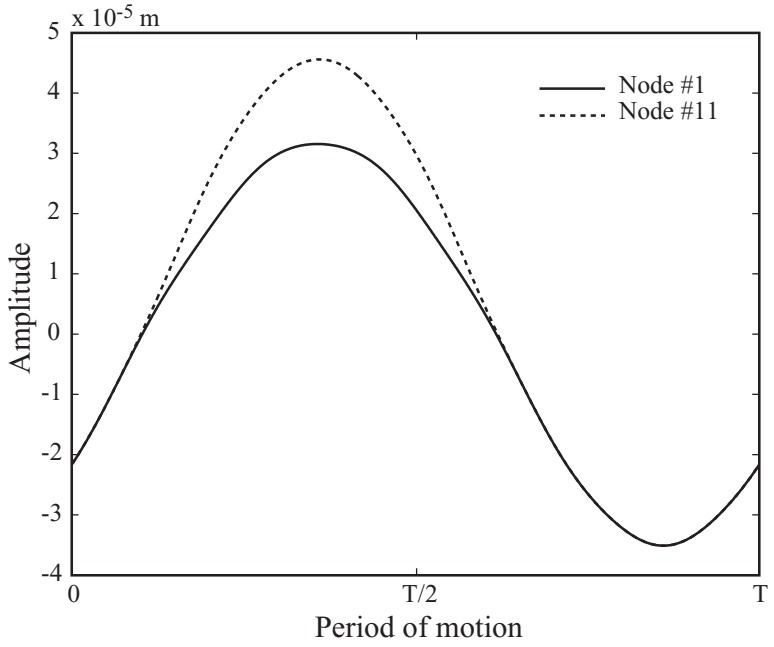

Figure 5.4: Time history of the displacement over one period of motion of the contacting crack nodes #1 and #11 (that is, the nodes located at the free edge of the crack) in the x direction, at the resonant nonlinear frequency (203.47 rad.s^{-1}).

Value of N_t	1024	512	256	128	64
Error on FS	-	0.37 %	0.39 %	0.34 %	0.62 %

Table 5.2: Influence of N_t on the accuracy of the prediction of the frequency shift FS.

closes during the other half.

In order to assess the impact that various choices of parameters have on the accuracy of the solution, a series of calculation is carried out and for each of these, all but one of the parameters are set to the values that correspond to the reference calculation. Tables (5.2)-(5.6) give – for various values of the parameter which is not fixed – the percentage of error found on the value of the frequency shift, with respect to the frequency shift obtained with the reference calculation.

Value of N_h	9	7	5	3	1
Error on FS	-	0.16 %	0.46 %	1.84 %	31.4 %

Table 5.3: Influence of N_h on the accuracy of the prediction of the frequency shift FS.

Value of k^*	10^{12} N.m^{-1}	10^{11} N.m^{-1}	10^{10} N.m^{-1}	10^{9} N.m^{-1}
Error on FS	-	0.03 %	0.24 %	1.89 %

Table 5.4: Influence of k^* on the accuracy of the prediction of the frequency shift FS.

The results show that the choice of the parameters chosen for the reference calculation corresponds indeed to a converged calculation, as slightly lower values of the parameters yield results with the same accuracy. Overall, the following conclusions can be drawn:

- The influence of N_t is very limited. As shown in Fig. (5.4), the time histories of the nonlinear degrees of freedom are relatively simple, and therefore a small number of points in the time domain provides a good description of their periodic waveforms. One should note however that other types of nonlinearities (contact with friction, for instance) would probably require large values of N_t.

- Similarly, the importance of the number of component modes N_{cm} retained in the reduced order model is very limited.

- The value of the penalty coefficient k^* plays a more significant role. Higher values of k^* ensure that the boundary conditions are efficiently enforced. The results show that the frequency shift is predicted within 1 % of error for values greater than 10^{10} N.m^{-1}. One should note that there exists a value of k^*, which, when exceeded, makes solving the nonlinear system describing the dynamics of the structure more difficult. This is due to the fact that for extremely high values of k^*, the linear and the nonlinear components of the nonlinear equations are not properly scaled with respect to each other. Therefore, the choice of an optimum value for k^* is necessarily constrained by the need for accuracy and by the capability of solving the nonlinear system of equations. For the cracked beam studied here, the higher bound for k^* was found around 10^{14} N.m^{-1}.

- The number of harmonics retained in the solution is also very important. The calculations show clearly that one-harmonic approximations of the dynamics of the system lead to grossly inaccurate predictions of the frequency shift. Five harmonics are enough to capture the periodic waveform of the nonlinear DOFs, and therefore the frequency shift can be predicted with an error smaller than 1 %.

- Finally, the number of nonlinear nodes describing the interface plays a great role. Interestingly, it seems that the crack needs to be finely described so that the overall dynamics of the system is accurately captured. Modeling the crack by a couple of pairs of nodes only is not sufficient to eliminate the mutual penetration occurring at the other non-selected nodes of the crack, due to the local modes of deformation of the crack interfaces.

The computational cost associated with these calculations is very low when compared to traditional methods such as direct time integration, which must integrate the nonlinear equations of motion over a very long time until the transient behavior of the structure dies out.

Results obtained with the parameters set to $N_{cm} = 20$, $N_t = 256$, $N_h = 5$, $k^* = 10^{10}$ N.m^{-1} and $N_n = 20$ show that the CPU cost associated to the calculation of the solution of the nonlinear set of equations, for a given frequency near the resonant frequency, is about 2.7 seconds on a laptop with a 1.8 GHz INTEL processor. Such calculation parameters yield a frequency shift within 0.5 % of the reference value.

As a consequence, the efficiency and speed of the method allows one to study various crack configurations very easily. The results presented in Fig. (5.5) show the evolution of

Value of N_{cm}	20	10	5	3	1
Error on FS	-	0.37 %	0.37 %	0.40 %	0.47 %

Table 5.5: Influence of N_{cm} on the accuracy of the prediction of the frequency shift FS.

Value of N_n	$20^{(1)}$	$10^{(2)}$	$8^{(3)}$	$6^{(4)}$	$4^{(5)}$	$2^{(6)}$	$2^{(7)}$	$2^{(8)}$
Error on FS	-	2.0 %	4.1 %	6.6 %	9.3 %	22 %	24 %	66 %

Table 5.6: Influence of the number of nonlinear nodes describing the crack on the accuracy of the prediction of the frequency shift FS. $^{(1)}$All the pairs of nodes (1-11), (2-12), ... (10,20) are selected. $^{(2)}$Nodes (1-11), (3-13), (5-15), (7-17) and (9-19). $^{(3)}$Nodes (1-11), (4-14), (7,17), and (10-20). $^{(4)}$Nodes (1-11), (5-15) and (9-19). $^{(5)}$Nodes (1-11) and (6-16). $^{(6)}$Nodes (1-11). $^{(7)}$Nodes (6-16). $^{(8)}$Nodes (10-20).

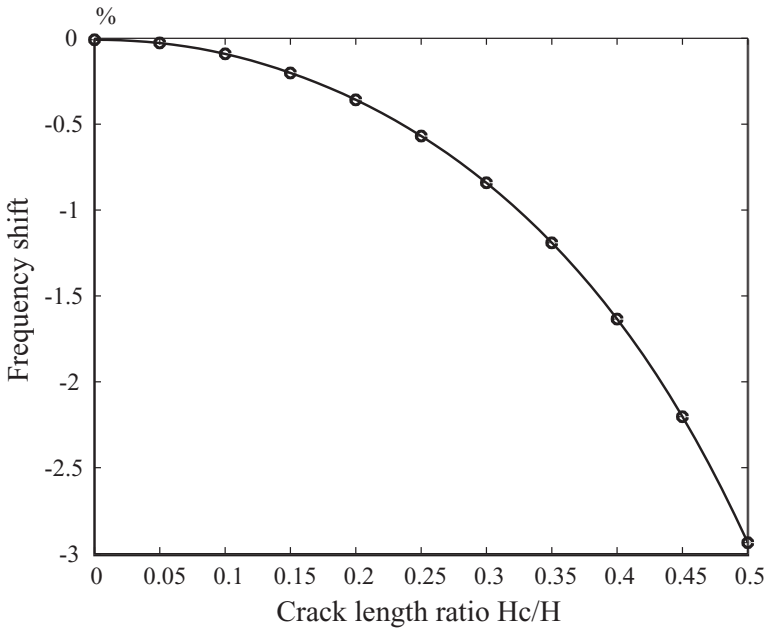

Figure 5.5: Frequency shift predicted for various crack lengths. The percentage of variation is calculated with respect to the natural frequency of the beam without crack.

the frequency shift for various crack length ratios, defined as the crack length H_c divided by the height H of the beam. A crack length ratio equal to zero corresponds to a beam without crack. A value of 0.5 corresponds to the reference calculation presented above, where the frequency shift is equal to -2.93 %.

5.4 Conclusion

A new method for the modeling and the analysis of the complex periodic forced response of structures with nonlinear boundary conditions such as cracks has been presented.

The method, based on (1) a multi-harmonic, frequency domain representation of the dynamics of the structure, and (2) a time domain enforcement of the nonlinear boundary conditions, yields results of excellent accuracy at an extremely low computational cost. An example of application has been studied. Finite element models of cracked beams have been used to illustrate the method's capabilities as well as to investigate the role of the various parameters defining the method. The results show clearly that mono-harmonic approximations of the dynamics of the structure cannot accurately predict the frequency shift due to the presence of the crack, and that a relatively precise description of the crack interfaces in terms of number of nonlinear nodes is also necessary. The performance of the method in terms of accuracy and speed makes it compatible with extensive parametric studies. It is for instance possible to obtain very rapidly the relationship existing between the frequency shift and the length of the crack, a tool of significant importance for monitoring the evolution of damaged, cracked structures.

Although the example of application presented here is relatively simple in terms of geometry, one should note that the method's flexibility allows for studies of structures with more complicated crack characteristics, as well as systems with different types of displacement dependent nonlinearities, such as friction, impacts, or nonlinear stops, for instance. The method shows a great potential for the efficient prediction of the nonlinear forced response of structures represented by complex finite element models featuring a large number of nodes subject to nonlinear boundary conditions.

CHAPTER VI

THEORETICAL AND NUMERICAL ANALYSIS OF ADVANCED MODELS OF FRICTION DAMPERS

6.1 Introduction

Predicting with accuracy the forced response of a friction-damped structure requires the precise modeling of the nonlinear contact interfaces. In the case of bladed-disk assemblies with friction dampers attached, this requirement translates into a need for accurately modeling the physical properties of the friction dampers.

The inherent complexity of nonlinear systems involving friction dampers has however led most of the studies on the subject to focus on approximate models of dampers that are more amenable to efficient numerical parametric studies. One of the most common approximations consists in assuming that the behavior of the dampers can be reduced to that of a simple hysteretic model represented by a single stiffness value, a friction coefficient and a constant or variable normal load. Very few attempts have been made to take into account the exact structural properties of the dampers, and even in that case the models developed have still been approximations of the real structure. For instance, in the structure-like model of damper proposed by Guillen *et al.* [6], the stiffness of the damper is represented by a set of coefficients that are not derived from a finite element model representation of the damper, and therefore are relatively hard to determine. The same

model allows only four contact nodes with constant normal load, and the analysis of the contact efforts stems from a combinatorial approach of the various states of the damper, which severely hinders the generalization of this method to the case of dampers with more contact points.

The theoretical developments and the associated numerical studies addressed in this chapter show that the two methods developed in this dissertation can be applied to realistic structures featuring complex damper models. First, a new model of a flexible wedge damper is presented, and the forced response of an industrial turbine bladed disk is investigated. In this case, the nonlinear operator approach outlined in Chapter II is used to model the effect of the damper on the cyclic structure. Then, using the direct contact approach developed in Chapter III, a flexible, structure-like model of damper is introduced. In this case the properties of the dampers are directly derived from the finite element model of the damper. The DOFs of the damper become in fact part of the system studied, and the nonlinear behavior of the blade-disk-damper assembly is fully described by contact elements between the structure and the damper. As a consequence, this approach is readily applicable to the study of the forced response of friction-damped systems with many contact interfaces, without sacrificing the accuracy of the modeling of any of the components of such assemblies.

6.2 Nonlinear equations of motion in the frequency domain

Following the theoretical analysis developed in Chapter II, the general equations of motion for the friction-damper structure can be expressed in the time domain as

$$\tilde{\mathbf{M}}\ddot{\tilde{\mathbf{x}}} + \tilde{\mathbf{C}}\dot{\tilde{\mathbf{x}}} + \tilde{\mathbf{K}}\tilde{\mathbf{x}} = \tilde{\mathbf{f}}_l + \tilde{\mathbf{f}}_{nl}[\tilde{\mathbf{x}}], \tag{6.1}$$

where $\tilde{\mathbf{x}}$ represents the DOFs of *all* the sectors of the complete assembly, and $\tilde{\mathbf{f}}_{nl}[\tilde{\mathbf{x}}]$ represents the displacement-dependent, nonlinear forces due to the contact efforts.

Using cyclic symmetry properties of the structure, the equations of motion of the nonlinear system can be simplified so as to involve the DOFs of the reference cyclic sector only, and their formulation in the frequency domain is given by the following set of coupled, nonlinear algebraic equations:

$$\underline{\mathbf{\Lambda}}_k^{q(k,e_o)}\underline{\mathbf{x}}_k^0 - \underline{\mathbf{f}}_{l,k}^0 - \underline{\mathbf{f}}_{nl,k}^0(\underline{\mathbf{x}}_0^0, \ldots, \underline{\mathbf{x}}_{n_h}^0) = \mathbf{0}, \quad \text{with} \quad k = 0, \cdots, n_h, \tag{6.2}$$

where $\underline{\mathbf{x}}_k^0$ is the vector containing the Fourier coefficients describing the k-th harmonics of the nonlinear DOFs, n_h is the total number of harmonics retained to approximate the dynamics of the structure, $q(k, e_o)$ represents the relationship between spatial and temporal harmonics

$$q(k, e_o) - ke_o \equiv 0 \; [n_s], \tag{6.3}$$

and the complex matrices $\underline{\mathbf{\Lambda}}_k^q$ are given by

$$\underline{\mathbf{\Lambda}}_k^q = -(k\omega)^2\underline{\mathbf{M}}^q + \underline{j}k\omega\underline{\mathbf{C}}^q + \underline{\mathbf{K}}^q, \tag{6.4}$$

where $\underline{\mathbf{M}}^q$, $\underline{\mathbf{K}}^q$ and $\underline{\mathbf{C}}^q$ represent the complex mass, stiffness and damping matrices associated with the normal modes of vibration of the reference sector, where these modes of vibration feature q nodal diameters.

The calculation of the contact efforts is performed according to the two types of methods described in Chapters II and IV: in the case of the wedge damper, the nonlinear operator approach introduced in Chapter II is used, and therefore the damper is not represented as a structure in the frequency domain equations of motion. The wedge damper DOFs are only used for the calculations performed in the time domain. For the direct contact interactions that describe the efforts exerted by a structure-like damper on the platforms, the DOFs of the damper appear in the frequency domain equations of motions and the analytical formulation developed in Chapter IV is used.

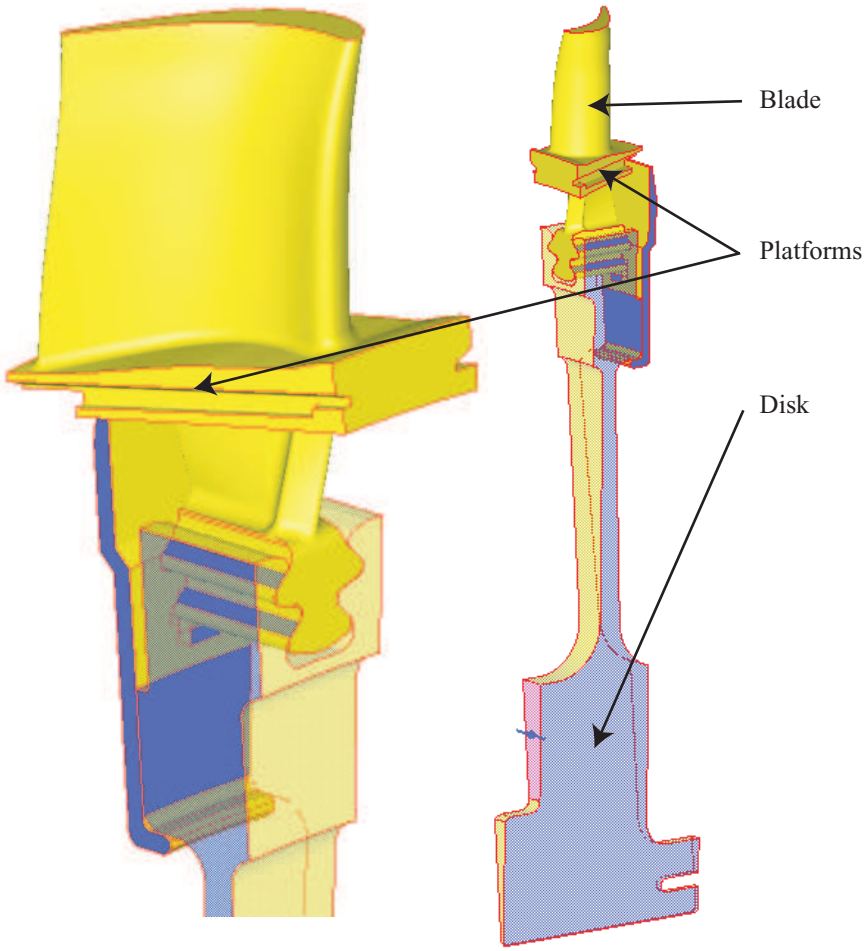

Figure 6.1: Cyclic sector of the turbine studied. Specifically designed slots machined in the platforms of adjacent blades accommodate the dampers, which are maintained in position by the centrifugal load created by the rotation of the engine.

6.3 Model of turbine bladed-disk assembly

The turbine disk studied features 64 blades. A cyclic sector of the bladed disk assembly is shown in Fig. 6.1. The original finite element model of a cyclic sector of the assembly is made of about 130000 DOFs, and this sector is condensed out using a Craig-Bampton component mode synthesis adapted to structures with cyclic boundary conditions. The reduced-order mass and stiffness matrices obtained for each nodal diameter of the cyclic free response of the structure are made of (1) the degrees of freedom associated with the friction nodes of the platform, (2) the DOFs where the linear excitation representing the aerodynamic forcing is applied, and (3) 19 modal coordinates corresponding to the normal modes of vibration of the cyclic sector when the physical DOFs mentioned above are fixed. The physical DOFs are made of three pairs of nodes located under the platforms – where the dampers are attached – and two nodes located at the tip of the blade – where the linear excitation is applied.

Therefore, the condensation of the original structure yields 64 complex, 43-by-43 mass and stiffness matrices which satisfy the conjugate relations $\underline{\mathbf{M}}_p = \overline{\underline{\mathbf{M}}}_q$ and $\underline{\mathbf{K}}_p = \overline{\underline{\mathbf{K}}}_q$ if $p+q = 64$, with $p, q \in [0, \ldots, 63]$. The eigenfrequencies associated to each couple $(\underline{\mathbf{M}}_p, \underline{\mathbf{K}}_p)$ – that is, the frequencies of the natural modes of vibration of the complete bladed-disk when it vibrates with a p nodal-diameter pattern – are shown in Fig. 6.2. Since the modes of vibration can exhibit a strong dependency on the number of nodal diameters of the response of the structure – in particular for small nodal diameters – the exact formulation of the equations of motion of the nonlinear system must take into account these different mass and stiffness matrices.

The engine order of the linear excitation that represents the aerodynamic forcing due to the wake flow of upstream stator elements is 43. The set of harmonic components defining

the linear forcing is $H_l = \{1, 2, 3\}$, that is, the linear forcing is written as:

$$\underline{\mathbf{F}}_l(t) = \underline{\mathbf{F}}_l^1 e^{\underline{j}\omega t} + \underline{\mathbf{F}}_l^3 e^{\underline{j}3\omega t} + \underline{\mathbf{F}}_l^5 e^{\underline{j}5\omega t}, \tag{6.5}$$

where the norm of the third and fifth harmonic components of the excitation are chosen to be respectively 70% and 30% of the norm of the first harmonic. The frequency of this forcing is chosen so as to excite the mode of interest for this study, which is the first bending mode of the blade, found at ω_0.

6.4 Analysis of the forced response with a wedge-damper attached

In this section the forced response of the turbine disk with a wedge damper (also referred to as cottage-roof damper) is analyzed, and the influence of the design parameters of the damper is investigated.

6.4.1 Model of wedge damper

The model of wedge damper used for this study is shown in Fig. 6.3. It is characterized by a 4-by-4 stiffness matrix $\mathbf{K_d}$ corresponding to the tangential and normal DOFs associated with the two contact points of the damper with the platform. This stiffness matrix is derived from the finite element model representation of the damper, and by considering the fact that the damper can only translate in space in the $\mathbf{e_x}$ and $\mathbf{e_y}$ direction. The elimination of the possible rotation of the damper along the $\mathbf{e_z}$ axis means that the rank of $\mathbf{K_d}$ is 2.

The centrifugal efforts applied to the damper are denoted C_1 and C_2. They are derived from the mass properties of the damper, the angular speed of the bladed-disk assembly, and the distance between the dampers and the axis of rotation of the engine. The geometry of the damper is characterized by the angles γ_1 and γ_2, which allows for the study of non-symmetric configurations.

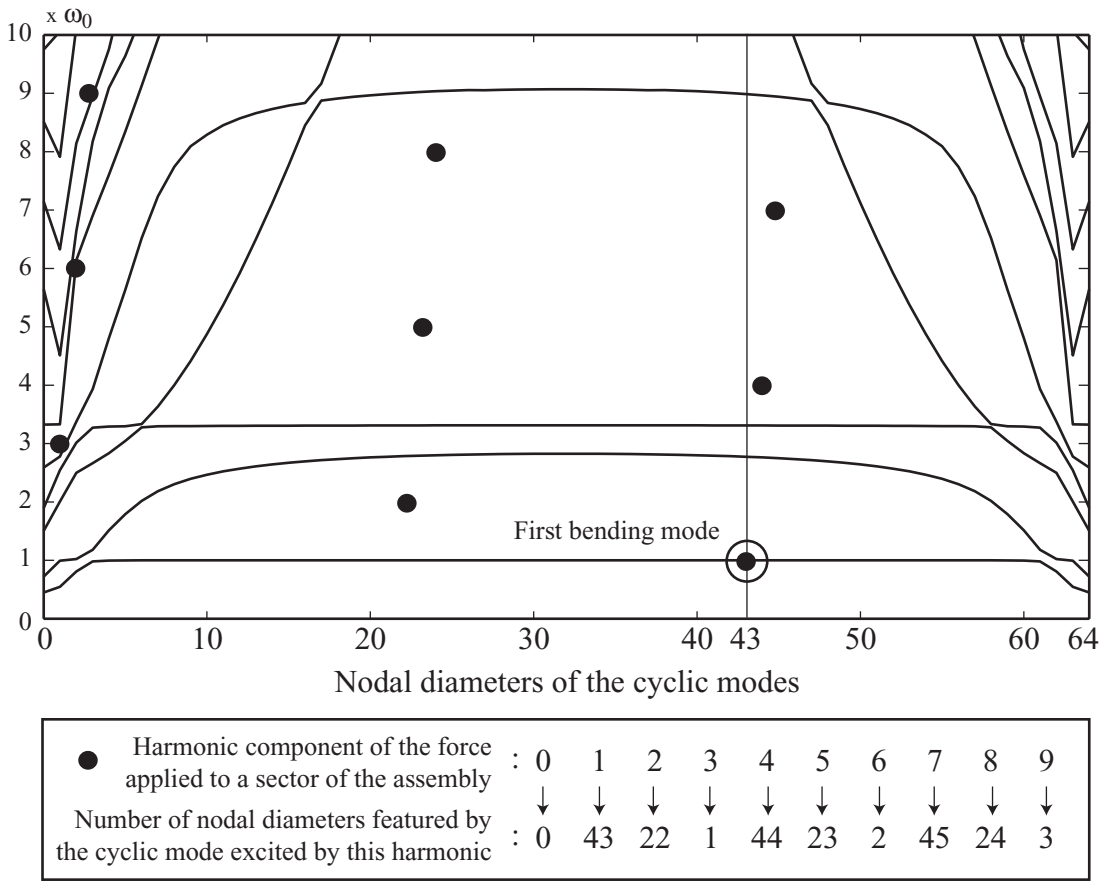

Figure 6.2: *Top*: Normalized frequencies of the cyclic modes of the 64-sector bladed disk assembly, as a function of the number of nodal diameters featured by these modes. The mode of interest for this study corresponds to the first bending mode of the blade associated with an engine-order 43 linear excitation. *Bottom*: Relation between the harmonics of the linear and nonlinear forces applied to a cyclic sector of the assembly and the number of nodal diameters featured by the cyclic modes excited by these harmonics. The first harmonic corresponds to the frequency of the first bending mode studied, with 43 nodal diameters. Higher harmonics excite the structure for different nodal diameters, as illustrated by the dots on the top figure.

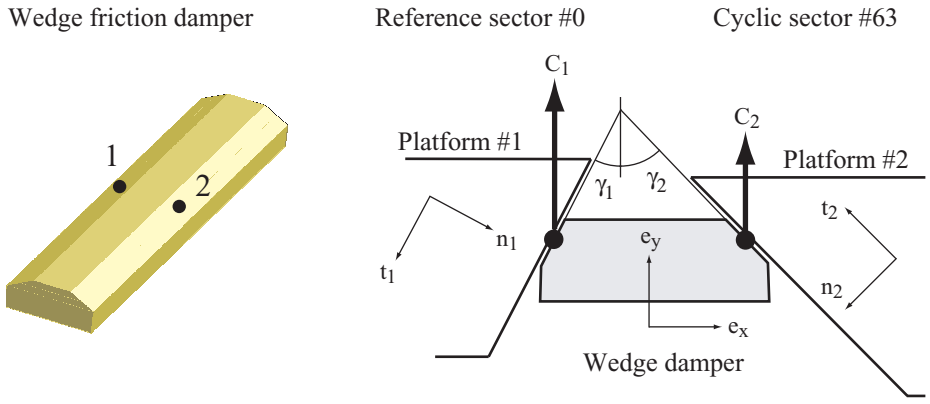

Figure 6.3: Model of wedge friction damper and description of its geometric configuration with the platforms of the turbine bladed disk.

6.4.2 Time-domain analysis of the contact forces

The contact law used to model the contact interface is a simple, constant coefficient Coulomb friction law. Denoting by F_1^t, F_1^n, F_2^t and F_1^n the contact efforts exerted by the damper on the platforms, the following quasi-static equilibrium must be verified at all time:

$$-\mathbf{K}_d\{u_1^t, u_1^n, u_2^t, u_2^n\} + \mathbf{C}_1 + \mathbf{C}_2 = \{F_1^t, F_1^n, F_2^t, F_2^n\}, \tag{6.6}$$

where u_1^t, u_1^n, u_2^t, and u_2^n represent the DOFs of the damper. As described in the method presented in Chapter II, this equation is evaluated in the time domain for every input motion provided by the nonlinear solver, and as a consequence the tangential and normal forces applied to the structure vary as a function of this motion. The contact interfaces can therefore exhibit complicated behaviors with alternating stick and slip phases on each of the platforms.

Now, assuming that x_1^t, x_1^n, x_2^t, and x_2^n represent the nonlinear DOFs of the platforms, the following state equations entirely characterize the behavior of the damper:

- If the first contact node of the damper is in the slip state, the following relations must

be satisfied:

$$F_1^t = \mu F_1^n \quad \text{and} \quad \dot{u}_1^t < \dot{x}_1^t \quad \text{(positive slip)} \tag{6.7}$$

$$\text{or} \quad F_1^t = -\mu F_1^n \quad \text{and} \quad \dot{u}_1^t > \dot{x}_1^t \quad \text{(negative slip)}, \tag{6.8}$$

$$\text{and} \quad u_1^n = x_1^n, \tag{6.9}$$

with similar relations existing for the second contact point.

- If the first contact node of the damper is in the stick state, the following relations must be respected:

$$\dot{u}_1^t = \dot{x}_1^t \quad \text{and} \quad |f_1^t| < \mu |f_1^n|, \tag{6.10}$$

$$\text{and} \quad u_1^n = x_1^n, \tag{6.11}$$

with similar relations existing for the second contact point.

One should note that only the stick, positive slip and negative slip states are mentioned above as possible configurations for the damper: the case of separation is not considered as it does not correspond to a physically realistic configuration, since the wedge dampers – due to their specific geometry – maintain contact with both platforms at all time. This requirement is expressed as an additional condition describing the wedge angles and the friction coefficient of the interfaces:

$$\mu < 1/\tan\gamma_1 \quad \text{and} \quad \mu < 1/\tan\gamma_2. \tag{6.12}$$

The wedge damper can therefore be described by 9 distinct states: stick/stick, stick/positive slip, stick/negative slip, positive slip/stick, positive slip/positive slip, positive slip/negative slip, negative slip/stick, negative slip/positive slip and finally, negative slip/negative slip.

The description of this model of damper is completed by the mathematical criteria that govern the transitions between these states. Assuming that t^* represents the time at which a transition occurs, these criteria can be expressed as:

- *Slip-to-stick transition*. This transition is characterized by the fact that the relative slip velocity is zero. For the first contact point, this can be written as:

$$t < t^*,\ \dot{x}_1^t(t) - \dot{u}_1^t(t) \neq 0 \quad \text{and} \quad \dot{x}_1^t(t^*) - \dot{u}_1^t(t^*) = 0. \tag{6.13}$$

  In addition, the transition must be validated by the fact that the relationship between the contact forces, evaluated at t^* with the stick assumption, do not allow for slip, that is:

$$\mu \frac{\mathrm{d}}{\mathrm{dt}} |F_1^n| > \frac{\mathrm{d}}{\mathrm{dt}} |F_1^t|. \tag{6.14}$$

  Similar conditions exist for the second contact point.

- *Stick-to-slip transition*. The conditions for this transition are obtained by comparing the norm of the tangential and normal components of the contact forces:

$$t < t^*,\ |F_1^t(t)| < \mu |F_1^n(t)| \quad \text{and} \quad F_1^t(t^*) = \mu F_1^n(t^*) \quad \text{(stick/pos. slip)}, \tag{6.15}$$

  or

$$t < t^*,\ |F_1^t(t)| < \mu |F_1^n(t)| \quad \text{and} \quad F_1^t(t^*) = -\mu F_1^n(t^*) \quad \text{(stick/neg. slip)}. \tag{6.16}$$

  In addition, the transition must be validated by the fact that the relationship between the contact forces, evaluated at t^* with the stick assumption, allows for slip, that is:

$$\mu \frac{\mathrm{d}}{\mathrm{dt}} |F_1^n| < \frac{\mathrm{d}}{\mathrm{dt}} |F_1^t|. \tag{6.17}$$

  Similar conditions exist for the second contact point.

Assuming that simultaneous transitions are not physically realistic (that is, state transitions can not occur on both platforms at the same time) due to the usually non-symmetric geometry of the damper and motion of the platforms, and assuming that positive-slip to negative slip and negative-slip to positive-slip transitions are not allowed, the conditions described above yield a maximum of 24 distinct transitions.

The evaluation of the time-domain periodic waveforms of the contact forces is performed using a variation of the time-integration procedure described in Chapter II. A third degree polynomial interpolation of the input motion provided at each iteration by the non-linear solver is used to represent the motion of the platforms. In other words, the motion of the platforms over the intervals $[t_i, t_{i+1}]$ (where $t_1, \cdots, t_{n_t}$ represent the time points for which displacement values describing the motion of the platforms are obtained by Fourier transforms) is interpolated as follows:

$$x_1^t(t) = x_{1,i,0}^t + x_{1,i,1}^t t + x_{1,i,2}^t t^2 + x_{1,i,3}^t t^3 \quad \text{for} \quad t \in [t_i, t_{i+1}], \tag{6.18}$$

with similar expressions for the other variables $x_1^n(t)$, $x_2^t(t)$ and $x_2^n(t)$. The interpolation coefficients $x_{1,i,0}^t$, $x_{1,i,1}^t$, $x_{1,i,2}^t$ and $x_{1,i,3}^t$ are chosen so that they ensure the following continuity conditions:

$$x_1^t(t_i^+) = x_1^t(t_i^-) \quad \text{and} \quad \dot{x}_1^t(t_i^+) = \dot{x}_1^t(t_i^-). \tag{6.19}$$

As a consequence of this formulation, the equations governing the state of the damper as well as the transition criteria can be expressed, for each of the n_t time intervals $[t_i, t_{i+1}]$ of a period of motion, as functions involving these interpolation coefficients. The functions obtained by substituting these interpolation coefficients into the state and transition equations lead to polynomial equations of maximum degree equal to 3. The solutions of these equations can therefore be obtained analytically, without actually performing the numerical time-integration of the equations describing the forces and the displacement of the

damper points. This exact procedure yields significant computational time savings, as it does not require a step size $\delta_t = T/n_t$ as small as that used for a direct time integration. Furthermore, the exact transition times are detected without using numerical approximations.

This procedure is repeated over several periods of the input motion of the platforms, until the steady state of the motion of the damper (and therefore, the steady state of the contact forces applied to the platforms) is reached.

Finally, the proper phase conditions described in Chapter II are applied to the periodic waveforms of the contact forces, so as to derive accurately the Fourier coefficients involved in the frequency-domain equations of motion.

6.4.3 Results

The forced response of the turbine bladed disk has been conducted for several numerical parameters that directly influence the accuracy of the results, so as to identify the value of these parameters beyond which no noticeable accuracy improvement is observed.[1]

- The reduced order matrices obtained for each nodal diameter must represent accurately the dynamics of the structure. This can be controlled by selecting a relatively high number of component modes c_{nm} in the Craig-Bampton synthesis. One should note that these reduced order matrices *do* depend on the nodal diameter featured by the modes of vibration they represent. Figure 6.2 clearly illustrate how the harmonics of the linear and nonlinear forces couple modes of vibrations with various nodal diameters. The method developed herein allows for the accounting of the exact properties of the cyclic structure, instead of taking into account the reduced order

[1] The physical parameters of this study, such as the values used for the centrifugal load, damper stiffness, excitation forcing, structural damping, friction coefficient and frequency range are proprietary. The results are presented here in terms of relative quantities.

matrices calculated for the engine order of the linear excitation only.

- The Hybrid Frequency-Time domain method requires two parameters. The most important one is the number of harmonics, n_h, which defines the set of harmonics $H_{nl} = \{0, 1, \ldots, n_h\}$ used to capture the periodic time histories of the contact forces as well as the time histories of the friction DOFs. The second one is the number of points, n_{time}, used in the time domain to perform the FFT operations required by the method as well as the calculation of the contact forces for a given input motion of the platforms.

The nonlinear forced responses obtained for various numerical parameters as well as several wedge damper configurations are presented in Fig. 6.4. It is shown that the HFT method is numerically converged when the following numerical parameters are chosen: $c_{nm} = 11$, $H_{nl} = \{0, 1, \ldots, 9\}$ and $n_{time=1024}$. These parameters define the reference nonlinear calculation. The analysis of the results presented yields the following conclusions:

- A very effective damping effect is observed for the nominal wedge damper design. The resonant peak of the corresponding nonlinear response is about 12 times smaller than the resonant peak of the forced response of the turbine disk when there are no dampers.

- A one-harmonic approximation of the dynamics of the structure does not provide an accurate estimation of the amplitude of the nonlinear forced response, as the relative error observed with respect to the reference calculation is more than 70%. At least 5 harmonics are required to estimate the value of the resonant peak within a 5% error margin. One should note that neglecting the higher harmonics of the linear forcing is also an important source of inaccuracy (15% error). Although the harmonics 3 and

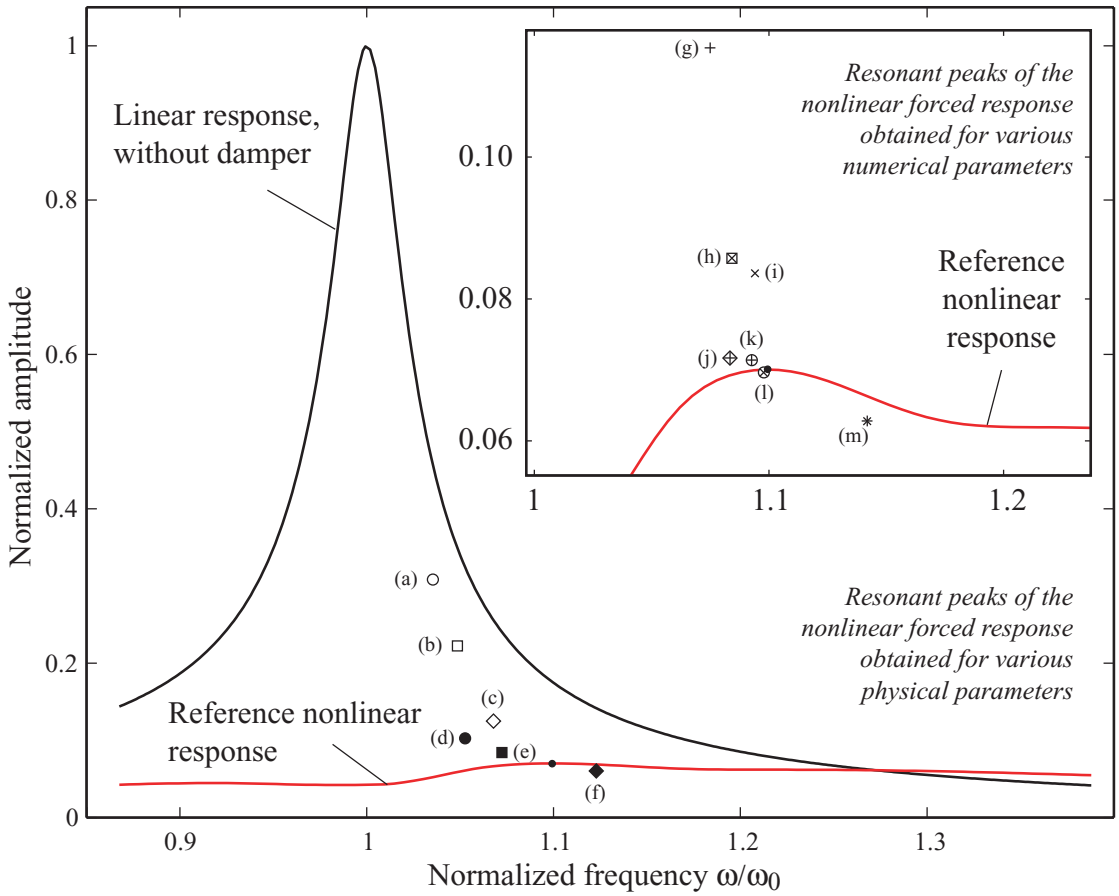

Figure 6.4: Amplitude of the forced response of the tangential component of the first friction node, for various numerical parameters as well as for various damper configurations. The reference calculation is performed for the nominal damper design ($\mathbf{K_d}^n$,γ_1^n,γ_2^n,C_1^n,C_2^n) with the following numerical parameters: $H_l = \{1,3,5\}$, $H_{nl} = \{0,1,2,\ldots,9\}$, $n_{cm} = 11$, and $n_{time} = 1024$. The other results presented in this figure have been obtained by varying one or more of these parameters, the others remaining unchanged with respect to the reference calculation. For the sake of clarity, only the nonlinear resonant peaks corresponding to the forced responses obtained with these modified parameters are plotted above; these peaks are identified by a symbol and a letter which refers to the calculations indicated below. *Resonant peaks obtained for various damper configurations*: (a) $\mathbf{K_d} = \mathbf{K_d}^n/10$; (b) $\mathbf{K_d} = \mathbf{K_d}^n/5$; (c) $\mathbf{K_d} = \mathbf{K_d}^n/2$; (d) $C_1 = 0.94 \times C_1^n$ and $C_2 = 0.94 \times C_2^n$; (e) $\gamma_1 = \gamma_1^n + 1^o$ and $\gamma_2 = \gamma_2^n - 1^o$; (f) $\gamma_1 = \gamma_1^n - 1^o$ and $\gamma_2 = \gamma_2^n + 1^o$. *Results obtained for various numerical parameters*: (g) $H_{nl} = \{0,1\}$; (h) $H_{nl} = \{0,1,2,3\}$; (i) $H_l = \{1\}$; (j) resonant peak obtained with the nominal parameters by assuming that the reduced stiffness and mass matrices of a cyclic sector of the assembly are independent of the number of nodal diameters, that is: $\underline{\mathbf{M}}_p = \underline{\mathbf{M}}_{43}$ and $\underline{\mathbf{K}}_p = \underline{\mathbf{K}}_{43}$, for $p = 0,\ldots,64$; (k) $H_{nl} = \{0,1,2,3,4,5\}$; (l) $H_{nl} = \{0,1,\ldots,15\}$, $c_{nm} = 16$, $n_{time} = 2048$; (m) $c_{nm} = 1$.

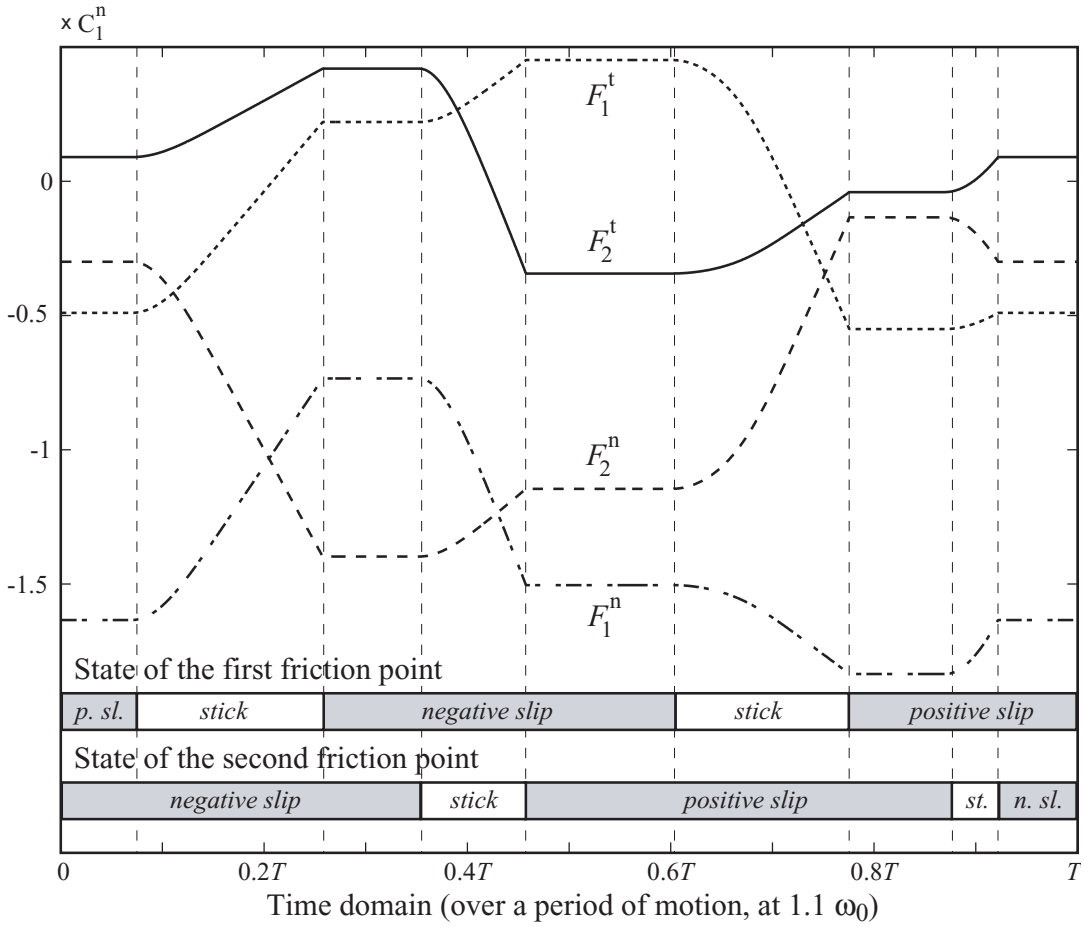

Figure 6.5: Time histories of the tangential and normal components of the contact forces observed at the two friction points of the damper, and time histories of the state (stick or slip) of the contact points. For each contact point *positive slip* is characterized by $F^t = \mu F^n$, and *negative slip* is characterized by $F^t = -\mu F^n$. The results are obtained at $\omega = 1.1\ \omega_0$ which corresponds to the resonant peak of the nonlinear response with nominal parameters. The time histories presented correspond to the actual forces exerted by the damper on the first contact point of the reference sector and the second contact point of the adjacent sector.

5 of the linear force do not affect the forced response in the linear case (the modes they excite are decoupled), they play a significant role in the nonlinear case as the modes of the structure become coupled by the nonlinear force.

- The damper configurations tested show that the nonlinear forced response is highly sensitive to the wedge damper design. The response seems most affected by small changes in the values of the normal loads and the wedge angles, whereas it takes huge variations of the stiffness of the damper to introduce significant amplitude differences.

The time histories of the contact forces applied to the bladed disk at the frequency of the resonant nonlinear peak are shown in Fig. 6.5. They illustrate the complicated nature of the contact interactions between the damper and the platforms, as eight state transitions are observed over a single period of motion. The complex periodic waveforms observed explain why a high number of harmonics is necessary to accurately capture the dynamics of such systems.

The efficiency of the method developed should also be underscored: the nonlinear forced response has been calculated for 150 frequencies in less than 15 minutes on a laptop with a Intel 1.8 GHz processor. The HFT method is therefore a very efficient and accurate tool for the parametric study of flexible wedge friction dampers.

6.5 Analysis of the forced response with a structure-like damper attached

In this section the forced response of the same cyclic structure is studied; the model of friction damper is however very different: it is represented by a finite element model, and the stiffness properties associated to the DOFs of this model are included in the frequency domain equations of the nonlinear system. The interaction of the damper and the structure

is modeled by a set of contact elements according to the direct contact approach defined in Chapter IV.

A simple example is first studied to show the equivalence between the nonlinear operator approach used to model friction dampers and introduced in Chapter II, and the direct contact approach which requires the damper DOFs to be part of structure analyzed, and which was developed in Chapter IV. Then the friction-damped, forced response of the turbine blade assembly is investigated with a complex damper represented by an elastic structure having four contact points with the platforms.

6.5.1 Theoretical analysis

Let $\tilde{\mathbf{K}}$ denote the stiffness matrix of the system made of *all* the sectors of a bladed disk assembly. Assuming that each cyclic sector of the assembly is associated with a local reference frame deduced by successive rotations of that of the reference sector, and that the DOFs of each cyclic sector are expressed in these local coordinate systems, $\tilde{\mathbf{K}}$ can be written as:

$$\tilde{\mathbf{K}} = \begin{bmatrix} \mathbf{K_s} & \mathbf{K_c} & \mathbf{0} & \mathbf{0} & \mathbf{0} & \cdots & \mathbf{K_c} \\ \mathbf{K_c} & \mathbf{K_s} & \mathbf{K_c} & \mathbf{0} & \mathbf{0} & \cdots & \mathbf{0} \\ \mathbf{0} & \mathbf{K_c} & \mathbf{K_s} & \mathbf{K_c} & \mathbf{0} & \cdots & \mathbf{0} \\ \vdots & \vdots & \vdots & \vdots & \vdots & \ddots & \vdots \\ \mathbf{K_c} & \mathbf{0} & \mathbf{0} & \mathbf{0} & \mathbf{0} & \mathbf{K_c} & \mathbf{K_s} \end{bmatrix}, \tag{6.20}$$

where $\mathbf{K_s}$ and $\mathbf{K_c}$ represent, respectively, the stiffness of a sector and the elastic coupling existing between the adjacent sectors. Now, assuming that an additional, elastic damper is appended to each of the cyclic sectors, and that it is structurally independent from the cyclic assembly, then the new stiffness matrix $\tilde{\mathbf{K}}^{+}$ of the augmented assembly can be

written as:

$$\tilde{\mathbf{K}}^{+} = \begin{bmatrix} \mathbf{K}_\mathbf{s}^{+} & \mathbf{K}_\mathbf{c}^{+} & \mathbf{0} & \mathbf{0} & \mathbf{0} & \cdots & \mathbf{K}_\mathbf{c}^{+} \\ \mathbf{K}_\mathbf{c}^{+} & \mathbf{K}_\mathbf{s}^{+} & \mathbf{K}_\mathbf{c}^{+} & \mathbf{0} & \mathbf{0} & \cdots & \mathbf{0} \\ \mathbf{0} & \mathbf{K}_\mathbf{c}^{+} & \mathbf{K}_\mathbf{s}^{+} & \mathbf{K}_\mathbf{c}^{+} & \mathbf{0} & \cdots & \mathbf{0} \\ \vdots & \vdots & \vdots & \vdots & \vdots & \ddots & \vdots \\ \mathbf{K}_\mathbf{c}^{+} & \mathbf{0} & \mathbf{0} & \mathbf{0} & \mathbf{0} & \mathbf{K}_\mathbf{c}^{+} & \mathbf{K}_\mathbf{s}^{+} \end{bmatrix}, \tag{6.21}$$

where

$$\mathbf{K}_\mathbf{s}^{+} = \begin{bmatrix} \mathbf{K_s} & \mathbf{0} \\ \mathbf{0} & \mathbf{K_d} \end{bmatrix} \quad \text{and} \quad \mathbf{K}_\mathbf{c}^{+} = \begin{bmatrix} \mathbf{K_c} & \mathbf{0} \\ \mathbf{0} & \mathbf{0} \end{bmatrix}, \tag{6.22}$$

and where $\mathbf{K_d}$ is the stiffness matrix of the damper. Since the dampers are not physically attached to the rest of the structure, there are no coupling terms between the dampers and the sectors, and of course there are no coupling terms between the dampers themselves. The absence of coupling terms also signifies that the dampers retain all of the six DOFs associated to rigid body motions.

Following the same analysis as the one performed in Chapter II, the set of nonlinear frequency-domain equations that govern the forced response of the structure can be written as:

$$\underline{\mathbf{\Lambda}}^{+q(k,e_o)}_{k}\underline{\mathbf{x}}^{+0}_{k} - \underline{\mathbf{f}}^{+0}_{l,k} - \underline{\mathbf{f}}^{+0}_{nl,k}(\underline{\mathbf{x}}^{+0}_{k}, \ldots, \underline{\mathbf{x}}^{+0}_{n_h}) = \mathbf{0}, \quad k = 0, \ldots, n_h \tag{6.23}$$

with the following definitions:

- The vector representing the Fourier coefficients of the k-th harmonic of the nonlinear DOFs of the reference sector, $\underline{\mathbf{x}}^{+0}_{k}$, is partitioned as:

$$\underline{\mathbf{x}}^{+0}_{k} = \begin{bmatrix} \underline{\mathbf{x}}^{0}_{k} \\ \underline{\mathbf{x}}_{\mathbf{d}}{}^{0}_{k} \end{bmatrix} \tag{6.24}$$

- The jacobian matrices $\underline{\mathbf{\Lambda}}^{+q(k,e_o)}_{k}$ are given by

$$\underline{\mathbf{\Lambda}}^{+q}_{k} = -(k\omega)^2\underline{\mathbf{M}}^{+q} + \underline{j}k\omega\underline{\mathbf{C}}^{+q} + \underline{\mathbf{K}}^{+q}, \tag{6.25}$$

where

$$\underline{\mathbf{M}}^{+q} = \begin{bmatrix} \underline{\mathbf{M}}^{q} & \mathbf{0} \\ \mathbf{0} & \mathbf{0} \end{bmatrix}, \quad \underline{\mathbf{C}}^{+q} = \begin{bmatrix} \underline{\mathbf{C}}^{q} & \mathbf{0} \\ \mathbf{0} & \mathbf{0} \end{bmatrix}, \quad \underline{\mathbf{K}}^{+q} = \begin{bmatrix} \underline{\mathbf{K}}^{q} & \mathbf{0} \\ \mathbf{0} & \mathbf{K_d} \end{bmatrix}, \tag{6.26}$$

and where $\underline{\mathbf{M}}^{q}$, $\underline{\mathbf{C}}^{q}$, $\underline{\mathbf{K}}^{q}$ correspond to the complex matrices of the cyclic reference sector alone.

- The relation between the spatial and temporal harmonics is unchanged:

$$q(k, e_o) - k e_o \equiv 0[n_s]. \tag{6.27}$$

- The Fourier coefficients corresponding to the k-th harmonic of the linear forcing $\underline{\mathbf{f}}^{+0}_{l,k}$ are defined as

$$\underline{\mathbf{f}}^{+0}_{l,k} = \begin{bmatrix} \underline{\mathbf{f}}^{0}_{l,k} \\ \underline{\mathbf{f}}_{\mathbf{d}}{}^{0}_{l,k} \end{bmatrix}. \tag{6.28}$$

  Usually, the definition of the linear forcing applied to the dampers only includes the constant, real terms due to the centrifugal efforts applied to them.

- The Fourier coefficients corresponding to the k-th harmonic of the nonlinear contact forces are defined as:

$$\underline{\mathbf{f}}^{+0}_{nl,k} = \begin{bmatrix} \underline{\mathbf{f}}^{0}_{nl,k} \\ \underline{\mathbf{f}}_{\mathbf{d}}{}^{0}_{nl,k} \end{bmatrix}. \tag{6.29}$$

  Now, if the dampers attached to the assembly are not straddling adjacent cyclic sectors, one can derive from the law of action and reaction the following relation:

$$\underline{\mathbf{f}}^{0}_{nl,k} = -\underline{\mathbf{f}}_{\mathbf{d}}{}^{0}_{nl,k}. \tag{6.30}$$

  However, this relation is usually not verified in the more general – and common – case of a damper straddling two adjacent cyclic sectors. In this case, the reference sector is subject to the contact forces created by the damper straddling the reference

sector (defined as the sector $\#0$) and the sector $\#N_s - 1$, and it is also subject to the contact forces created by the damping straddling the reference sector and the sector $\#1$.

Assuming that $f_{D_i \to S_j}(t)$ is the force exerted by the damper $\#i$ onto the cyclic sector $\#j$ and $f_{S_i \to D_j}(t)$ is the force exerted by the sector $\#i$ onto the damper $\#j$, and using the phase ϕ_t introduced in Chapter II, the following relations can be written:

$$f_{D_0 \to S_0}(t) = -f_{S_0 \to D_0}(t), \tag{6.31}$$

$$f_{D_1 \to S_0}(t) = -f_{S_0 \to D_1}(t), \tag{6.32}$$

$$f_{D_1 \to S_0}(t) = f_{D_0 \to S_{N_s-1}}(t - \phi_t) = -f_{D_{N_s-1} \to S_0}(t - \phi_t), \tag{6.33}$$

and the Fourier coefficients of $\underline{\mathbf{f}}^{+0}_{nl,k}$ reflect the phase differences expressed in these relations.

Finally, the time-domain calculation of the contact efforts is made by the same type of time-marching or time-integration procedures as presented in Chapter II.

With this approach, any type of elastic structure can be appended to the matrices representing the cyclic sectors of the bladed-disk assembly.

6.5.2 Validation of the direct-contact approach

For simple models of dampers, the nonlinear operator approach and the direct contact approach should yield the same results. In this study, the forced response of the turbine bladed disk is analyzed with these two methods when a simple, platform-to-platform friction damper with constant normal load is attached. The results are presented in Fig. 6.6

The parameters defining the nonlinear operator and the structure-like friction damper are chosen so that the behavior of the two systems becomes identical when the stiffness k^* of the contact element required by the direct contact approach tends towards infinity. In

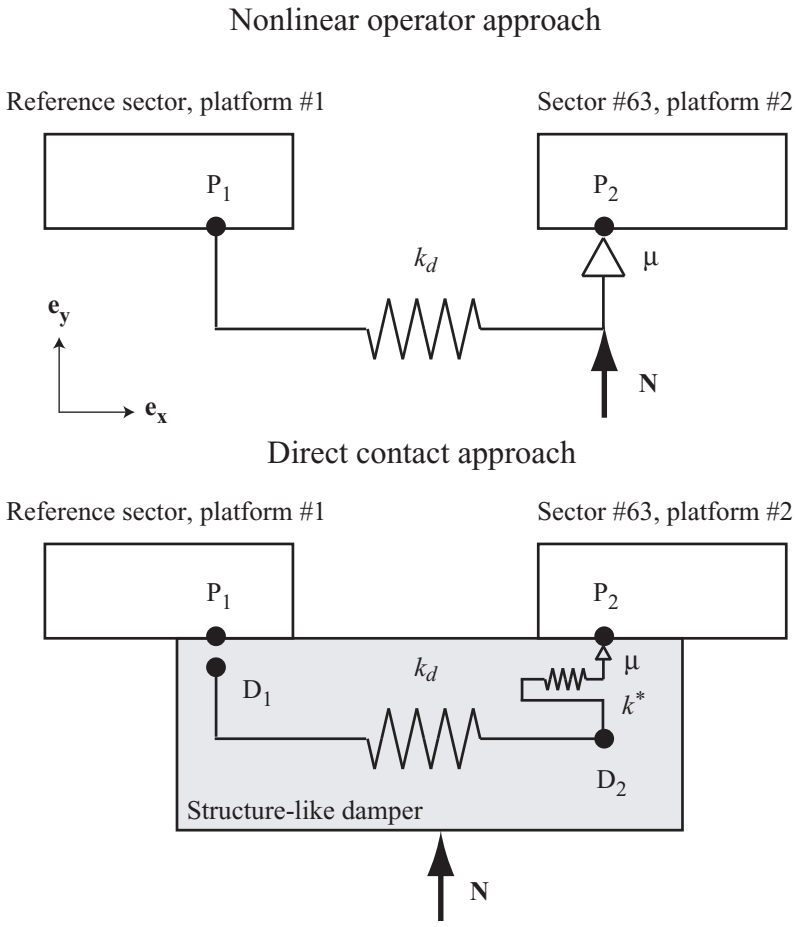

Figure 6.6: Equivalent analysis techniques for a simple model of friction damper attached to the cyclic sectors of the turbine bladed disk. *Nonlinear operator approach (top).* In this approach the damper is considered as a nonlinear operator providing the contact efforts at the platform DOFs P_1 and P_2 as a function of their displacement. The parameters of the operator are k_d, N and μ. *Direct contact approach (Bottom).* Here the damper is modeled by a structure – a very simple spring of stiffness k_d – with DOFs associated to its two nodes D_1 and D_2. In order to make the comparison with the first method, and in order to eliminate the rigid body mode of the damper associated with the $\mathbf{e_x}$ direction, the *relative* motion between P_1 and D_1 is eliminated. The second node D_2 directly rubs onto the platform P_2 and the method requires that a contact element must be inserted between these two DOFs. The behavior of this system converges towards that of the first, when the stiffness k^* of the contact element tends towards infinity.

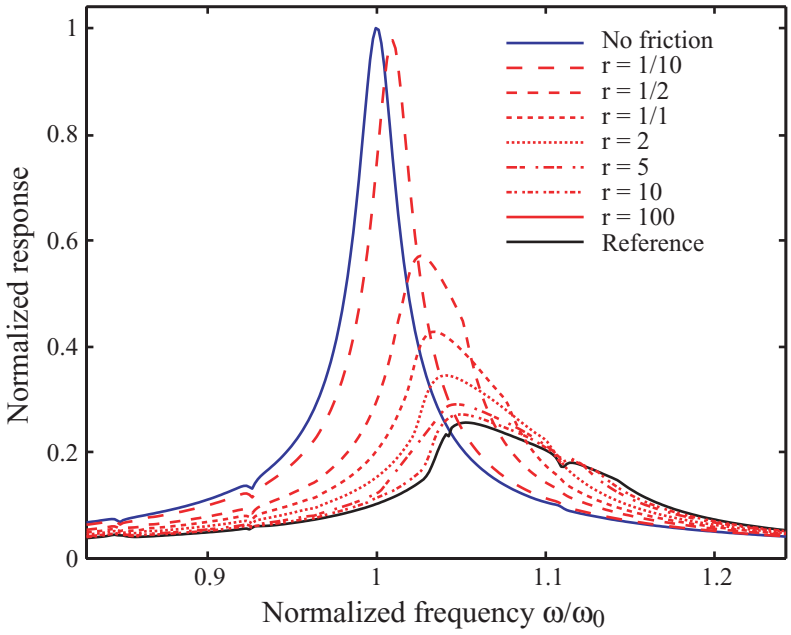

Figure 6.7: Comparison of the forced response of the tangential component of the displacement of one of the friction nodes of the platforms, when calculated with the nonlinear operator approach and with the direct contact approach. The reference calculation corresponds to the results obtained with the nonlinear operator approach, and it is compared to the responses obtained for various ratios $r = k^*/k_d$ with the direct contact approach.

addition, the same number of harmonics is kept in both methods.

The results of this comparison are presented in Fig. 6.7. The forced response obtained for various ratios $r = k^*/k_d$ with the direct contact method is compared to the reference calculation obtained with the nonlinear operator approach. As expected, the two methods yield similar results when k^* tends towards infinity. Actually, an excellent agreement is already obtained when the value of the stiffness of the contact element is just ten times that of the damper itself, and when this ratio exceeds 100 the two responses are virtually indistinguishable. For these values of r, the augmented system (since the cyclic sector of the blade-disk-damper assembly is now made of 45 DOFs) captures very accurately the nonlinear behavior due to the damper. The CPU cost for the direct contact method is similar to that for the nonlinear operator approach: the CPU time required to calculate the

response at a nonlinear frequency is on average about 0.2s with a personal laptop running at 1.8GHz.

The benefits of the direct contact approach are obvious: the dampers can now be represented by finite element models, and no approximations regarding their geometry are necessary anymore. Although the system studied here is indeed simple, since the definition of the damper as a structure is restricted to its minimum definition (a 2-DOF spring), it is clear that the technique is readily applicable to models of dampers with many more structural DOFs, with the advantage that the stiffness properties of these dampers are integrally part of the system studied. This great flexibility of analysis means that systematic parametric studies can be carried out with ease, since they are now based on a finite element model representation of the dampers. This is of great importance on a design standpoint.

6.5.3 Model of structure-like damper

The forced response of the cyclic assembly with a more complicated structure-like damper attached is now analyzed. The model of damper is shown in Fig. 6.8.

The damper is represented by a structure whose shape is more or less that of a hollow cube, with an opening at the bottom surface. The geometry of the damper is defined by its outer dimensions L, l, and h, and its wall thickness w. The material properties of the damper are its Young modulus, Poisson ratio and density ρ, as well as the friction coefficient of the top surface[2]. The mass of the damper is deduced from its geometry, and is used to calculate the centrifugal efforts C_A, C_B, C_C and C_D. These efforts are applied in the $\mathbf{e_z}$ direction on each of the four points of contact between the damper and the platforms of the structure. The damper straddles two adjacent sectors of the cyclic assembly: the points of contact A and B are interacting with the platform of the reference assembly, and the points of contact C and D are interacting with the platform of the sector

[2]The exact values of the damper parameters are proprietary.

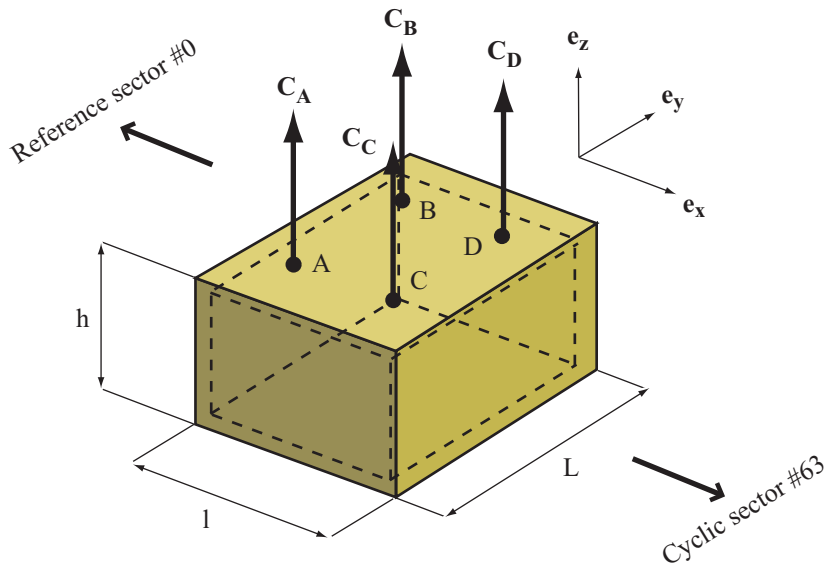

Figure 6.8: Model of structure-like damper with multiple contact nodes.

#63.

A finite element model that takes into account all these physical properties is constructed. Since this FE model contains many more DOFs than necessary for the present study, a Craig-Bampton condensation method is applied and yields a reduced-order model made of the 12 physical DOFs associated to the contact nodes, and 10 modal coordinates. Since the damper is not subject to boundary conditions other than the nonlinear interactions occuring at the platform interfaces, its reduced-order stiffness matrix $\mathbf{K_d}$ allows for all of the six rigid body modes of the damper.

6.5.4 Choice of boundary conditions and contact elements

The augmented system representing the blade-disk-damper assembly features 65 DOFs and ideally, this friction-damped system can be described without assumptions by enforcing 3-D friction conditions at each of the points of contact between the damper and the platforms.

This approach allows however the structure-damper assembly to feature the rigid body

modes associated with the translations of the damper in the $\mathbf{e_x}$ and $\mathbf{e_y}$ directions, as well as the rotation about the $\mathbf{e_z}$ axis. The presence of these rigid body modes has proved to be a source of extreme numerical complications and in most cases the nonlinear forced response could not be calculated. Among the possible explanations for these difficulties, one can note that (1) allowing for the *creep* or *drift* of the damper under the platforms may prevent the damper to reach a periodic steady state, (2) the full structural coupling existing between the *tangential* and *normal* friction components at each contact point may not ensure the uniqueness of the response of the damper, and (3) the full structural coupling existing between the *contact nodes* of the damper prevents the nonlinear solver from converging towards the solution representing the nonlinear force, because of the intricate nature of a full 3-D contact at each of the four nodes. These possible explanations are difficult to investigate independently, even when using exact analysis techniques such as time integration, due to the overall complexity of the structure studied.

In order to alleviate these problems, a more stringent set of boundary conditions is used:

- The relative displacement of the damper with respect to the platform is eliminated in the $\mathbf{e_x}$ and $\mathbf{e_y}$ directions for the point A.
- The relative displacement of the damper with respect to the platform is eliminated in the $\mathbf{e_x}$ direction for the point B.

These boundary conditions eliminate the rigid body modes corresponding to the translation of the damper in the $\mathbf{e_x}$ and $\mathbf{e_y}$ directions. The rotation of the damper about the $\mathbf{e_z}$ axis is also eliminated. The elimination of these relative DOFs is achieved by simple linear manipulations of the rows and columns of the structural matrices of the augmented assembly. Thus, the dampers and the structure become structurally coupled with respect

to these particular DOFs.

This coupling can actually be interpreted as a natural enforcement of the actual boundary conditions applied to the dampers: the dampers usually fit snuggly into cavities under the platform that precisely accommodate their geometry, thus preventing the rigid body modes mentioned above, or to the least strongly limiting the corresponding relative displacements.

The three rigid body modes that are not eliminated correspond to the translation of the damper along the $\mathbf{e_z}$ axis and to the two rotations about the $\mathbf{e_x}$ and $\mathbf{e_y}$ axis. The presence of these rigid body modes is necessary to allow for the isostatic determination of the configuration of the damper as a function of the position of the four platform nodes. For instance, if the four nodes of the platform are at a given time displaced by the same amount in the $\mathbf{e_z}$ direction, the damper must be able to follow the same motion to maintain the contact – thanks to the centrifugal efforts – with the platforms.

The contact elements chosen to model the interaction between the damper and the platform reflect the computational need for simplification of the complexity of the system:

- The contact element acting on the node A takes into account the variable normal efforts in the $\mathbf{e_z}$ direction and this direction only (since there is no relative motion at this point in the other directions).

- The contact elements chosen for the nodes B,C and D allow for friction along a predetermined direction and variable normal load. The direction of friction is deduced from the study of the linear response of the assembly without damper attached, and is defined by the direction in which the largest component of the response if observed. In the case studied, and given the type of excitation chosen, this direction of privileged motion coincides with the $\mathbf{e_x}$ tangential direction. One should note

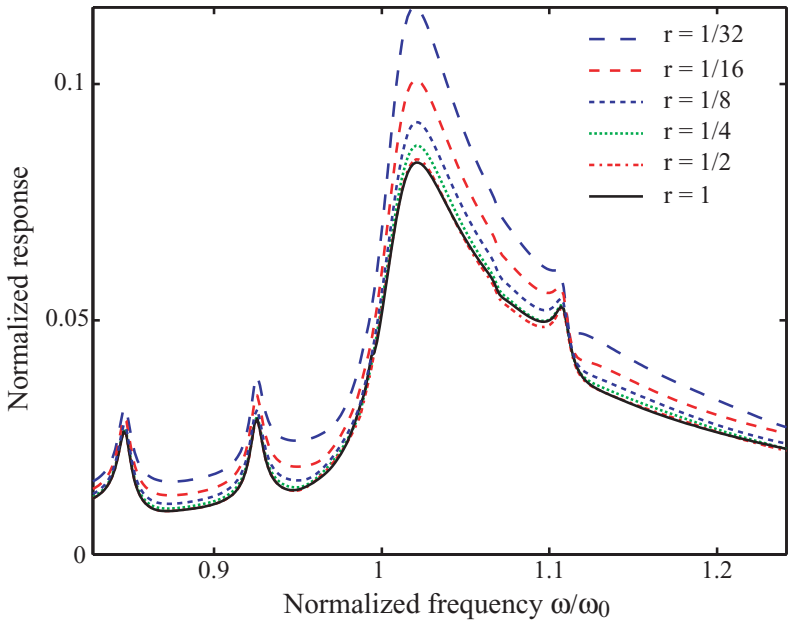

Figure 6.9: Forced response of the tangential component of the node A of the platform. The reference calculation is obtained with the contact parameter k^*_{ref}. The ratio r is defined as $r = k^*/k^*_{ref}$, and the forced responses obtained for various values of r are calculated.

however that if needed, the choice of another direction could be easily enforced by rotating these contact elements appropriately.

With these modeling assumptions, the damper/structure interface is modeled by a set of 14 nonlinear DOFs.

6.5.5 Results

The nonlinear forced response of the turbine bladed disk is presented in Fig. 6.9. The amplitude of the forced response of the $\mathbf{e_x}$ component of the displacement of the blade at the contact node A is given for various values of the method parameter k^*. The calculations are performed with 9 harmonics, a number which corresponds to the converged case. The forced response presented in Fig. 6.9 shows the convergence of the direct contact method with respect to k^*. Values of k^* beyond that used for the reference calculation do not yield any noticeable improvement of the forced response.

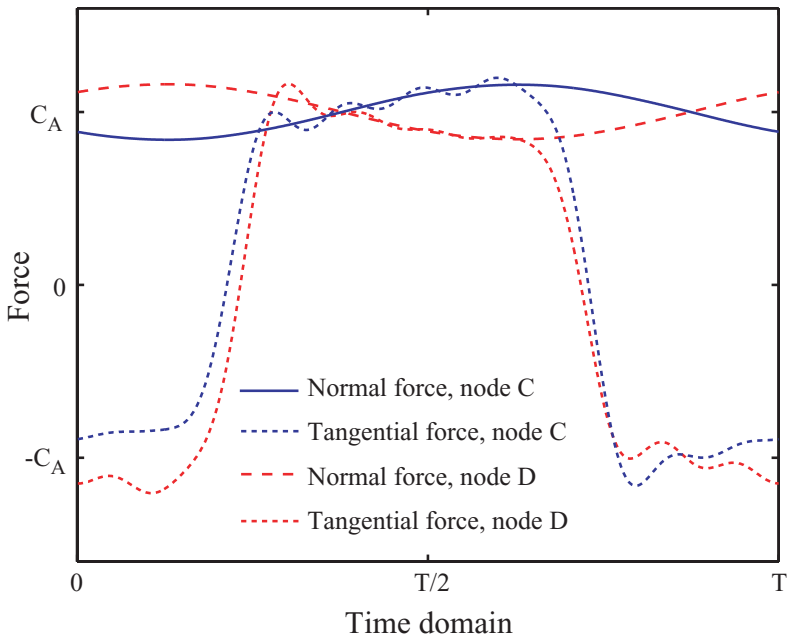

Figure 6.10: Time histories of the periodic waveforms of the contact forces applied by the damper to the nodes C and D of the platform. These forces are approximated by 9 harmonics, and are obtained at the frequency of the resonant nonlinear peak. C_A is the value of the normal load applied to the node A of the damper. In this study all the normal loads applied to the damper are equal to each other.

The results illustrate the effectiveness of the friction damper, since the amplitude of the nonlinear resonant peak is about 0.08 times that of the linear case. The presence of additional resonances (which were absent in the wedge damper study) also illustrate the increase of complexity due to the use of a realistic structure-like friction damper. And the forced responses are obtained very efficiently: the response at each frequency is calculated in about 0.3s.

The Figure 6.10 shows the time histories of the contact forces obtained with the reference calculation. The tangential and normal components of the forces applied by the damper on the structure (at the nodes C and D) are depicted over a period of motion. These time histories are obtained at the frequency corresponding to the resonant nonlinear peak. The normal efforts applied by the damper are clearly variable, and they vary around

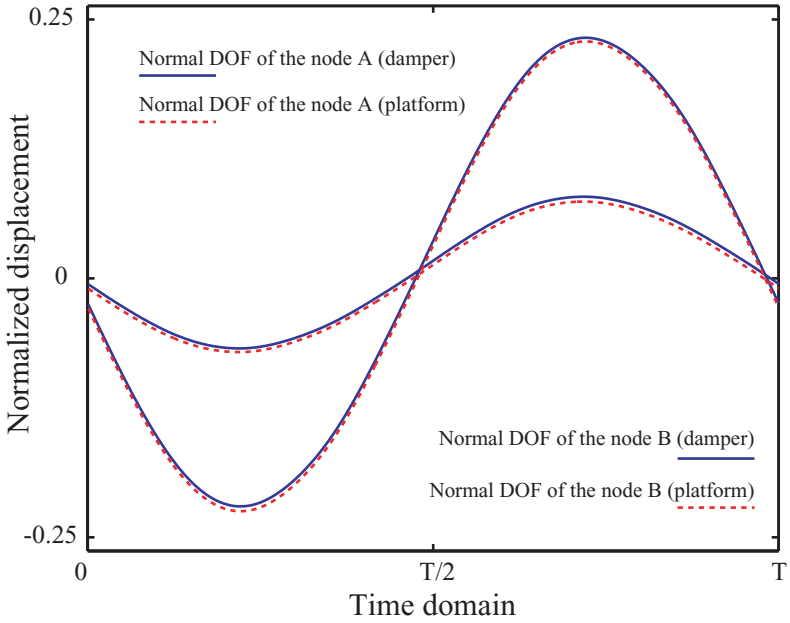

Figure 6.11: Time histories of the normal DOFs of the damper and the platform at the contact nodes A and B, obtained at the nonlinear resonant peak frequency.

the value of the centrifugal forces applied to the four nodes of the damper. One can also check that at all times, the sum of the normal efforts applied by the damper on the platform is constant and equal to the sum of the centrifugal forces applied to the damper.

The Figure 6.11 shows the time histories of the normal component of the displacement of the contact nodes A and B, for the damper and platform DOFs. One can observe that at all times, there exists a small penetration of the damper nodes in the platform. This is a consequence of the direct contact approach. The low value of the penetration is due to the good convergence of the forced response as a function of k^*.

6.6 Conclusion

Two new models of dampers have been presented. The first one is a flexible wedge damper, which takes advantage of the nonlinear operator approach of modeling the displacement-dependent forces created by the damper. The second damper is a flexible structure that is appended to the system it interacts with. The direct contact approach,

which is based on the definition of contact elements that characterize the relationship between the damper and the structure, has been applied to this model with great success.

The nonlinear forced responses of an industrial turbine bladed-disk assembly have been studied with the two models of dampers. In both cases, the complexity of the response of the structure as well as the complexity of the contact efforts has been highlighted. These examples show that the dynamics of friction damped systems can be obtained very accurately and at a low computational cost. The studies conducted in this chapter also demonstrate the fact that strong approximations regarding the modeling of friction dampers are not required anymore. In particular, the flexibility and efficiency of the direct contact method should allow the investigation of friction damped systems – and other systems with displacement-dependent nonlinearities – with an unprecedented degree of realism. Since in this method the dampers are represented by their finite element models, the direct contact approach should also be applicable to many different types of systems, independently of their geometry or the number of contact points.

CHAPTER VII

CONCLUSIONS

7.1 Dissertation contributions

The main contributions of this work are as follows:

- The formulation of the Hybrid Frequency-Time (HFT) method used for the study of structures with displacement-dependent nonlinearities has been generalized, and in particular its application to the theoretical analysis of bladed-disk assemblies with friction dampers has been extended.
  - Modifications of the original HFT method have been introduced in order to meet the demanding requirements and constraints associated with the study of the friction-damped, forced response of realistic industrial structures. A new method of condensation of the frequency-domain, nonlinear equations has been developed. It is particularly adapted to the study of nonlinear systems with a large number of degrees of freedom (DOFs). An efficient formulation for the calculation of the jacobian of the nonlinear equations describing systems with a large number of friction dampers has also been introduced.
  - The theoretical analysis of structures with cyclic symmetry has been introduced. It has been shown that the exact forced response of a cyclic assembly

with friction dampers can be deduced rigorously from the analysis of the behavior of a single cyclic sector of the assembly. A relation between the spatial harmonics of the response of the structure and the temporal harmonics of the excitation has been exhibited. This new modeling technique takes into account the variation of the elastic properties of cyclic assemblies as a function of the spatial harmonics of the response and, by extension, as a function of the temporal harmonics of the nonlinear forces.

  - The framework for the theoretical modeling of friction dampers as nonlinear operators as been established. Within this framework, the procedures used to handle the time-domain representation of the nonlinear forces have been delineated for several models of dampers, including a 3-D model with variable normal load, and particular attention has been paid to establish the rigorous way of calculating these forces in the case of systems with cyclic symmetry.

- These developments have been applied to several case studies. The analysis of the forced response of stand-alone structures, cyclic and mistuned assemblies has been carried out for various types of frictional configurations. The results obtained have highlighted the capability of the HFT method in terms of its accuracy, speed, and its potential for conducting efficient parametric studies of friction-damped structures. These studies have shown how complex the dynamics of systems with friction damping can be, when effects like 3-D contact or localization of energy due to mistuning are present.

- A new direct contact approach based on the HFT method has been developed, for the study of the nonlinear forced response of systems experiencing contact phenomena which are not necessarily due to the action of friction dampers. This new method is

still based on a dual time-domain/frequency domain representation of the dynamics of such systems; however, the analysis of the boundary conditions at the contact interfaces replaces that of the contact efforts used in the regular HFT method, thus offering a significant advantage when the periodic waveforms of the contact efforts are complicated. In this method, special contact elements are added to the structure at the friction or impact interfaces, and the stiffness of these extra contact elements is iteratively increased. In other words, a series of forced responses derived from the linear response of the structure – obtained when the nonlinear boundary conditions are ignored, i.e, when the stiffness of the extra contact elements is zero – is calculated, until satisfactory convergence of the results is observed. The new direct contact approach has been successfully applied to simple nonlinear systems. The method has also been validated by comparing its results with those obtained by performing an exact numerical time integration of the nonlinear equations.

- A new method for the modeling and analysis of structures with nonlinear boundary conditions such as cracks has been presented. The forced response of a beam with a crack has been investigated with this method. This study has shown that the exact dynamics of complex nonlinear systems derived from large finite elements can be captured very accurately at a computational cost which is several orders of magnitude lower than that of traditional numerical methods. It has also highlighted the fact that the accuracy of the response depends significantly on the degree of realism of the modeling of the crack.

- Two new complex, flexible models of friction dampers have been developed. The nonlinear forced response of a realistic turbine bladed disk assembly has been studied for each of these dampers.

- The first model introduced is a wedge damper developed within the nonlinear operator framework. The theoretical analysis of the contact forces in the time domains has been presented and it has been shown that a very efficient numerical implementation of the calculation of the contact forces is possible. A parametric study of the design parameters of the wedge damper and their effect on the forced response of the turbine disk has been performed. It has exhibited the great sensitivity of the response with respect to the geometric and physical properties of the damper.
- The second model of damper developed takes advantage of the flexibility of the direct contact approach and is represented by the finite element model of an elastic structure. The model allows for friction with variable normal load on each of its contact points. The interaction between the damper and the turbine disk is fully described by (1) a set of boundary conditions applied to some of the relative DOFs representing the motion of the damper with respect to the motion of the platforms, and (2) a choice of contact elements for the damper-platform interfaces. To the author's knowledge, this is the first time that a flexible, structure-like model of damper that allows for the rigid body mode in the normal direction is developed and applied to a realistic industrial structure with cyclic symmetry.

The forced responses of the turbine bladed disk obtained with these two types of dampers have shown the added layer of complexity that a realistic modeling of these dampers entails. In particular, the complicated nature of the periodic waveforms of the contact efforts as well as the frequency response of the structure was presented. These studies have shown that it is now possible to investigate, at a very low compu-

tational cost and with excellent accuracy, the effect of friction damping when very realistic modeling assumptions regarding the friction-damped structure as well as the dampers are made.

7.2 Direction for future research

Following are some ideas for future research that would complement and further advance the topics addressed in this dissertation.

7.2.1 Friction damper modeling

The results obtained in Chapter VI have shown that it is now possible to use finite element models to describe the physical properties of friction dampers, and that the exact stiffness properties of the dampers can be taken into account. However, during the course of this dissertation work, significant numerical obstacles have been encountered when trying to extend the realism of the modeling of the friction dampers by *simultaneously* taking into account (1) their mass properties, (2) the exact 3-D nature of the contact points with the platforms, (3) the specific constraints associated with systems with cyclic symmetry; and (4) without enforcing specific boundary conditions regarding some of the relative rigid body modes of the damper with respect to the structure.

Ideally of course, the periodic forced response of friction damped systems should be obtained by simply using the finite element models of the structure and the friction dampers, and by enforcing general 3-D contact conditions on *all* the contact interfaces between the dampers and the blades. In other words, the dampers would only be subject to the periodic motion of the platforms and the centrifugal force. Although the methods developed in this dissertation theoretically allow to do so, the effective numerical investigation of such a general case has proved to be extremely tedious and difficult and to this day the reason why is not well understood. Explanations for these difficulties are needed

and would probably require the investigation of some of the following topics:

- *Influence of the mass properties of the dampers*. Studies including the inertia properties of a friction damper are a subject of notorious difficulty. Taking into account such properties may lead to a loss of the periodic behavior of the damper and may require a different type of analysis method than the HFT.

- *Drift and creep*. If no restrictions are applied to some of the relative DOFs between the damper and the structure, it is possible that the friction dampers may exhibit drifting or creeping withing the cavities they are inserted in, which may also lead to the loss of the periodic nature of the behavior of the damper and the contact efforts.

- *Nonlinear solver*. Although the hybrid Powell algorithm used in this dissertation work has shown excellent capabilities for the study of complicated friction damped systems, it may be of interest to assess the capabilities of other nonlinear solvers, and this may alleviate some of the convergence issues observed when the four modeling assumptions mentioned above are taken into account simultaneously.

7.2.2 Modeling of structures with a very large number of nonlinear contact DOFs

The most advanced structures that can be currently analyzed while incurring a reasonable computational cost feature at most a few hundreds nonlinear DOFs. Since the cost of solving the nonlinear equations derived from the HFT method increases with the cube of the number of nonlinear variables, the application of the HFT method to systems featuring more nonlinear DOFs seems impractical.

With the notable exception of mistuned assemblies that require the modeling of a great number of independent contact interfaces, the structures that require a high number of nonlinear contact points are usually structures with a few contact interfaces where each contact interface is described by a precise mesh of many contact nodes.

In this case, the following modification of the HFT method could be implemented:

- The nonlinear DOFs of the interface would be approximated by a series of interface normal modes similar to that commonly used in component modes techniques. These interface modes would be represented in the frequency domain by a set of Fourier coefficients.

- The actual, physical nonlinear DOFs would be used in the time domain to evaluate the efforts at the contact interface.

- These efforts would be projected back onto the interface modes, in the frequency domain.

This approach should allow the study of structures featuring thousands or more of nonlinear DOFs, thus preserving the accuracy of the contact interfaces, while limiting the increase of computational effort currently required for such systems.

7.2.3 New applications of the direct-contact approach

The direct method approach presented herein has been applied to friction damped systems as well as to a model of beam with a crack. The potential of the method however expands well beyond these types of applications. In fact, the periodic response of many types of structural systems with cracks, gaps or plays, impact and friction seems now readily accessible. The author believes that the study of the behavior of systems of unprecedented realism is now possible, and that the method offers great research opportunities.

APPENDICES

APPENDIX A

Definition and properties of the Kronecker product

Given a p-by-q matrix $\mathbf{A}$ and a matrix $\mathbf{B}$, the Kronecker product of A and B is defined as:

$$\mathbf{A} \otimes \mathbf{B} = \begin{bmatrix} \mathbf{A}(1,1)\mathbf{B} & \dots & \mathbf{A}(1,q)\mathbf{B} \\ \vdots & & \vdots \\ \mathbf{A}(p,1)\mathbf{B} & \dots & \mathbf{A}(p,q)\mathbf{B} \end{bmatrix}$$

It also satisfies the following property:

$$(\mathbf{A} \otimes \mathbf{B})(\mathbf{C} \otimes \mathbf{D}) = (\mathbf{AC}) \otimes (\mathbf{BD})$$

APPENDIX B

Definition and properties of Fourier matrices

The complex Fourier matrix $\underline{\mathbf{E}}$ is defined for a n_s-sector cyclic assembly as:

$$\underline{\mathbf{E}}(p,q) = \frac{1}{\sqrt{n_s}} e^{\frac{2j\pi}{n_s}(p-1)(q-1)}, \quad (p,q) \in [1, n_s].$$

Assuming that the number of DOFs of a cyclic sector of the assembly is n, the block version $\underline{\tilde{\mathbf{E}}}$ of the Fourier matrix (referred to as extended Fourier matrix) is given by:

$$\underline{\tilde{\mathbf{E}}} = \underline{\mathbf{E}} \otimes \mathbf{I}_n,$$

where $\mathbf{I}_n$ is the n-by-n identity matrix, and $\otimes$ represents the Kronecker product. The inverse of $\underline{\tilde{\mathbf{E}}}$ is $\underline{\tilde{\mathbf{E}}}^*$, and $\underline{\mathbf{E}}$ satisfies the following property:

$$\underline{\mathbf{E}}^* \underline{\mathbf{u}}_k^{e_o} = \frac{1}{\sqrt{n_s}} \begin{Bmatrix} 0 \\ \vdots \\ 1 \\ \vdots \\ 0 \end{Bmatrix} \leftarrow \begin{array}{l} \text{line } q+1 \text{ such that} \\ q - k e_o \equiv 0 \ [n_s], \end{array}$$

where $\underline{\mathbf{u}}_k^{e_o}$ is defined as:

$$\underline{\mathbf{u}}_k^{e_o} = \left[1, \ldots, e^{(2j\pi p e_o k)/n_s}, \ldots, e^{(2j\pi (n_s-1) e_o k)/n_s}\right]^T.$$

Also, if $\mathbf{A}$ is a $(n \times n_s)$-by-$(n \times n_s)$, real, block-circulant matrix with blocks of size n, then

$$\underline{\tilde{\mathbf{E}}}^* \mathbf{A} \underline{\tilde{\mathbf{E}}} = \mathbf{BDiag}\big[\underline{\mathbf{A}}^0, \ldots, \underline{\mathbf{A}}^{n_s-1}\big],$$

where $\underline{\mathbf{A}}^0, \ldots, \underline{\mathbf{A}}^{n_s-1}$ are n-by-n complex matrices.

BIBLIOGRAPHY

BIBLIOGRAPHY

[1] T. Cameron and J. Griffin. An alternating frequency/time domain method for calculating the steady-state response of nonlinear dynamic systems. *Journal of Applied Mechanics*, 56:149–154, 1989.

[2] F.H. Ling and X.X. Wu. Fast galerkin method and its application to determine periodic solutions of non-linear oscillators. *International Journal of Non-Linear Mechanics*, 22(2):89–98, 1987.

[3] J. Guillen and C. Pierre. An efficient, hybrid, frequency/time domain method for the dynamics of large-scale dry-friction damped structural systems. In *Proceedings of the IUTAM symposium on Unilateral Multibody Dynamics*, Munich, Germany, 1998.

[4] J. Guillen. *Studies of the Dynamics of Dry-Friction-Damped Blade Assemblies*. PhD thesis, The University of Michigan, 1999.

[5] J. Guillen and C. Pierre. An efficient, hybrid, frequency-time domain method for the dynamics of large-scale dry-friction damped structural systems. In F. Pfeiffer and Ch. Glocker, editors, *IUTAM Symposium on Unilateral Multibody Contacts*, Dordrecht, Netherlands, 1999. Kluwer Academic Publishers.

[6] J. Guillen, T. Lagrange, and C. Pierre. An advanced damper model for the dynamics of dry friction damped systems. In *Proceedings of the 17th Biennial Conference on Mechanical Vibration and Noise, ASME paper DETC99/VIB-8083*, Las Vegas, Nevada, September 1999.

[7] J.P. Den Hartog. Forced vibrations with combined coulomb and viscous friction. In *Transactions of the ASME*, volume 53–9, pages 107–115, 1931.

[8] R. Ibrahim. Friction-induced vibration, chatter, squeal, and chaos. part i: Mechanics of contact and friction. *Applied Mechanics Review*, 47(7):209–226, 1994.

[9] R. Ibrahim. Friction-induced vibration, chatter, squeal, and chaos. part ii: Dynamics and modeling. *Applied Mechanics Review*, 47(7):227–253, 1994.

[10] B. Feeny, A. Guran, N. Hinrichs, and K. Popp. A historical review on dry friction and stick-slip phenomena. *Applied Mechanics Review*, 51(5):321–341, 1998.

[11] A.A. Ferri. Friction damping and isolation systems. *Journal of Engineering for Gas Turbines and Power*, 117:196–206, 1995. Special 50-th Anniversary Design Issue.

[12] E.S. Levitan. Forced oscillation of a spring-mass system having combined coulomb and viscous damping. *Journal of the Acoustical Society of America*, 32(10):1265–1269, 1960.

[13] M.S. Hundal. Response of a base excited system with coulomb and viscous friction. *Journal of Sound and Vibration*, 64(3):371–378, 1979.

[14] G.C.K. Yeh. Forced vibrations of a two-degree-of-freedom system with combined coulomb and viscous damping. *Journal of the Acoustical Society of America*, 32(10):14–24, 1960.

[15] T.K. Pratt and R. Williams. Non-linear analysis of stick-slip motion. *Journal of Sound and Vibration*, 74(4):531–542, 1981.

[16] I. Korkmaz, J.J. Barrau, M. Berthillier, and S. Creze. Theoretical dynamic analysis of a cantilever beam damped by a dry friction damper. In *DE-Vol. 84-1, ASME Design Engineering Technical Conferences, Volume 3 - Part A*, 1995.

[17] W.E. Whiteman and A.A. Ferri. Suppression of bending-torsion flutter through displacement-dependent dry friction damping. *AIAA Journal*, 37(1):79–83, 1999.

[18] A. Toufine, J.J. Barrau, and M. Berthillier. Dynamic study of a simplified mechanical system with presence of dry friction. *Journal of Sound and Vibration*, 225(1):95–109, 1999.

[19] A. Toufine, J.J. Barrau, and M. Berthillier. Dynamic study of a structure with flexion-torsion coupling in the presence of dry friction. *Nonlinear Dynamics*, 18:321–337, 1999.

[20] A. Nayfeh and D. Mook. *Nonlinear Oscillations*. John Wiley & Sons, 1979.

[21] E.H. Dowell. The behavior of a linear, damped modal system with a non-linear spring-mass-dry friction damper attached. *Journal of Sound and Vibration*, 89(1):65–84, 1983.

[22] E.H. Dowell and H.B. Schwartz. Forced response of a cantilever beam with a dry friction damper attached, part i: Theory. *Journal of Sound and Vibration*, 91(2):255–267, 1983.

[23] E.H. Dowell and H.B. Schwartz. Forced response of a cantilever beam with a dry friction damper attached, part ii: Experiment. *Journal of Sound and Vibration*, 91(2):269–291, 1983.

[24] A.A. Ferri and E.H. Dowell. The behavior of a linear, damped modal system with a non-linear spring-mass-dry friction damper attached, part ii. *Journal of Sound and Vibration*, 101(1):55–74, 1985.

[25] A.A. Ferri and A.C. Bindemann. Damping and vibration of beams with various types of frictional support conditions. *Journal of Vibration and Acoustics*, 114:289–296, 1992.

[26] C.H. Menq and J.H. Griffin. A comparison of transient and steady state finite element analyses of the forced response of a frictionnally damped beam. *Journal of Vibration, Acoustics, Stress and Reliability in Design*, 107:19–25, 1985.

[27] W.E. Whiteman and A.A. Ferri. Displacement-dependent dry friction damping of a beam-like structure. *Journal of Sound and Vibration*, 198(3):313–329, 1996.

[28] W.E. Whiteman and A.A. Ferri. Multi-mode analysis of beam-like structures subjected to displacement-dependent dry friction damping. *Journal of Sound and Vibration*, 207(3):403–418, 1997.

[29] Y.-J. Go, Y.-H. Kim, and H.-G. Chang. An analysis of the behavior of a simply supported beam with a dry friction damper attached. *Applied Acoustics*, 55(1):31–41, 1998.

[30] E. Bazan, J. Bielak, and J.H. Griffin. An efficient method for predicting the vibratory response of linear structures with friction interfaces. *Journal of Engineering for Gas Turbines and Power*, 108:633–640, 1986.

[31] J.H. Griffin. Friction damping of resonant stress in gas turbine engine airfoils. *Journal of Engineering for Power*, 102:329–333, 1980.

[32] A.V. Srinivasan and D.G. Cutts. Dry friction damping mechanisms in engine blades. *Journal of Engineering for Gas Turbines and Power*, 105:525–530, 1983.

[33] A. Muszyńska and D.I. Jones. On tuned bladed disk dynamics: Some aspects of friction related mistuning. *Journal of Sound and Vibration*, 86(1):107–128, 1983.

[34] A. Sinha and J.H. Griffin. Effects of static friction on the forced response of frictionally damped turbine blades. *Journal of Engineering for Gas Turbines and Power*, 106:65–69, 1984.

[35] K.Y. Sanliturk, M. Imregun, and D.J. Ewins. Harmonic balance vibration analysis of turbine blades with friction dampers. *Journal of Vibration and Acoustics*, 119:96–103, 1997.

[36] A. Sinha and J.H. Griffin. Friction damping of flutter in gas turbine engine airfoils. *Journal of Aircraft*, 20(4):372–375, 1983.

[37] A. Sinha and J.H. Griffin. Effects of friction dampers on aerodynamically unstable rotor stages. *AIAA Journal*, 23:262–270, 1985.

[38] A. Sinha and J.H. Griffin. Stability of limit cycles in frictionally damped and aerodynamically unstable rotor stages. *Journal of Sound and Vibration*, 103(3):341–356, 1985.

[39] A. Sinha, J.H. Griffin, and R.E. Kielb. Influence of friction dampers on torsional blade flutter. *Journal of Engineering for Gas Turbines and Power*, 108:313–318, 1986.

[40] J.H. Griffin and A. Sinha. The interaction between mistuning and friction in the forced response of bladed disk assemblies. *Journal of Engineering for Gas Turbines and Power*, 107:205–211, 1985.

[41] D. Cha and A. Sinha. Computation of the optimal normal load of a friction damper under different types of excitation. In *Presented at the International Gas Turbine & Aeroengine Congress and Exhibition, paper 99-GT-413*, Indianapolis, Indiana, June 1999.

[42] D. Cha and A. Sinha. Statistics of responses of a mistuned and frictionally damped bladed disk assembly subjected to white noise and narrow band excitations. In *Proceedings of the ASME Turbo Expo 2000*, Munich, Germany, May 2000.

[43] D. Cha and A. Sinha. Computation of the optimal normal load for a mistuned and frictionally damped bladed disk assembly under different types of excitation. In *Proceedings of the ASME Turbo Expo 2001, paper 2001-GT-0278*, New Orleans, Louisiana, June 2001.

[44] S.L. Lau and Y.K. Cheung. Amplitude incremental variational principle for nonlinear vibration of elastic systems. *Journal of Applied Mechanics*, 48:959–964, 1981.

[45] S.L. Lau, Y.K. Cheung, and S.Y. Wu. Incremental harmonic balance method with multiple time scales for aperiodic vibration of nonlinear systems. *Journal of Applied Mechanics*, 50:871–876, 1983.

[46] S.L. Lau and W.S. Zhang. Nonlinear vibrations of piecewise-linear systems by incremental harmonic balance method. *Journal of Applied Mechanics*, 59:153–160, 1992.

[47] A.A. Ferri. On the equivalence of the incremental harmonic balance method and the harmonic balance-newton raphson method. *Journal of Applied Mechanics*, 53:455–457, 1986.

[48] C. Pierre and E.H. Dowell. A study of dynamic instability of plates by an extended incremental harmonic balance method. *Journal of Applied Mechanics*, 51:693–697, 1985.

[49] C. Pierre, A.A. Ferri, and E.H. Dowell. Multi-harmonic analysis of dry friction damped systems using an incremental harmonic balance method. *Journal of Applied Mechanics*, 52(4):958–964, 1985.

[50] A.A. Ferri and E.H. Dowell. Frequency domain solutions to multi-degree-of-freedom, dry-friction damped systems. *Journal of Sound and Vibration*, 124(2):207–224, 1988.

[51] S.T. Wei and C. Pierre. Effects of dry friction damping on the occurrence of localized forced vibrations in nearly cyclic structures. *Journal of Sound and Vibration*, 129(3):397–416, 1989.

[52] T.N. Shiau and Y.D. Yu. Frictional damping on the dynamic behaviour of composite blades. In *Proceedings of the 6-th International Symposium on Transport Phenomena and Dynamics of Rotating Machinery*, volume 1, pages 262–271, Honolulu, Hawaii, 1996.

[53] T.N. Shiau, J.S. Rao, Y.D. Yu, and S.T. Choi. Steady-state response and stability of rotating composite blades with frictional damping. *Journal of Engineering for Gas Turbines and Power*, 120:131–139, 1998.

[54] Y.B. Kim and S.T. Noah. Stability and bifurcation analysis of oscillators with piecewise-linear characteristics: A general approach. *Journal of Applied Mechanics*, 58:545–553, 1991.

[55] A. Cardona. A multiharmonic method for nonlinear vibration analysis. *International Journal for Numerical Methods in Engineering*, 37:1593–1608, 1994.

[56] M. Berthillier, C. Dupont, P. Chanez, and F. Saurat. Réponse forcée aéroélastique des aubes de turbomachines. *Revue Française de Mécanique*, 4, 1998.

[57] M. Berthillier, C. Dupont, R. Mondal, and J.J. Barrau. Blades forced response analysis with friction dampers. *Transactions of the ASME*, 120:468–474, April 1998.

[58] J.H. Wang and W.K. Chen. Investigation of the vibration of a blade with friction damper by hbm. *Journal of Engineering for Gas Turbine and Power*, 115:294–299, 1993.

[59] Y. Ren and C.F. Beards. A new receptance-based perturbative multi-harmonic balance method for the calculation of the steady state response of non-linear systems. *Journal of Sound and Vibration*, 172(5):593–604, 1994.

[60] T. Ge and A.Y.T. Leung. A toepliz jacobian matrix/fast fourier transformation method for steady-state analysis of discontinuous oscillators. *Shock and Vibration*, 2(3):205–218, 1995.

[61] A.Y.T. Leung and T. Ge. Toepliz jacobian matrix for nonlinear periodic vibration. *Journal of Applied Mechanics*, 62:709–717, 1995.

[62] Y. Wang. Stick-slip motion of frictionally damped turbine airfoils: A finite element in time (fet) approach. In *DE-Vol. 84-1, 1995 ASME Design Engineering Technical Conferences, Volume 3 – part A*, pages 1071–1082, 1995.

[63] Y. Wang. An analytical solution for periodic response of elastic-friction damped systems. *Journal of Sound and Vibration*, 189(3):299–313, 1996.

[64] A.A. Ferri and B.S. Heck. Vibration analysis of dry-friction damped turbine blades using singular perturbation theory. *Transactions of the ASME*, 120:588–595, 1998.

[65] E.J. Berger and C.M. Krousgrill. On friction damping modeling using bilinear hysteresis elements. *Journal of Vibration and Acoustics*, 124:367–375, July 2002.

[66] S. Chen and A. Sinha. Probabilistic method to compute the optimal slip load for a mistuned bladed disk assembly with friction dampers. *Journal of Vibration and Acoustics*, 112:214–221, 1990.

[67] C.C. Lin and M.P. Mignolet. Effects of damping and damping mistuning on the forced vibration response of bladed disks. *Journal of Sound and Vibration*, 193(2):525–543, 1996.

[68] C.H. Menq, J. Bielak, and J.H. Griffin. The influence of microslip on vibratory response, part i: A new microslip model. *Journal of Sound and Vibration*, 107:279–293, 1986.

[69] C.H. Menq, J.H. Griffin, and J. Bielak. The influence of a variable normal load on the forced vibration of a frictionally damped structure. *Journal of Engineering for Gas Turbines and Power*, 108:300–305, 1986.

[70] B.D. Yang and C.H. Menq. Modeling of friction contact and its application to the design of shroud contact. *Journal of Engineering for Gas Turbines and Power*, 119:958–963, 1997.

[71] J.H. Wang and W.L. Shieh. The influence of a variable friction coefficient on the dynamic behavior of a blade with friction damper. *Journal of Sound and Vibration*, 149(1):137–145, 1991.

[72] J.R. Anderson and A.A. Ferri. Behavior of a single-degree-of-freedom system with a generalized friction law. *Journal of Sound and Vibration*, 140(2):287–304, 1990.

[73] J.H. Griffin and C.H. Menq. Friction damping of circular motion and its implications to vibration control. *Journal of Vibration and Acoustics*, 113:225–229, 1991.

[74] J.H. Griffin, W.T. Wu, and Y. El-Aini. Friction damping of hollow airfoils: Part i - theoretical developments. *Journal of Engineering for Gas Turbines and Power*, 120:120–125, 1998.

[75] K.Y. Sanliturk and D.J. Ewins. Modelling two-dimensional friction contact and its application using harmonic balance method. *Journal of Sound and Vibration*, 193(2):511–523, 1996.

[76] C.H. Menq and B.D. Yang. Non-linear spring resistance and friction damping of frictional constraint having two-dimensional motion. *Journal of Sound and Vibration*, 217(1):127–143, 1998.

[77] B.D. Yang and C.H. Menq. Characterization of 3d contact kinematics and prediction of resonant response of structures having 3d frictional constraint. *Journal of Sound and Vibration*, 217(5):909–925, 1998.

[78] B.D. Yang and C.H. Menq. Characterization of contact kinematics and application to the design of wedge dampers in turbomachinery blading: Part 1 – stick-slip contact kinematics. *Journal of Engineering for Gas Turbines and Power*, 120:410–417, 1998.

[79] B.D. Yang, C.H. Menq, and J.J. Chen. Prediction of resonant response of shrouded blades with three-dimensional shroud constraint. *Journal of Engineering for Gas Turbines and Power*, 121:523–529, 1999.

[80] G. Csaba. Forced response analysis in time and frequency domains of a tuned bladed disk with friction dampers. *Journal of Sound and Vibration*, 214(3):395–412, 1998.

[81] G. Csaba. *Modelling Microslip Friction Damping and its Influence on Turbine Blade Vibrations*. PhD thesis, Linköping University, Sweden, 1998.

[82] G. Csaba. Modelling of a microslip friction damper subjected to translation and rotation. In *Presented at the International Gas Turbine & Aeroengine Congress and Exhibition, paper 99-GT-149*, Indianapolis, Indiana, June 1999.

[83] M. Jareland and G. Csaba. Friction damper mistuning of a bladed disk and optimization with respect to wear. In *Proceedings of the ASME Turbo Expo 2000, paper 2000-GT-363*, Munich, Germany, May 2000.

[84] M. Jareland. A parametric study of a cottage-roof damper and comparison with experimental results. In *Proceedings of the ASME Turbo Expo 2001, paper 2001-GT-0275*, New Orleans, Louisiana, June 2001.

[85] K.Y. Sanliturk, D.J. Ewins, and A.B. Stanbridge. Underplatform dampers for turbine blades: Theoretical modeling, analysis, and comparison with experimental data. *Journal of Engineering for Gas Turbines and Power*, 123:919–929, 2001.

[86] F. Pfeiffer and M. Hajek. Stick-slip motion of turbine blade dampers. *Philosophical Transactions of the Royal Society of London A*, 338:503–517, 1992.

[87] A.B. Kaiser, J.P. Cusumano, and J.F. Gardner. Modeling and dynamics of friction wedge dampers in railroad freight trucks. *Vehicle System Dynamics*, 38(1):55–82, 2002.

[88] L. Panning, W. Sextro, and K. Popp. Optimization of interblade friction damper design. In *Proceedings of the ASME Turbo Expo 2000, paper 2000-GT-541*, Munich, Germany, May 2000.

[89] J.J. Chen and C.H. Menq. Prediction of periodic response of blades having 3d nonlinear shroud constraints. In *Proceedings of the International Gas Turbine & Aeroengine Congress and Exhibition, paper 99-GT-289*, Indianapolis, Indiana, June 1999.

[90] J.J. Chen, B.D. Yang, and C.H. Menq. Periodic forced response of structures having three-dimensional frictional constraints. *Journal of Sound and Vibration*, 229(4):775–792, 2000.

[91] J.J. Chen and C.H. Menq. Periodic response of blades having three-dimensional nonlinear shroud constraints. *Journal of Engineering for Gas Turbines and Power*, 123:901–909, 2001.

[92] S. Nacivet, C. Pierre, F. Thouverez, and L. Jézéquel. Analysis of periodic frictional contact in finite elements problems. In *Proceedings of DTEC'01, 2001 ASME Design Engineering Technical Conferences, paper DETC2001/VIB-21735*, Pittsburgh, Pennsylvania, USA, September 2001.

[93] S. Nacivet, C. Pierre, F. Thouverez, and L. Jézéquel. A dynamic lagrangian frequency-time method for the vibration of dry-friction damped systems. *Journal of Sound and Vibration*, 265:201–219, 2003.

[94] E. Seinturier, J.-P. Lombard, M. Dumas, C. Dupont, and V. Sharma. Forced response prediction methodology for the design of hp compressor bladed disks. In *Proceedings of the ASME Turbo Expo 2004, paper GT-2004-53372*, volume 6, pages 317–326, Vienna, Austria, July 2004.

[95] E.P. Petrov and D.J. Ewins. Analytical formulation of friction interface elements for analysis of nonlinear multi-harmonic vibrations of bladed disks. *Journal of Turbomachinery*, 125:364–371, April 2003.

[96] E.P. Petrov. A method for use of cyclic symmetry properties in analysis of nonlinear multiharmonic vibrations of bladed disks. *Journal of Turbomachinery*, 126:175–183, January 2004.

[97] E.P. Petrov. Method for direct parametric analysis of nonlinear forced response of bladed disks with friction contact interfaces. *Journal of Turbomachinery*, 126(4):654–662, October 2004.

[98] E.P. Petrov and E.J. Ewins. Method for analysis of nonlinear multiharmonic vibrations of mistuned bladed disks with scatter of contact interface characteristics. *Journal of Turbomachinery*, 127:128–136, 2005.

[99] S. Nacivet. *Modélisation du frottement en pied d'aube par une approche fréquentielle*. PhD thesis, Ecole Centrale de Lyon, France, 2002.

[100] D. Charleux, F. Thouverez, and J.-P. Lombard. Three-dimensional multiharmonic analysis of contact and friction in dovetail joints. In *Proceedings of the 22nd International Modal Analysis Conference, paper 348*, Dearborn, Michigan, June 2004.

[101] D. Charleux, D. Gibert, F. Thouverez, and J. Dupeux. Numerical and experimental study of friction damping blade attachments of rotating bladed disks. *International Journal of Rotating Machinery*, 2006, 2006.

[102] E.P. Petrov and E.J. Ewins. Analysis of essentially non-linear vibration of large-scale models for bladed discs with variable contact and friction at root joints. In *Proceedings of the 8th International Conference on Vibrations in Rotating Machinery*, pages 163–172, Swansea, UK, September 2004.

[103] E.P. Petrov and E.J. Ewins. Effects of damping and varying contact area at blade-disk joints in forced response analysis of bladed disk assemblies. *Journal of Turbomachinery*, 128:403–410, 2006.

[104] B.D. Yang, M.L. Chu, and C.H. Menq. Stick-slip-separation analysis and non-linear stiffness and damping characterization of friction contacts having variable normal load. *Journal of Sound and Vibration*, 210(4):461–481, 1998.

[105] T. Lagrange. A study of the dynamics of friction-damped blade assemblies: Cyclic symmetry and structure-like dampers. Master's thesis, The University of Michigan, 1999.

[106] R. Craig and M. Bampton. Coupling of substructures for dynamic analysis. *AIAA Journal*, 8(7):1313–1319, 1968.

[107] M.J.D. Powell. A hybrid method for nonlinear equations. In P. Rabinowitz, editor, *Numerical Methods for Nonlinear Equations*. Gordon and Breach, London, U.K., 1969.

[108] B.S. Garbow, K.E. Hillstrom, and J.J. More. User guide for minpack-1. Technical report, National Argonne Laboratory, 1980.

[109] H. Cho and J.R. Barber. Dynamic behavior and stability of simple frictional systems. *Mathl. Comput. Modelling*, 28(4–8):37–53, 1998.

[110] H. Cho and J.R. Barber. Stability of the three-dimensional coulomb friction law. In *Proceedings of the Royal Society of London A*, volume 455, pages 839–861, 1999.

[111] M. Castanier and C. Pierre. Consideration on the benefits of intentional blade mistuning for the forced response of turbomachinery rotors. In *in Analysis and Design Issues for Modern Aerospace Vehicles, presented at the 1997 ASME International Mechanical Engineering Congress and Exhibition and Exhibition, ASME Publication AD*, volume 55, pages 419–425, Dallas, Texas, November 1997.

[112] M.-H. Shen and C. Pierre. Natural modes of bernoulli-euler beams with symmetric cracks. *Journal of Sound and Vibration*, 138(1):115–134, 1990.

[113] M.-H. Shen and C. Pierre. Free vibrations of beams with a single-edge crack. *Journal of Sound and Vibration*, 170(2):237–259, 1994.

ABSTRACT

MODELING AND ANALYSIS OF THE DYNAMICS OF DRY-FRICTION-DAMPED STRUCTURAL SYSTEMS

by

Olivier J. Poudou

Chair: Christophe Pierre

The benefits of intentional friction damping to reduce the occurrence of wear and premature failure of turbomachinery bladed-disk assemblies are well known and many studies on this topic have focused on the analysis and prediction of the complicated nonlinear forced response exhibited by these structures. In this research, extensions of the recently introduced multi-harmonic Hybrid Frequency-Time method are proposed for the efficient analysis of the response of realistic structures featuring displacement-dependent nonlinearities, such as the friction and impact phenomena that may occur in the presence of friction dampers or when two parts of the same structure periodically contact each other. These theoretical extensions are adapted to the study of large scale, industrial bladed-disk structures that may feature cyclic symmetry or mistuning.

Two analysis techniques are developed for the modeling of displacement-dependent nonlinearities. In the first technique friction dampers are modeled as nonlinear operators representing the contact forces acting on the blades, from the simple case of mono-directional friction with constant normal load to the more complex case of three dimensional contact with variable normal load. The analysis of the forced response of several

nonlinear systems illustrates the capabilities of this approach as well as the complexity of the typical behavior exhibited by friction damped structures. The second technique introduced helps analyze structures experiencing intermittent contact or friction between two parts or sub-components of the same assembly. This method is applied to the study of the forced response of several simple systems and is used with great efficiency to predict the nonlinear behavior of a beam with a crack. This approach also allows the dampers to be modeled realistically as stand-alone components appended to the bladed disk assembly. In this case the bladed disk assembly as well as the friction dampers are modeled as independent structures that interact at their contacting interfaces. This allows the use of detailed finite element models of dampers rather than having to make simplifying assumptions regarding their geometry. These two methods are applied to the study of the nonlinear forced response a realistic bladed-disk assembly featuring a wedge damper model and a structure-like damper model.